Adsorption and desorption of cellulose derivatives

Promotoren: Dr. B.H. Bijsterbosch,
emeritus hoogleraar in de Fysische- en Kolloïdchemie

Dr. M.A. Cohen Stuart,
hoogleraar in de Fysische Chemie met bijzondere aandacht voor de Kolloïdchemie

Co-promotor: Dr. A. de Keizer,
universitair docent bij het departement Biomoleculaire Wetenschappen

C.W. Hoogendam

Adsorption and desorption of cellulose derivatives

Proefschrift
ter verkrijging van de graad van doctor
op gezag van de rector magnificus
van de Landbouwuniversiteit Wageningen,
Dr. C.M. Karssen,
in het openbaar te verdedigen
op woensdag 23 september 1998
des namiddags te half twee in de Aula.

Hoogendam, Cornelis Willem

Adsorption and desorption of cellulose derivatives
Cornelis Willem Hoogendam. -[S.I. : s.n.]
Thesis Wageningen - with refs. - with summary in Dutch
ISBN 90-5485-881-8
Subject headings: polymer adsorption, cellulose derivatives

printing: Grafisch Service Centrum, Wageningen

The work reported in this thesis ("Adsorption and desorption of cellulose derivatives") was supported by the Dutch Programme for Innovation Oriented Carbohydrate Research (IOP-k).

Stellingen

(1)

Het gedrag van cellulose derivaten aan een vast-vloeistof grensvlak wordt in hoge mate beïnvloed door de stijfheid van deze moleculen.
dit proefschrift, Hoofdstukken 4 en 5

(2)

De hydrodynamische laagdikte van een geadsorbeerd polymeer bepaald door middel van dynamische lichtverstrooiing heeft alleen betekenis als de effectieve viscositeit van de polymeer oplossing gebruikt wordt.
dit proefschrift, Hoofdstuk 6

(3)

De beschrijving van polyelectroliet adsorptie aan een geladen oppervlak van Vermeer et al., waarbij gebruik wordt gemaakt van een theorie die uitgaat van een evenwichtssituatie, is niet volledig. Voor polyelectrolieten is, vooral bij lage zoutconcentraties, een lange tijd nodig om een toestand van evenwicht in de adsorptie te bereiken.
A.W.P. Vermeer, F.A.M. Leermakers, L.K. Koopal, Langmuir 13 (1997) 4413

(4)

De theoretische beschrijving van de effectieve viscositeit is (nog) verre van volledig.
G.D.J. Phillies, C. Malone, K. Ullmann, G.S. Ullmann, J. Rollings, and L.P. Yu, Macromolecules 20 (1987) 2280.

(5)

Gelpermeatie chromatografie in combinatie met statische lichtverstrooiing is een elegante methode om de (intrinsieke) ketenstijfheid van een polymeer te bepalen.
dit proefschrift, Hoofdstuk 2

(6)

Voor een goed begrip van de adsorptie van polyelectrolieten is het noodzakelijk om ook de adsorptie kinetiek in beschouwing te nemen.
dit proefschrift, Hoofdstukken 3 en 4

(7)

In een aantal gevallen kan de uitkomst van het regeringsaccoord van Paars II worden aangemerkt als een vorm van kiezersbedrog.

(8)

De moderne aanduiding van diverse begrippen (zoals target, helpdesk, en helicopterview) en beroepen (bijvoorbeeld sales manager, computer operator, en designer) door middel van een Engelse naamgeving in Nederland is misschien wel het beste voorbeeld van een "overdone" taalgebruik.

(9)

De vernieuwing van de Nederlandse spelling is niet duidelijk en gaat niet ver genoeg.
Woordenlijst Nederlandse taal, Sdu Uitgevers 1997, Achtste oplage.

(10)

Zwaar bier maakt het hoofd licht, light bier ligt zwaar op de maag.

(11)

Experimenteren is een spel van vraag en antwoord tussen de experimentator en de natuur. Dat bij het stellen van een zorgvuldig geformuleerde vraag in veel gevallen ondoorgrondelijk antwoord wordt gegeven, stelt het incasseringsvermogen van de experimentator regelmatig tot het uiterste op de proef.

(12)

Het toenemend aantal vetarme producten is een verrijking van ons voedselaanbod.

(13)

Als het niet gaat zoals het moet, dan moet het maar zoals het gaat.
Gehoord van Ben Spee in de koffiekamer

(14)

De materiaalkennis van de Landbouwuniversiteit is op z'n minst twijfelachtig te noemen. Dit blijkt uit de opmerking: "!! niet in papiercontainer: ... papier met kunststof, **cellulose**, en metaalfolie als oppervlakte of tussenlaag...". Papier bestaat voor het overgrote deel uit cellulose.
Folder Bedrijfsafval gescheiden inzamelen, Landbouwuniversiteit Wageningen, Bureau Veiligheid en Milieuhygiëne Huishoudelijke dienst, oktober 1997.

Stellingen
behorende bij het proefschrift
"Adsorption and desorption of cellulose derivatives"
door C.W. Hoogendam
Landbouwuniversiteit Wageningen, 23 september 1998.

Contents

Chapter 1

Introduction

1.1 General

The importance of polymers is generally recognised. The use of polymers covers a broad range of applications. Roughly speaking one can classify these applications in terms of plastics, as thickening agents, or as coating materials. The work described in this thesis is related to polymers applied as a coating material.

Often synthetic polymers are being used as a coating material. For instance, they provide the colloidal stability of the pigment in paints. Polysaccharides like starch and cellulose which are chemically modified often provide a good alternative for synthetic polymers. The raw materials are widely available from natural sources, they are non-toxic, and cause less harm to the environment than synthetic polymers. Since the interest in chemically modified polysaccharides is still growing, more research concerning their behaviour at solid-liquid interfaces is needed. Insight in this behaviour may result in optimisation of current uses and may also lead to new applications.

1.2 Cellulose treatment, cellulose derivatives and their applications

Cellulose is the most abundant and one of most widely used organic polymers in the world. Because of its ample availability (cellulose is the major constituent of plant material), cellulose is a relatively low-cost polymer. Among cellulose sources wood and cotton are by far the most important ones. On a dry basis, wood contains about 40 to 50% cellulose. Besides cellulose, wood also contains other polysaccharides as lignin (20 to 30%) and hemicellulose (10 to 30%) and components as gums, proteins, and minerals [1]. Because of the high amount of non-cellulose components, a profound treatment of wood is needed in order to obtain purified cellulose. In the preparation of cellulose from wood, usually wood chips are heated under pressure with reagents (e.g. sodium hydroxide, sodium sulfite, and calcium hypochlorite) [2]. Despite an intensive purification it still contains a substantial amount of other polysaccharides (about 15% [1]). Furthermore, the harsh chemical and mechanical treatment causes a cleavage of the cellulose chain. As a raw material, cotton fibers contain the highest amount of cellulose (about 85% [1]). Treatment of cotton is similar to that of wood, however the conditions employed are less rigorous because the amounts of impurities to be removed are much smaller. Purified cotton cellulose usually is of outstanding

quality and has a high degree of polymerisation.

Because cellulose is a polyhydroxyl alcohol, its functional groups (hydroxyl groups) allow numerous chemical modifications. Most of the chemically modified cellulose polymers are accounted for by cellulose esters and cellulose ethers (sometimes referred to "classical cellulose derivatives"). Cellulose nitrate is the oldest known cellulose derivative and by far the most important ester of cellulose. It is being used for the manufacture of materials such as coatings, celluloid plastics, and certain military explosives [3]. Cellulose acetate finds large application in rayon which is used in many textile products [3]. The most important representatives of the group of cellulose ethers are methyl cellulose, hydroxyethyl cellulose and carboxymethyl cellulose. Methyl cellulose is employed, amongst others, in pharmaceutics (e.g. as coating agent in tablets), in the food industry (e.g. as thickeners), and in cement [2,3].

Hydroxyethyl cellulose (HEC) is prepared by treating alkali cellulose (cellulose in a hot aqueous solution containing about 50% sodium hydroxide [3]) with ethylene oxide ($O(CH_2)_2$). Sodium hydroxide is needed to swell the cellulose (breaking the crystalline structure), thereby improving its reactivity and catalysing the etherification. As the hydroxyl group of the hydroxyethyl substituent can be further etherified by ethylene oxide, HEC usually has polyethylene oxide side chains. Since HEC is a water-soluble polymer it is applied as a thickener and pigment-protective colloid in water-based paints [4]. Further it has applications in cement, in pharmaceutical emulsions, as a binder in tablets, and in cosmetic products (e.g. shampoos).

Sodium carboxymethyl cellulose (NaCMC, formerly named sodium cellulose glycolate) or cellulose gum is an anionic cellulose ether which is prepared by the reaction of sodium monochloroacetic acid ($ClCH_2COONa$) and alkali cellulose [3,5]. Though most applications concern the sodium salt of CMC, it is generally referred to CMC. As CMC has such abilities as thickening water, suspending solids in aqueous media and forming films it has proven to be of great commercial value. CMC is successfully applied as a thickener for textile printing pastes, as a soil-suspending agent in synthetic detergents, as a coating for powders and tablets, and as thickener and suspending agent in water-based paints [1-4].

An important characteristic of cellulose derivatives is the average number of substituents per glucose monomer (degree of substitution ds). Below ds=0.4, CMC is not soluble in water, therefore commercially available CMCs usually have a ds ranging from 0.4 to 1.4 [5]. The quality of CMC is related to the uniformity of the distribution of the substituents over the cellulose chain. The main problem to obtain a uniform distribution originates from the highly ordered crystalline structure of natural cellulose. Though swelling of cellulose can be achieved by treatment with sodium hydroxide, which improves the accessibility of the hydroxyl groups considerably, the process of substitution cannot be easily controlled. The CMC samples that were used in the work described in this thesis were synthesised from cotton cellulose on a laboratory scale under well-defined experimental conditions, which highly enhances achievement of uniformly distributed substituents.

1.3 Usage of carboxymethyl cellulose in pelletisation of iron ore and in papermaking

In this paragraph we discuss two applications of carboxymethyl cellulose which are related to the work described in this thesis.

Raw iron ore contains about 25-30% iron as mined. The iron content can be increased to 60-65% by magnetic separating drums [4]. Though the iron concentrate has an acceptable chemical quality for processing raw ore into iron, it must be agglomerated into a coarser form before it can be used in blast-furnaces. The most desirable size for blast-furnace feed ranges from 6 to 25 mm [4]. Methods of size enlargement have been known for over hundred years. Of all methods available, sintering and pelletisation are the most important ones. In the sintering process, a mixture of iron concentrate and coke fines is ignited by passing them underneath an ignition burner that is fired with natural gas and air. As the coke fines burn, the generated heat sinters the iron ore concentrate into larger lumps. Then the sinter is crushed to remove extra large lumps and cooled.

Because the agglomerates as obtained from pelletisation are the most desirable ones for the blast-furnace, this process accounts for most of the agglomerate production. In the pelletisation process, ore of very fine size (< 75 μm), usually in a moist state, is rolled into small balls of 10-20 mm in diameter in a balling drum or disk [4]. These so-called green pellets are then dried and hardened by passing combustion gasses through the bed of the agglomerates. The wetting of the particles causes capillary binding forces which hold them together. Gradually nuclei arise which grow into balls, while through the rotational movement simultaneously the strength of the balls is mechanically consolidated. The strength can be substantially enhanced by the addition of a binder. Commonly used types of binders are CaO, $CaCl_2$ and bentonite [6]. However, the main disadvantage of such inorganic binders is that they can cause serious contamination of the final product. Organic binders (polymers) are combusted in the pellet melting process, thereby strongly reducing the amount of contamination. Especially CMC has been successfully applied as an alternative for inorganic binders in the pelletisation process [7]. The success of this application depends critically on the structure of the interfacial CMC layer.

Cellulose (mainly wood cellulose) is the raw material for paper. Roughly speaking in the process of papermaking three steps can be distinguished. First cellulose fibers are dispersed in water, next they are beaten to roughen the fiber surface (which increases the strength of the paper), after which the fiber mat is dried. To enhance its properties (e.g. to achieve uniformity of the surface and enhance opacity [2,8]) usually coatings are applied to paper. The main components of coatings are pigment (or a combination of pigments), dispersants for the pigment, and adhesives to bind the pigment to the paper. The most common pigments used in papermaking are China clay, calcium carbonate, aluminium trihydrate, and titanium dioxide. Titanium dioxide is chemically inert, non-toxic, and insoluble in any liquid employed in

papermaking. It exists in two forms, anatase and rutile. Both forms, especially rutile, have exceedingly high refractive indices which make them highly suitable to enhance the opacity of paper.

The main importance of carboxymethyl cellulose in papermaking relates to two applications. CMC is used alone, or in conjunction with starch, to increase dry strength properties and to improve surface characteristics [9]. CMC is also applied in combination with pigments. In order to achieve an optimal opacity with titanium dioxide, the pigments have to be of small particle size [9]. Therefore, to ensure optimal realisation it is essential that the pigments are sufficiently stabilised against flocculation by other coating ingredients. As CMC adsorbs on titanium dioxide it is frequently applied as stabiliser. Furthermore, because of its excellent binding strength, which implies that it is capable to penetrate into the cellulose network, CMC anchors the pigments onto the paper surface. So, CMC acts as an adhesive as well.

1.4 Adsorption of uncharged polymers and polyelectrolytes

As mentioned in previous sections, many applications of polymers are a consequence of their adsorption at a solid-liquid interface. Adsorption of polymer segments will take place if the interaction energy (adsorption energy) of the segments is larger than the interaction between solvent molecules and the surface. In solution the segments have many degrees of freedom which are (strongly) diminished when they adsorb. Thus, the energy of adsorption has to overcome the loss of conformational entropy [10]. When polymers adsorb, conformational entropy is maintained through sections of the chain which are not attached to the surface (loops and tails). The sequence of segments which are attached to the surface is called a train. Loops are sections between two trains, tails consist of segments at the end of the chain dangling in the solution. Parameters that affect the conformation of the adsorbed polymer layer (i.e. the contribution of trains, loops, and tails) are the adsorption energy, the adsorbed amount of polymer, and the molar mass of the polymer (i.e. the length of the chain). In case the ratio of free surface sites and adsorbing segments is high (at low polymer concentration), the adsorption energy contribution is the leading parameter. The adsorbed amount is low, and most of the segments are situated in trains. At higher surface coverage, and if the adsorption energy is not high, loops and tails are also present. In general, for uncharged polymers, the size of the loops and tails increases with the length of the chain. Consequently, the adsorbed amount increases with molar mass. If polymer segments have high adsorption energy this quantity keeps dominating the adsorption. The conformation of the adsorbed layer is flat and the adsorbed amount does not depend on the chain length [10].

Polyelectrolytes are charged polymers. One can distinguish polyelectrolytes with fixed charges (strong polyelectrolytes) and those with charges that depend on pH and salt concentration (weak polyelectrolytes). Electrostatic interactions play an important role in

polyelectrolyte adsorption. Not only the charge of the polymer but also the charge of the substrate surface affects the adsorption. When polyelectrolyte and substrate have the same sign, electrostatics work against the adsorption. Adsorption can only take place if the non-electrostatic interaction is high enough to overcome the electrostatic repulsion between segments and substrate and the mutual repulsion between segments. As salt screens these electrostatic interactions, it can increase the adsorbed amount. Adsorption on an uncharged surface can also be enhanced by salt. If polyelectrolyte and substrate have opposite signs of charge, electrostatics favour the adsorption. Now salt can have either the effect of increasing or decreasing the adsorption. If the interaction is merely electrostatic (i.e. there is little non-electrostatic interaction) salts screens interactions between charged segments and the substrate, leading to less adsorption at higher salt concentration (screening-reduced adsorption [11]). On the other hand, if the non-electrostatic interaction is high, the adsorption increases with salt concentration (screening-enhanced adsorption [11]). The interaction between segments and substrate with opposite charge is strong. As a consequence, at low salt concentration polyelectrolytes adapt a flat conformation when they adsorb; the adsorption does not depend on the chain length.

If both the surface and polyelectrolyte segments carry variable charges, electrostatics become a very complicated factor in the adsorption. When adsorption takes place, additional charges are introduced on the surface as well as on the polyelectrolyte. The presence of charged segments near the surface affects the charge of the surface and visa versa. Both the surfaces used in this study (TiO_2, Fe_2O_3, and SiO_2) and CMC have variable charges. At the inorganic surfaces metal-OH groups are present, CMC has COOH groups.

Theoretical descriptions dealing with polymer adsorption are based on the assumption that the process of adsorption attains the lowest value of the free energy. When the lowest value of the free energy is reached the process is said to be at equilibrium. So, by using thermodynamics one is able to calculate the adsorbed amount at equilibrium as a function of parameters such as polymer concentration, chain length or interaction energy. Thermodynamics do not provide information about the time that is needed to reach equilibrium. If a polymer chain has to overcome a barrier before it can adsorb, the adsorption process will be hampered. The existence of such a barrier is comparable to the activation energy of chemical reactions or the barrier for coagulation of colloidal particles in the DLVO theory. For neutral polymers the barrier originates from loops and tails of adsorbed molecules, which obstruct the motion of chains to a surface (steric hindrance) [12]. In case of polyelectrolytes also long-range electrostatic interactions between a charged surface and chains approaching the surface are present. Hence, it is obvious that kinetic barriers in the adsorption process, especially for polyelectrolytes, cannot be ignored. Experimental work (see for instances refs. 13 and 14) indicates that a barrier for polyelectrolyte adsorption exists. From a theoretical point of view, the subject of adsorption kinetics was recently studied in detail for uncharged polymers by Semenov and Joanny [15]. The subject of the adsorption

kinetics of polyelectrolytes has not been considered theoretically to a large extent. A proposal for the description of polyelectrolyte adsorption taking into account the kinetics is formulated in this thesis.

1.5 Outline of this thesis

The main aim of the work described in this thesis is to gain insight in the mechanisms that play a role in the adsorption of cellulose derivatives (CMC and HEC) on inorganic oxides. By varying parameters like pH, salt concentration, substrate surface, chain length, and degree of substitution information can be obtained about mechanisms of adsorption. Understanding the adsorption behaviour is needed to develop new and to improve current applications.

Most adsorption experiments were carried out with CMC. In **chapter 2** the characterisation of the CMC samples by means of size exclusion chromatography in combination with static light scattering (SEC-MALLS) is described. By SEC-MALLS the relation between the radius of gyration and the molar mass is obtained experimentally. The electrostatic wormlike chain model is used to analyse the data and to determine the intrinsic persistence length of CMC. The intrinsic persistence length, which characterises the local stiffness of the cellulose backbone, is also obtained from potentiometric titrations.

Chapter 3 deals with the kinetics of polyelectrolyte adsorption. Analogous to the Kramers' rate theory for chemical reactions [16] a model is presented which is based on the assumption that a polyelectrolyte encounters a barrier in its motion towards an adsorbing surface. The influence of the salt concentration, the surface charge and the polymer charge on the height of the barrier is examined. Taking into account the height of the barrier, we calculate the adsorption as a function of time. On the basis of such calculations we judge if equilibrium in adsorption is reached on the time scale of an experiment.

The adsorption of CMC on TiO_2 and Fe_2O_3 is discussed in **chapter 4**. We investigate the effect of pH, NaCl concentration, molar mass and degree of substitution of CMC on the adsorption. Attention is paid to the kinetics of the adsorption by comparing the time dependent adsorption with calculations using the model presented in chapter 3. Furthermore we discuss the effect of increasing the pH on both the adsorbed amount and the layer thickness after initially adsorbing CMC at low pH.

In **chapter 5** we discuss the adsorption of HEC and quaternary ammonium substituted HEC (QNHEC) on SiO_2 and TiO_2 as a function of pH and NaCl concentration. As in chapter 4, experimental data are compared with model calculations.

The diffusion of spherical SiO_2 particles (inert probes) in various CMC solutions is studied in **chapter 6**. From the diffusion behaviour we determine the viscosity as experienced by these probes (effective viscosity). An interpretation of the diffusion behaviour is given in terms of a model in which the probes are supposed to be surrounded by a polymer free layer.

The effective viscosity is applied to determine the adsorbed layer thickness of CMC and HEC on Fe_2O_3 and SiO_2, respectively.

References

1. E. Ott, H.M. Spurlin, M.W. Grafflin, *Cellulose Part II 2th ed.*, Interscience Publishers, New York (1963).
2. K.W. Britt (Ed.), *Handbook of Pulp and Paper Technology 2th ed.*, Van Nostrand Reinhold Company, New York (1970).
3. R.E. Kirk and D.F. Othmer (Ed.), *Encyclopaedia of Chemical Technology*, The Interscience Encyclopedia, Inc., New York (1949).
4. R.L. Whistler, J.N. BeMiller, *Industrial Gums, Polysaccharides and Their Derivatives* 2th Ed, Academic Press, London (1973).
5. M. Grayson (Ed.), *Encyclopaedia of Chemical Technology Vol. 5*, John Wiley & Sons, New York (1979).
6. H.C.W. Foerst and H. Buchholz-Meisenheimer (Eds), *Ullmans Encyklopädie der technischen Chemie*, Urban & Schwarzenberg, Berlin (1970).
7. AQUALON CO, U.S. Patent US 4948-430-A (1990).
8. J.A. Clark, *Pulp Technology and Treatment for Paper*, Miller Freeman Publications, Inc., San Fransisco (1978).
9. J.P. Casey (Ed.), *Pulp and Paper, Chemistry and Chemical Technology 2th ed. vol. IV*, John Wiley & Sons, New York (1983).
10. G.J. Fleer, M.A. Cohen Stuart, J.M.H.M. Scheutjens, T. Cosgrove, B. Vincent, *Polymers at Interfaces*, Chapman & Hall, London (1993).
11. H.G.M. van de Steeg, M.A. Cohen Stuart, A. de Keizer, and B.H. Bijsterbosch, *Langmuir* **8** (1992) 2538.
12. J.C. Dijt, *Kinetics of Polymer Adsorption, Desorption and Exchange*, Ph. D. thesis, Wageningen Agricultural University (1993).
13. J. Meadows, P.A. Williams, M.J. Garvey, R.A. Harrop, and G.O. Phillips, *Colloids Surfaces* **32** (1988) 275.
14. P.F. Luckham and J. Klein, *J. Chem. Soc. Faraday Trans. 1* **80** (1984) 865.
15. A.N. Semenov and J.F. Joanny, *J. Phys. II (Paris)* **5** (1995) 859.
16. H.A. Kramers, *Physica* **7** (1940) 284.

Chapter 2

Persistence length of carboxymethyl cellulose as evaluated from size exclusion chromatography and potentiometric titrations

Abstract

The intrinsic persistence length of carboxymethyl cellulose (CMC) is determined by size exclusion chromatography in combination with multiangle laser light scattering (SEC-MALLS) as well as from potentiometric titrations. Samples with degree of substitution (ds) ranging from 0.75 to 1.25 were investigated. The relation between molar mass M and radius of gyration R_g as obtained by SEC-MALLS is determined in 0.02, 0.1, and 0.2 mol l^{-1} $NaNO_3$. Using the electrostatic wormlike chain theory a bare (intrinsic) persistence length L_{p0} of CMC is assessed at 16 nm, irrespective of the degree of substitution. A somewhat lower value (12 nm) is obtained when Odijk's theory for the description of polyelectrolyte dimensions is applied. The difference between L_{p0} assessed from both models is discussed briefly. Potentiometric titrations were carried out in NaCl solutions (ranging from 0.01 to 1 mol l^{-1}). From the titrations the radius of the CMC backbone was obtained by application of the model of a uniformly charged cylinder. The radius amounts to 0.95 nm for CMC ds=0.75, and increases to 1.15 nm for CMC with ds=1.25. The pK for the intrinsic dissociation constant of the carboxyl groups (i.e., at zero degree of dissociation) amounted to 3.2. L_{p0} was also deduced from potentiometric titrations. A model developed by Katchalsky and Lifson, which relates the dissociation behaviour of a polyelectrolyte to the stiffness of its chain, was applied to CMC. From analyses of the potentiometric titrations an intrinsic persistence length of 6 nm was deduced. The difference between L_{p0} assessed from SEC-MALLS and potentiometric titrations is discussed briefly.

2.1 Introduction

The macroscopic properties of polymer solutions are determined by microscopic (molecular) parameters. For example, the viscosity of a polymer solution is influenced by the molar mass of the polymer, its radius of gyration R_g, and its flexibility. Thickening properties of a polymer solution are related to the rigidity of the polymer backbone, which is characterised by the persistence length L_p. Knowledge of microscopic parameters is also

required to describe polymer adsorption at a solid-liquid interface. A general finding is the preferential adsorption of molecules with large molar mass [1], implying that for a polydisperse polymer the composition of the mixture, i.e. the molar mass distribution, is of importance. Although at present little is known about the influence of the local stiffness on the adsorption properties of polymers, its effect on solution properties is generally recognised. Polymers having equal molar masses will be more extended when they have a higher persistence length. The larger extension manifests itself in a slower motion (diffusion) of the molecule.

For many years, viscometry has been applied as a method to determine the persistence length. By measuring the concentration dependence of the viscosity the intrinsic viscosity of a polymer solution is determined. The intrinsic viscosity is related to the dimension and the molar mass of a polymer. As the former is related to the persistence length, viscometry enables determination of L_p. However, the molar mass must be determined separately (e.g. by means of the Mark-Houwink relation). Furthermore, quantities obtained by viscometry are averages. So, for (nearly) monodisperse polymers, viscometry might be used as a suitable technique to determine L_p, but if applied to polydisperse samples, additional information about the molar mass distribution is needed. Information about the distribution is accessible from size exclusion chromatography (SEC). In this technique, which is also known as gel permeation chromatography (GPC), molecules are separated according to their size, yielding the molar mass distribution.

Cellulose derivatives are well known for their thickening properties. In this connection, most cellulose compounds are characterised by a persistence length in the range 5-20 nm [2]. In this chapter we focus on the determination of the persistence length of carboxymethyl cellulose (CMC). As CMC is a polyelectrolyte, repulsion between charged segments will affect the persistence length; i.e., L_p will depend on the degree of dissociation of the polyelectrolyte and on the salt concentration. Hence, the parameter that characterises the local stiffness originating from the polymer backbone is the magnitude of L_p in the absence of any electrostatic effects. It is denoted as the bare or intrinsic persistence length L_{p0}. From viscometry Rinaudo [3] obtained L_{p0}=5.0 nm at high salt concentrations where electrostatic interactions are negligible. L_p was calculated from the intrinsic viscosity according to Yamakawa et al. [4]. The same value is obtained by Kamide et al. [5] who applied various theoretical models (Benoit-Doty [6] and Yamakawa [4]) to published viscosity data. A value of 8.5 nm was obtained by Lavrenko et al. [7] from viscosity measurements of CMC solutions in mixtures of water and cadoxen (Cd^{2+}-ethylenediamine complex).

We used size exclusion chromatography in combination with multiangle laser light scattering (SEC-MALLS) to determine the intrinsic persistence length of CMC. The use of light scattering as the detection method for SEC offers the possibility of analysing a polymer sample in terms of the distribution of molar mass and molecular dimensions. The latter is represented by the radius of gyration R_g. The advantage of light scattering over viscometry as

the detection method is that with the former M_w and R_g are determined in an absolute way, i.e. unlike viscometry where a calibration is needed to relate the detector signal to the required quantity. CMC samples with different numbers of substituted groups per monomeric unit (degree of substitution, ds from 0.75 to 1.25) and molar masses (30 to 10^3 kg mol^{-1}) were prepared from the same cellulose source by a homogeneous substitution reaction. By this approach a well-defined set of CMC samples is obtained so that the relation between M and chain dimensions can be determined as a function of ds over a broad range of M. The relation between M and R_g reveals information about the persistence length of a polymer. The electrostatic wormlike chain model is used to analyse this relation and to determine L_{p0}. In our analysis we follow the approach proposed by Davis [8]. Besides Davis's approach we will discuss our data in terms of Odijk's model [9]. The two approaches yield somewhat different values for the intrinsic persistence length. We will discuss briefly the difference between L_{p0} value as obtained from the two models.

In addition to SEC-MALLS the CMC samples were characterised with respect to their dissociation behaviour by means of potentiometric titrations. The latter were interpreted in terms of a uniformly charged cylinder, which serves as a model for a CMC molecule on a length scale of L_p. In this way information about the cross-section of the CMC backbone is obtained. Potentiometric titrations were also used to estimate L_{p0}. For this purpose a modified analysis proposed by Katchalsky [10-12] was used.

2.2 Theoretical background

2.2.1 The electrostatic wormlike chain model

First, the theory describing the dimensions of a (charged) wormlike polyelectrolyte will be briefly outlined. For a more comprehensive review of the electrostatic wormlike chain model, the reader is referred to a paper by Davis [8].

The size of a macromolecule in solution is often characterised by its radius of gyration R_g. This quantity measures the root-mean-square distance of the segments from the centre of mass of the chain. For a linear flexible homopolymer, R_g can be calculated to a first approximation from the random walk model. Dividing the chain into N_K segments each of length L_K (Kuhn length), the radius of gyration for a random chain is given by [13]:

$$R_{g0}^2 = \frac{1}{6} N_K L_K^2 \qquad (2.1)$$

In the random walk model, excluded volume effects are neglected; R_g calculated in this manner is called the unperturbed radius of gyration R_{g0}. Equation 2.1 only applies to a chain for which the length scale L_p of the local stiffness is small compared to the length of the stretched chain (contour length L_c). More generally, the unperturbed dimension of a chain can

be expressed in terms of L_p and L_c by means of the wormlike chain model [14a]:

$$R_{g0}^2 = L_c^2\left[\frac{1}{3}x - x^2 + 2x^3 - 2x^4\left(1 - e^{-1/x}\right)\right] \qquad (2.2)$$

where $x=L_p/L_c$. Equation 2.2 is quite general, it includes (as limits) both the Gaussian coil and the rigid rod. It can be shown that for long wormlike chains $L_K=2L_p$ [14a]. Then the limit corresponding to the former (equation 2.1) is recovered when $L_c/L_p >> 1$. For the other limit (rigid rod) the equation approaches $R_{g0}^2=\frac{1}{12}L_c^2$, namely when $L_c/L_p << 1$ (i.e. if bending between adjacent segments is not allowed). In equation 2.2 the mutual interaction between polymer segments and interaction between segment and solvent is not taken into account (i.e. excluded volume effects are neglected). Excluded volume effects are taken into account by introducing a linear expansion factor (α_{ev}). The dimension of the chain is written as a product of the unperturbed dimension and the chain expansion factor: $R_g=\alpha_{ev}R_{g0}$. Since R_g is composed of two parameters (R_{g0} and α_{ev}), this approach is often denoted as the two-parameter model. In general, α_{ev} depends on the molar mass, the local stiffness of the chain, and the solvent quality. In a θ-solvent α_{ev} is unity; the mutual attraction between segments is exactly counterbalanced by repulsive interactions between segments. If repulsion between segments prevails a chain will adopt a more extended conformation: $\alpha_{ev} > 1$. The linear expansion factor is a function of the excluded volume parameter z. We will use the expression for α_{ev} derived by Yamakawa and Tanaka [14b]:

$$\alpha_{ev}(z) = \left[0.541 + 0.459\left(1 + 6.04z\right)^{0.46}\right]^{\frac{1}{2}} \qquad (2.3)$$

The expression for z in case of a wormlike chain is [15]

$$z = \frac{1}{32}\left(\frac{3}{\pi L_p^2}\right)^{\frac{3}{2}}\left(\frac{L_c}{L_p}\right)^{\frac{1}{2}}\beta\,\frac{3}{4}\,K(N_K) \qquad (2.4)$$

where β is the excluded volume per Kuhn segment. The function $K(N_K)$ reflects the probability of contact between Kuhn segments in a chain. For a Gaussian chain ($N_K >> 1$) $K(N_K)$ has a limiting value 4/3, so that $3/4K(N_K)=1$. For $N_K \rightarrow 0$ $K(N_K)$ becomes zero [15,16]. Hence, the function $K(N_K)$ takes into account that shorter or stiffer chains have a more rodlike conformation with a lower probability of Kuhn segments making contact, thereby reducing the excluded volume. Values of $K(N_K)$ may be obtained from tables given in ref. [15].

Repulsion between charged sites causes the chain to stretch. Unlike the case of uncharged polymers, the value of L_p is not solely determined by the primary structure of the polymer backbone but is also affected by repulsion between charged sites. Hence, for polyelectrolytes the charge density on the chain and the electrolyte concentration will also

affect α_{ev}. It was shown by Odijk [17], and by Fixman and Skolnick [18], that L_{p0} and the electrostatic contribution to the persistence length L_{pe} are additive: $L_p=L_{p0}+L_{pe}$. The electrostatic persistence length depends on the charge density of the polymer chain, which in turn is determined by the average distance L_q between two charges along the chain. Often, the charge density is discussed in terms of a dimensionless charge density parameter λ, which is defined as the ratio L_B/L_q, where L_B is the Bjerrum length given by

$$L_B = \frac{q_e^2}{4\pi\varepsilon_0\varepsilon_r kT} \tag{2.5}$$

Here, q_e represents the charge of an electron, is ε_0 the dielectric permittivity of vacuum, ε_r is the relative permittivity of the solvent, and kT has its usual meaning. In water at 298 K, L_B has a value of 0.714 nm. As will be discussed below, the presence of counterions close to the chain reduces the charge density on the chain causing the effective charge density parameter λ_{eff} to be different from λ. In the Odijk-Skolnick-Fixman (OFS) approach [17,18] the electrostatic persistence length L_{pe} is given in terms of the effective magnitude of the charge density parameter. Their expression for L_{pe} reads

$$L_{pe} = \frac{1}{4L_B\kappa^2}\lambda_{eff}^2 \tag{2.6}$$

where κ is the inverse Debye-Hückel screening length defined by $\kappa^2=2F^2c_{salt}/\varepsilon_0\varepsilon_rRT$ for a 1-1 electrolyte with concentration c_{salt}. In evaluating λ_{eff}, we will calculate its magnitude taking CMC as a line charge (according to Odijk [9,19]) and from the Poisson-Boltzmann equation for a uniformly charged cylinder [8,16].

In the wormlike chain model for polyelectrolytes the excluded volume β is composed of three additive contributions: a hard-core β_c, an electrostatic contribution β_e, and an attractive β_a. Treating a Kuhn segment as a cylinder, the hard-core contribution is the excluded volume of a cylinder with radius a and length $2L_p$: $\beta_c=\pi a(2L_p)^2$ [16]. The second contribution is the repulsive interaction between the charges on the chain. Fixman and Skolnick [20] derived the following expression for the electrostatic contribution β_e:

$$\beta_e = \frac{8L_p^2}{\kappa}R(\omega) \tag{2.7}$$

with ω being a parameter depending on λ_{eff}, the radius of the cylinder, and the ionic strength [16,20]. For our analyses values of $R(\omega)$ are interpolated from tabulated values given in ref.[20]. The third contribution, the attractive interaction between two segments, is calculated from the condition that β equals zero at the salt concentration for which θ-conditions are reached ($-\beta_a=\beta_c+\beta_e$). For CMC the salt concentration for θ-conditions is not known precisely.

Davis estimated it at 5 mol l^{-1} NaCl. In our calculations we will use his value for β_a (-197 nm^3 [8]). The electrostatic wormlike theory will be applied to the relation between M (or equivalently L_c) and R_g as inferred from SEC-MALLS. Assuming some value for L_{p0} , R_{g0} is calculated from M by using equation 2.2. The electrostatic persistence length is calculated with equation 2.6. The chain expansion factor is a function of L_p and L_c. R_g is calculated from R_{g0} and equations 2.3 and 4. At a given salt concentration L_{p0} is the only unknown parameter; it is used as a fitting parameter to match R_g, as inferred from SEC-MALLS with its calculated values.

As mentioned before, the charge density of a polyelectrolyte is affected by the presence of counterions. The charges on the chain will give rise to an electric field around the polyelectrolyte. Assuming a uniform distribution of the charged groups, a uniformly charged cylinder may serve as an adequate model for the evaluation of the local electrostatic field. This implies that the polymer backbone is supposed to be rigid on a length scale of several monomers. Within this model, the electrical potential ψ as a function of the distance from the chain can be obtained by solving the Poisson-Boltzmann (PB) equation for a charged cylinder. Besides the surface potential, the solution of the PB equation also provides the relation between λ and λ_{eff} [16]. Manning [21] derived an analytical expression for ψ by solving the PB equation in its linearised form, i.e. putting $\sinh \psi \approx \psi$. According to Manning's results $\lambda_{eff}=L_B/L_c=\lambda$ for $\lambda \leq 1$. However, when L_c becomes less than L_B ($\lambda>1$), the effective spacing length equals L_B: counterions become very strongly localised around the polyelectrolyte, reducing λ_{eff} to 1. Without the approximation $\sinh(\psi)\approx\psi$, the PB equation cannot be solved analytically. However, its solution can be obtained numerically. As in the counterion condensation theory, numerical calculations show that λ_{eff} may be lower than λ. The dependence, however, is quite different [22,23] from that proposed by Manning. In this chapter λ_{eff} was calculated numerically from the full PB equation. The numerical procedure is described in the appendix.

2.2.2 Dissociation of a polyacid in solution

In general the dissociation of a weak polyacid satisfies the equation

$$pH = pK_a + \log\left(\frac{\alpha}{1-\alpha}\right) = pK_0 + \Delta pK + \log\left(\frac{\alpha}{1-\alpha}\right) \qquad (2.8)$$

where α is the fraction of dissociated acid groups (degree of ionisation), pK_a is the negative logarithm of the effective (α-dependent) dissociation constant, and pK_0 is the negative the logarithm of the intrinsic dissociation constant (pK_a at $\alpha=0$). The ΔpK term represents shift in the dissociation constant that is due to the change in the electrostatic free energy G_e of a polyacid upon variation in the number n of negatively charged groups [10]:

$$\Delta pK = \frac{0.4343}{kT}\left(\frac{\partial G_e}{\partial n}\right)_\kappa \tag{2.9}$$

In the following, two models are treated which relate structural parameters to the dissociation behaviour of a polyelectrolyte in aqueous solution. Both consider the work that is needed to displace an electrical charge (a proton) from the surface of the polyacid to a distance far from the surface. This work is directly related to the difference in electrical potential at the surface of the polymer (ψ_0) and the potential at infinity (ψ_∞). Since ψ_∞ is zero by definition, ($\partial G_e/\partial n$) effectively equals $q_e\psi_0$. In the first model it assumed that the chain may be considered as a uniformly charged cylinder. A schematic picture of the cylindrical model is given in figure 2.1. The potential difference ψ_0 can be divided into two contributions. At a given degree of dissociation the charge density of the polyacid is represented by its corresponding value of λ. In the region from a to a+d the cylinder is surrounded by a Stern layer with a thickness d, which represents the distance of closest approach of ions to the polyacid surface. At distance $r > d$ the cylinder is surrounded by a diffuse double layer. The potential at a+d (ψ_{a+d}) is calculated from the numerical integration of the full PB-equation for a charged cylinder. Then, the potential difference over the Stern layer, the second contribution to ψ_0, is calculated from λ and the expression for the capacitance of a cylindrical capacitor. Considering CMC as a cylinder with radius a, the expression for ΔpK is [24]

$$\Delta pK = \frac{0.4343 q_e \psi_{a+d}}{kT} + \frac{0.8686 q_e^2 ds}{4\pi\varepsilon_0\varepsilon_r L_B kT}\,\alpha \ln\left(\frac{a+d}{a}\right) \tag{2.10}$$

In the previous paragraph the chain is considered as a uniformly charged cylinder, i.e. the presence of discrete charges is ignored. The localisation of the charges is explicitly taken into account by Katchalsky and Lifson [11]. They calculated ΔpK from the change in the electrostatic free energy that takes place upon charging an uncharged polymer. The process of

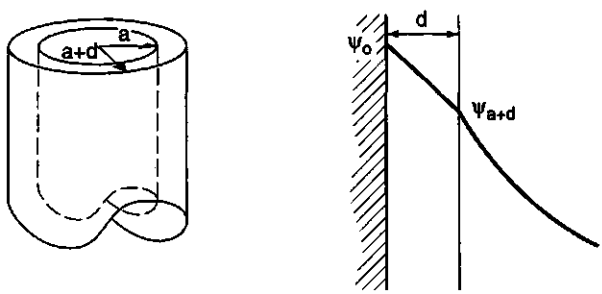

Figure 2.1 Schematic picture of a uniformly charged cylinder used as a model for a CMC molecule on a length scale L_p.

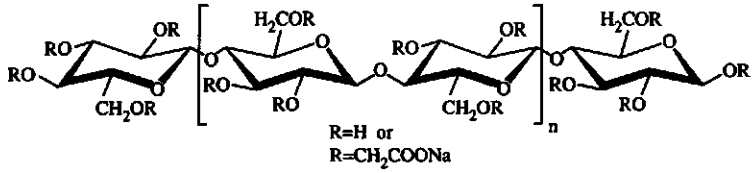

Figure 2.2 Repeating unit of carboxymethyl cellulose. The D-glucose units are linked through β-1,4 bonds. R represents a hydrogen-atom (unsubstituted hydroxyl group) or a CH_2COONa group (substituted hydroxyl group).

charging is divided into three steps, each contributing to G_e. Charges interact by a screened Debye-Hückel potential [~ exp(-κr)/r]. They are assumed to be equally spaced along the chain at a distance r. Summing up the contributions to G_e (stretching of the chain, buildup of the ionic atmosphere around charged groups, and averaging of exp(-κr)/r for all pairs of interacting charges over all chain configurations), they obtained for the variation in the electrostatic free energy [11,12]

$$\left(\frac{\partial G_e}{\partial n}\right)_\kappa = \frac{2nq_e^2}{4\pi\varepsilon_0\varepsilon_r h}\left[\ln(1+x) - \alpha\frac{(k_i - k_0)}{2k}\frac{x}{1+x}\right]$$
$$x = \frac{6h}{\kappa h_0^2} \qquad (2.11)$$

In equation 2.11, h_0 and h represent the end-to-end distance of the uncharged polymer and the chain carrying n charges respectively. The number of monomers in a Kuhn segment is denoted by k. For the uncharged chain, $k=k_0$. Charging the chain will increase the number of monomers per Kuhn segment eventually to k_i (the number of monomers in a Kuhn segment when the chain is fully dissociated). It is assumed that k is a linear function of α: $k=(1-\alpha)k_0+\alpha k_i$ [10]. Katchalsky and Lifson choose for h_0 the expression of the unperturbed end-to-end distance of a Gaussian coil. In their discussion about the choice for h, they state that the expression for a fully stretched molecule is applicable. In our opinion it is more realistic to consider the charged chain also as a random coil. Equation 2.11 can be used as the startingpoint for the determination of the intrinsic persistence length of a polyelectrolyte.

Let the number of monomeric units in the chain be denoted by Z, then the number of charges on a CMC molecule equals $n=\alpha Zds$. As we assume a Gaussian coil conformation for both the uncharged and the charged molecule, the expressions for the mean square of the end-to-end distances are represented by $h_0^2=Zk_0b^2$ and $h^2=Zkb^2$, respectively, where b is the length of a monomer (0.515 nm [26]). In the model of Katchalsky and Lifson excluded volume effects are not taken into account. The increase in the coil dimension, i.e. the swelling of the chain, is accounted for by increasing the number of monomers in a Kuhn segment from k_0 to k. Upon inserting these expressions for h_0 and h into equation 2.11, an expression is

obtained that contains a chain length dependence. In the limit of long chains ($Z\rightarrow\infty$, $x\rightarrow 0$) the Z-dependence vanishes. Realising that the ratio $(k-k_0)/k$ equals L_{pe}/L_p and $k_0 b = L_{K0} = 2L_{p0}$ for a long wormlike chain, combination of equation 11 with equations 2.8 and 2.9 yields

$$pH = pK_0 + \log\left(\frac{\alpha}{1-\alpha}\right) + \frac{0.4343}{kT}\frac{12q_e^2 ds}{4\pi\varepsilon_0\varepsilon_r\kappa 2L_{p0}b}\alpha\left(1-\frac{1}{2}\frac{L_{pe}}{L_{p0}+L_{pe}}\right) \qquad (2.12)$$

where we have used only the first term in the Taylor expansions for $\ln(1+x)$ and $x/(1+x)$, which amounts to x for both. The above equation offers the possibility of deducing the intrinsic persistence length from titration experiments.

2.3 Experimental

2.3.1 Materials

Carboxymethyl cellulose was prepared by Akzo Nobel by reaction of cellulose (cotton linters), NaOH, and sodium monochloro acetate ($ClCH_2COONa$). During the reaction hydrogen atoms at the glucose hydroxyl groups are substituted by CH_2COONa. The average number of substituents per glucose monomer is denoted as the degree of substitution (ds). In this way CMCs were prepared with ds=0.75, 0.91, 0.99 and 1.25 respectively, these samples will be denoted hereafter as samples 1. Subsequently, portions of these samples were treated with H_2O_2 in ethanolic slurry to cause random cleavage between glucose units, thereby reducing the molar mass. Adding different amounts of H_2O_2 yielded series with decreasing chain length (samples 2 to 5). In this way a set of 20 CMCs was prepared, varying in degree of substitution and chain length (see table 2.1). In figure 2.2 the structure of CMC is given schematically. The monomeric unit of the CMC backbone consists of D-glucose residues which are linked through β-1,4 bonds. Depending on whether the hydroxyl groups in a glucose unit are un-, mono-, di-, or tri-substituted, CMC molecules can in principle consist of eight different monomers. The composition of the CMC samples was analysed after acidic hydrolysis by HPLC and quantified from the refractive index by taking the peak height surface area in a 100 % analysis, yielding consistent and accurate data.

2.3.2 SEC-MALLS

CMC solutions were prepared in the following way. First, CMC was dissolved in demineralised water. While dissolving, the samples were gently shaken for 16 hours at room temperature. Then sodium nitrate solution was added to obtain an electrolyte concentration of 0.02 or 0.1 mol l^{-1}. In potentiometric titrations NaCl was used as the electrolyte; but as NaCl damages the SEC equipment, $NaNO_3$ was used as the electrolyte for SEC. The addition of salt

was carried out after dissolution in order to minimise the presence of aggregated, not fully dissolved, CMC. It was found that when CMC was dissolved in the presence of salt, the solution contained "scaly" particles, which is an indication that CMC was not dissolved completely. The presence of these particles was more pronounced at high salt concentrations.

The concentration of the polymer solutions was chosen such that the overlap concentration was not exceeded, but it was large enough to obtain a measurable light scattering intensity. The following concentrations were used: 1000, 1000, 1500, 2000 and 2500 mg l^{-1} for samples 1-5, respectively. Prior to the SEC measurements the samples were filtered over a 0.45 μm hydrophilic Durapore (Millipore) membrane.

The samples were eluted at pH=7 on a set of three columns (G6000 PW, G5000 PW, and G3000 PW) with a flow rate of about 0.95 ml min^{-1}. No adsorption on the columns was observed (i.e. all injected polymer was eluted from the columns). A DAWN-DSP-F (Wyatt Technology Co.) MALLS detector was used to obtain on-line determination of the absolute molar mass and the radius of gyration of each fraction eluting. The light scattering signal was detected simultaneously at eleven scattering angles θ, ranging from 44 to 151°. After the scattering intensity was converted into a Raleigh ratio R, the quantity Kc/R was plotted against $\sin^2(\theta/2)$ (Zimmplot [25]). In Kc/R, c is the CMC concentration and K is an optical constant given by $4\pi^2 n_D^2 (\partial n_D/\partial c)^2/\lambda_0^2 N_{AV}$, where λ_0 is the wavelength of the He-Ne laser, n_D is the refractive index of the solvent, and $\partial n_D/\partial c$ is the refractive index increment of CMC in aqueous solution. For each fraction, M and R_g were determined from the intercept and initial slope of the Zimmplot. The CMC concentration in eluted fractions was small enough for extrapolation to zero concentration to be of no concern. Both SEC and MALLS detection were carried out at 298 K.

Determination of the concentration was performed with an interferometric refractive index detector (Optilab Wyatt Technology Co). The refractive index increment ($\partial n_D/\partial c$) at a wavelength of 632.8 nm was established at 0.163 ml g^{-1}. The value of the refractive index increment did not depend on either ds or on M_w.

2.3.3 Potentiometric titrations

Sample preparation for titration experiments was nearly identical to the procedure in the SEC experiments. After CMC was dissolved, NaCl solution was added to obtain an electrolyte concentration in the range 0.01 to 1 mol l^{-1}. The polymer concentration was 1000 mg l^{-1} in all titration experiments. Initially, the solution pH was set to pH=3 by addition of 0.1 mol l^{-1} HCl. Flushing with purified nitrogen was used to remove any carbon dioxide from the solutions. Titrations to pH=11 (by addition of carbonate-free 0.1 mol l^{-1} KOH) and back-titrations to pH=3 were carried out in an atmosphere of purified nitrogen. For pH readings a glass electrode was used. The electrode was calibrated at 298 K against nine buffer

solutions in the pH range 3-11.

Titrations were performed at 298 K using a Schott Titronic T200 autoburette. The dosage of titrant was calculated on the basis of the change in pH according to previous additions. The minimum dosage volume was 0.01 ml; at the most, 0.5 ml of titrant was added. After addition of titrant, pH readings (accuracy of 0.001 pH units) were carried out. When the change in pH after addition was less than 0.01 pH unit per minute, new titrant was added. In general the time between two additions was about 5 minutes.

The proton release (forward titration with KOH) or take up (backward titration with HCl) by the polyelectrolyte were calculated from the dosage and the pH change due to the addition of titrant. The relation between the activity, calculated from the pH, and the concentration of free protons or hydroxyl ions was established through titration of HCl solution with the same electrolyte concentration as in the polyelectrolyte titration. The degree of ionisation (α) in the forward titration was calculated as

$$\alpha = \frac{c_p V ds - (n_{max} - n_r)}{c_p V ds} \tag{2.13}$$

where n_r is the amount of protons released from the polyelectrolyte, n_{max} is the maximum release of protons, c_p is the monomer concentration, and V is the volume in which the polyelectrolyte was dissolved. The value of n_{max} is identified as the point where the release of protons is zero; i.e., addition of base only leads to a change in pH. In the case of the back titration α is calculated from the proton uptake n_u by the polyelectrolyte: $\alpha=1-n_u/(c_p V ds)$.

2.4 Results and discussion

2.4.1 CMC monomer composition

The monomer composition of the samples as obtained from HPLC analysis is presented in figure 2.3. Spurlin [26] proposed a model from which the monomer composition of a sample with known ds can be calculated. In this model a relative rate constant is assigned to each of the hydroxyl groups at the 2-,3- or 6-position. It is assumed that substitution reaction occurs at random (i.e. all hydroxyl groups are equally accessible during the reaction) and that relative reactivities of the three hydroxyl groups do not change with ds. Furthermore, it is assumed that the rate of the substitution reaction is first order in the concentration of the hydroxyl groups. Calculated mole fractions based on Spurlin's statistical model are also included in figure 2.3 (solid curves). Mole fractions are calculated using the relative reaction rate constants that Reuben et al. [27] obtained from the monomer composition of a series of CMC samples having ds ranging from 0.55 to 2.17. Their calculated reaction rate constants were in good agreement with data reported in the literature (see for instance Buytenhuys and Bonn [28]). Therefore we assume that their data relate to a random distribution of the

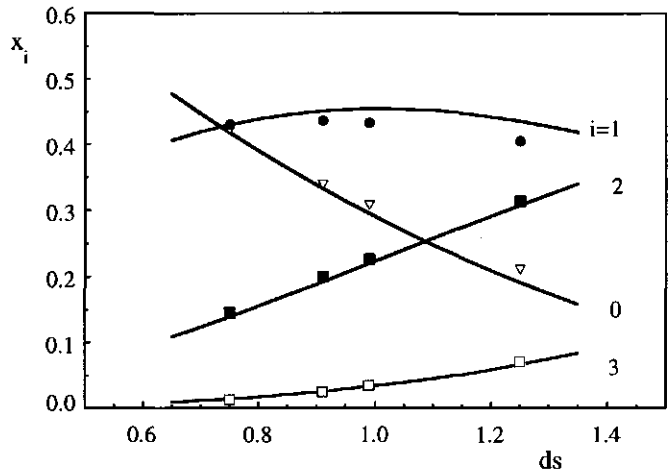

Figure 2.3 Composition of CMC samples by mole fraction (x_i) of substituted monomers. Numbers indicate the number of substituted hydroxyl groups per monomeric unit: i=0 (∇) unsubstituted glucose unit, i=1 (●) mono-, i=2 (■) di-, and i=3 (□) trisubstituted glucose. Solid curves refer to calculated mole fractions corresponding to a random distribution of the substituents. Compositions relate to samples 1. Identical results were obtained for the depolymerised samples.

substituents along the polymer chain. Ma et al. [29] determined for CMC ranging in ds from 0.51 to 1.55 the average number monomers that are present in blocks consisting of either substituted or unsubstituted glucose units by means of enzymatic cleavage. From their analysis they conclude that the crystalline structure of cellulose is almost completely absent in CMC and that substitution of glucose units takes place at random. Their analysis reveals that the average number of unsubstituted glucose units ranges from 3.4 to 1.8 monomeric units for ds=0.51 and 1.55, respectively. With respect to the monomeric composition the analysis in ref. 29 only yields information about the mole fraction of unsubstituted glucose units. In correspondence with random substitution, good agreement was found with Reuben for the amount of unsubstituted glucose. As can be seen from figure 2.3, the agreement between the monomer composition based on a random distribution of substituents and the composition of our samples is good. On the basis of this agreement, we conclude that in our samples the substituents are also randomly distributed over the polymer chain and that the number of long unsubstituted regions is negligible.

2.4.2 SEC-MALLS

In figure 2.4 some typical results for the molar mass distribution as obtained from SEC-MALLS measurements are given. The figure shows the differential molar mass distribution (DMMD) for CMC samples 1 and 4 with ds=0.91 determined in 0.02 and

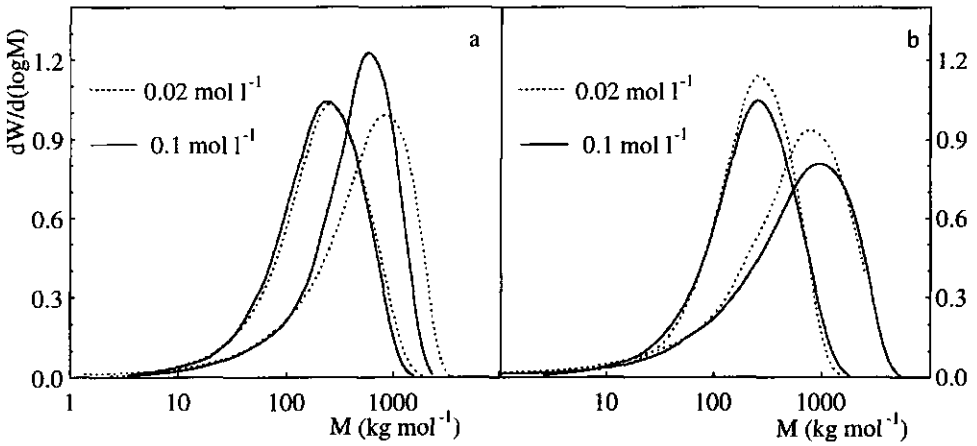

Figure 2.4 Molar mass distribution of two CMC samples (ds=0.91) M_w=1100 and 210 kg mol^{-1}. Distributions were determined in solutions containing 0.02 or 0.1 mol l^{-1} $NaNO_3$ (indicated in figure). Distributions were obtained (a) using a linear Zimmplot, (b) using a quadratic extrapolation to zero scattering angle.

0.1 mol l^{-1} $NaNO_3$ solution respectively. The molar mass distribution given in figure 2.4a is determined using a linear extrapolation of the scattered intensity to zero angle. Figure 2.4b shows the result when a non-linear extrapolation (second-order polynomial) is used. DMMD is determined by differentiation of the cumulative mass fraction W(M) (i.e. the mass fraction of molecules having a molecular mass less then M) with respect to the logarithm of M [30]. For a detailed description of the DMMD calculation from SEC data, the reader is referred to Shortt [30]. As the chain charge density, and accordingly ds, affects the size of polyelectrolytes, a distribution of ds within a sample would influence the fractionation. However, since all CMC samples were prepared under well-defined experimental conditions, probably the distribution in ds is negligible. Comparing the molar mass distributions for the high M sample (sample 1) as obtained at different electrolyte concentrations, it can be seen that the distribution depends significantly on the method of extrapolation to zero scattering angle. As can be seen from figure 2.4a the distribution for sample 1 is shifted to higher M at 0.02 mol l^{-1} $NaNO_3$ if a linear extrapolation is used. Since the distribution is an intrinsic property of a sample, it is not likely to depend on the electrolyte concentration. It might be supposed that a high electrolyte concentration leads to some aggregation of CMC. If the chains contain long regions of unsubstituted or slightly substituted monomers, screening of the few charges allows the formation of H-bridges between those regions which may lead to formation of aggregates. Since aggregates have a higher molar mass, their presence will shift the distribution to higher M compared to an unaggregated solution (i.e. a solution containing less electrolyte). However, the experiments show the opposite trend, indicating that the lack

of coincidence of distributions in 0.02 and 0.1 mol l^{-1} $NaNO_3$ is probably not caused by the presence of aggregates. Upon using a non-linear extrapolation method, both distributions of the low and high M sample are shifted to higher molar mass. The position of the peak in the DMMD now gives better agreement between distributions obtained in 0.02 and 0.1 mol l^{-1} $NaNO_3$. Though better agreement is found between the distributions, a discrepancy still exists between those obtained at low and at high salt concentrations. Complete treatment of the data requires a statistical treatment (F-test [31]) of the Zimmplot of each eluted fraction to decide which extrapolation method (linear or non-linear) should be used. Unfortunately, our set-up does not provide for such a treatment. We used the position of the peak as criterion to

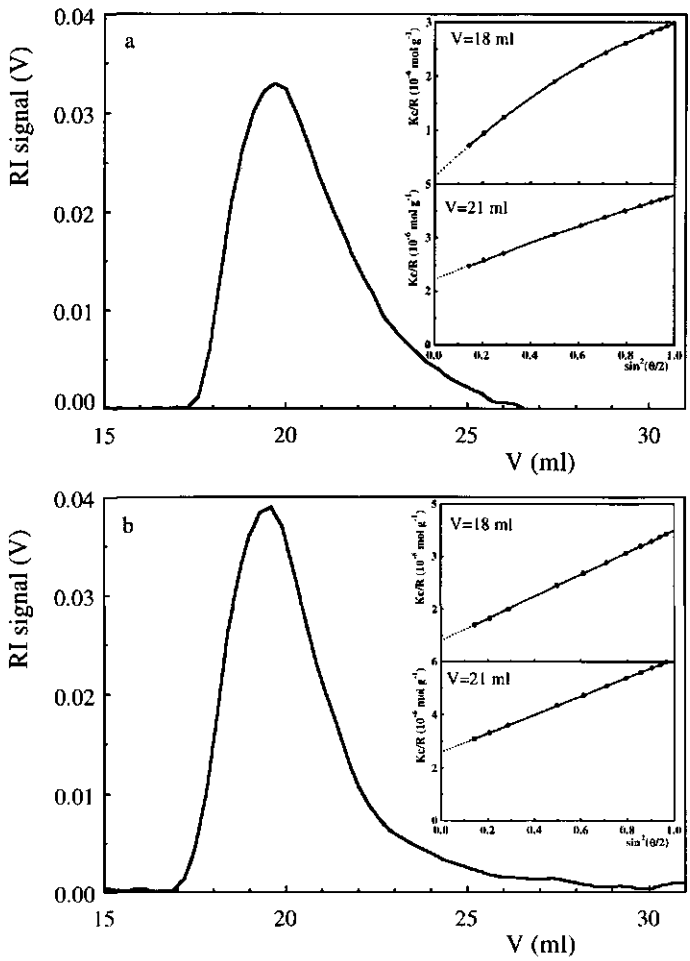

Figure 2.5 Elution chromatogram of CMC ds=0.91 (sample 1) as obtained in (a) 0.1 mol l^{-1} $NaNO_3$ and (b) 0.02 mol l^{-1} $NaNO_3$. The insets show Zimmplots at two elution volumes (indicated in figures). The molar mass of an eluted fraction decreases with increasing elution volume.

Table 2.1 Average molar masses M_w and M_n, polydispersity index M_w/M_n, and radius of gyration R_g of (depolymerised) CMC-samples with different degrees of substitution. Samples indicated by number 1 were not depolymerised. Numbers 2 up to 5 refer to samples which were depolymerised (by H_2O_2) to an increasing extent. Due to the low light scattering intensity, characterisation of some depolymerised samples could not be carried out.

ds	sample number	M_n (kg mol^{-1})	M_w (kg mol^{-1})	M_w/M_n	R_g(nm)
0.75	1	520	1100	2.2	140
	2	310	740	2.4	100
	3	200	400	2.0	75
	4	85	190	2.2	40
	5	45	120	2.7	30
0.91	1	510	1100	2.2	140
	2	470	880	1.9	120
	3	170	340	2.0	55
	4	100	210	2.1	40
0.99	1	570	1200	2.0	160
	2	390	640	1.6	95
	3	80	180	2.3	35
1.25	1	370	1100	2.9	130
	2	330	660	2.0	90
	3	200	380	1.9	50
	4	120	210	1.8	30

decide which extrapolation method is suitable for our data treatment. The other non-depolymerised CMC samples as well as the depolymerised fractions 2 and 3 show the same behaviour as presented in figure 2.4. Measurements on samples 4 and 5 (ds=0.75, 0.99 and 1.25) were not carried out in 0.02 mol l^{-1} $NaNO_3$.

The lack of coincidence of the molar mass distributions is caused by a downward curvature in Kc/R at low angles ($\theta < 75^o$). The downward curvature is illustrated by figure 2.5, where we give the concentration (measured by the index of refraction) of eluted fractions (CMC ds=0.91, sample 1) as a function of the elution volume. Insets show Zimmplots at different volumes in the chromatograms. As can be seen, nonlinearity is observed in 0.1 as well as in 0.02 mol l^{-1} $NaNO_3$, the effect being most pronounced in 0.1 mol l^{-1} $NaNO_3$ for CMC of high M. As the molar mass is obtained from the intercept of a Zimmplot (i.e. extrapolation of Kc/R to zero scattering angle), the magnitude of M is rather sensitive to the extrapolation method. The origin of the non-linear Zimmplots is not clear. As we stated in the previous paragraph, the presence of aggregated CMC is not likely the cause of the non-linearity. We will touch upon this in the following paragraphs. It was already pointed out by Mijnlieff et al. [32] that the use of a linear extrapolation may lead to errors in the determination of the molar mass of a polymer sample from static light scattering.

From figure 2.4 it can also be seen that the molar mass distribution is quite narrow, almost as narrow as in condensation polymers. The polydispersity is represented by the ratio,

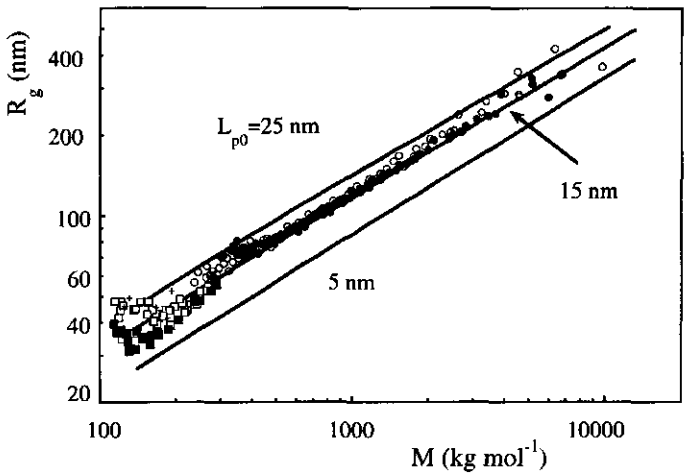

Figure 2.6 Relation between the radius of gyration R_g and molar mass M for CMC ds=0.91 SEC fractions. Samples with different degree of polymerisation are indicated by different symbols: ○: sample 1, ●: 2, □: 3, ■: 4. Solid curves refer to calculations using the wormlike chain model [8]. Different values for intrinsic persistence length L_{p0} are indicated.

M_w/M_n (table 2.1), where M_w and M_n are the weight and number molar mass averages respectively. The polydispersity ratio for the nondepolymerised samples (about 2.5) is comparable to M_w/M_n for cotton linters cellulose, which is about 2.2 [33], but is substantially lower as compared to the majority of commercial CMC types derived from wood cellulose, which show polydispersities from 6 to even 20. All results refer to experiments carried out in 0.1 mol l^{-1} $NaNO_3$. The molar mass of the nondepolymerised samples does not vary significantly with ds. As CMC samples with different ds were prepared from the same starting material, samples 1 do not differ much in average molar mass.

For CMC samples 1 to 4 with ds=0.91, but differing in average molar mass, the relation between radius of gyration and molar mass in 0.1 mol l^{-1} $NaNO_3$ is represented in figure 2.6. Both M and R_g were determined using by the non-linear extrapolation. For samples 5 the intensity of the scattered light was too low, so that characterisation could not be carried out accurately. Owing to the small proportions of the scattering molecules the low scattered intensity exhibited a high noise level. The samples supplement each other rather satisfactorily. Similar observations where made for samples with other ds. The full curves in the figure represent the relation between R_g and M calculated according to the wormlike chain model [8]. The relation was calculated using different values for the intrinsic persistence length. As can be seen from this figure, the value of L_{p0} lies in the range 15-25 nm.

A graph similar to figure 2.6 is presented in figure 2.7. In this figure the radius of gyration is given as a function of the number of Kuhn segments, N_K ($=L_c/2L_p$), for CMC

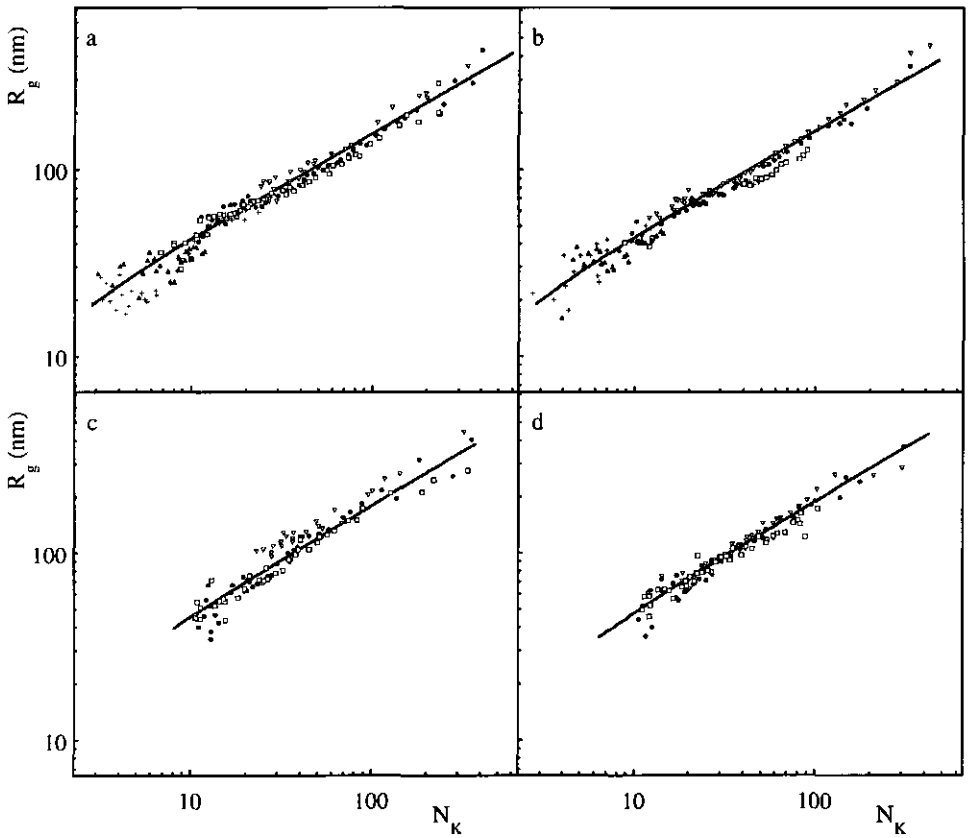

Figure 2.7 Relation between number of Kuhn segments N_K and radius of gyration R_g for CMC in a 1-1 electrolyte solution. Samples with different degrees of polymerisation are indicated by different symbols: ∇: sample 1, ●: 2, □: 3, ▲: 4, +:5. (a): CMC ds=0.75 in 0.1 mol l^{-1} $NaNO_3$, (b): ds=1.25 in 0.1 mol l^{-1} $NaNO_3$, (c): ds=0.75 in 0.02 mol l^{-1} $NaNO_3$, (d): ds=1.25 in 0.02 mol l^{-1} $NaNO_3$. The solid curves were calculated according to the wormlike chain model [8] using L_{p0}=17 nm for 0.02 mol l^{-1} $NaNO_3$ and L_{p0}=15 nm for 0.1 mol l^{-1} electrolyte respectively.

ds=0.75 and ds=1.25. The two upper figures relate to CMC samples 1-5 in 0.1 mol l^{-1} $NaNO_3$, the lower to CMC samples 1-3 in 0.02 mol l^{-1} $NaNO_3$. The relation between R_g and N_K calculated with the wormlike chain theory according to Davis is represented by the solid curves. Best fits to the experimental data were obtained when L_{p0} was set to 17 nm (0.02 mol l^{-1} $NaNO_3$) or 15 nm (0.1 mol l^{-1}), irrespective of ds. A linear relation between $\log N_K$ and $\log R_g$ is observed in 0.1 mol l^{-1} $NaNO_3$ for $N_K > 10$, indicating a random coil conformation of the polymer. For $N_K < 10$ the local rodlike character of the chain shows up from a slight downward bending of the curves. In 0.02 mol l^{-1} $NaNO_3$ the downward bending is observed for $N_K < 20$, illustrating that the local stiffness of the chain increases with

decreasing salt concentration. The increase of L_p with decreasing salt concentration also shows up from the dependence of R_g on the concentration $NaNO_3$. In 0.02 mol l^{-1} $NaNO_3$, R_g is found to be larger than in 0.1 mol l^{-1} $NaNO_3$. The electrolyte dependence of R_g can be deduced from figure 2.7, it is shown more clearly in figure 2.8. In figure 2.8 the relation between R_g and N_K is shown for CMC samples 2 with ds from 0.75 to 1.25 for two electrolyte concentrations. The lower curve (0.2 mol l^{-1} electrolyte) refers to CMC sample 1 (ds=0.91). The solution preparation of this sample was somewhat different from previous preparations. After dissolution in demineralised water, KOH solution was added to a concentration of 0.1 mol l^{-1}. After 15 hours the sample was brought to pH=7 with HNO_3, yielding a total $NaNO_3$ concentration of 0.2 mol l^{-1}. This treatment, carried out in a nitrogen atmosphere, was applied because in a highly basic medium hydroxyl groups are dissociated. The dissociation disrupts any hydrogen bonds between cellulose chains, the bond-breaking process being enhanced by the repulsion between charged groups. Thus, in a basic medium the presence of aggregated CMC is unlikely. The linear region in the relation between the radius of gyration and molar mass often obeys the scaling law $R_g \sim M^{\nu} \sim N_K^{\nu}$. The exponent ν contains information about structural properties of a macromolecule (e.g. if a chain is a random coil or is branched) and the solvent quality [34,35]. Schulz and Burchard [35] determined ν for CMC in 0.1 mol l^{-1} NaCl by viscometry and found ν=0.28. From this low number and determination of the hydrodynamic radius they concluded that their solutions contained a considerable amount of

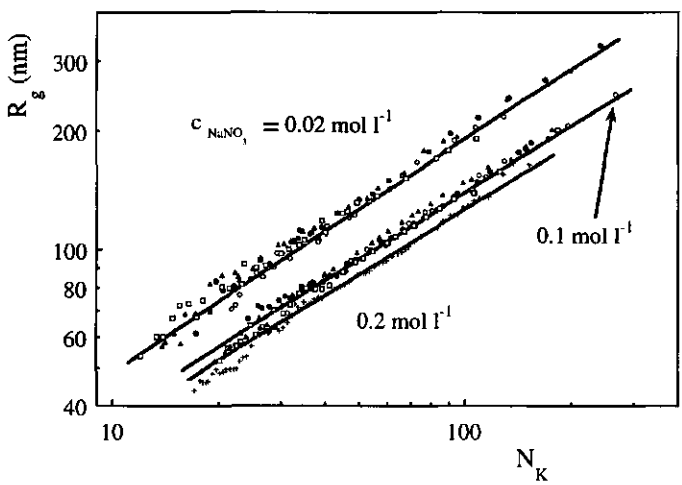

Figure 2.8 Relation between number of Kuhn segments (N_K) and radius of gyration (R_g) for CMC in a 1-1 electrolyte solution (indicated in figure). Different symbols refer to samples 2 differing in ds: ○: ds=0.75, ●: ds=0.91, □: ds=0.99, ▲: ds=1.25, and +: sample 1 ds=0.91. The solid curves were calculated according to the wormlike chain model [8] using L_{p0}=17 nm for 0.02 mol l^{-1} $NaNO_3$ and L_{p0}=15 nm for 0.1 and 0.2 mol l^{-1} electrolyte respectively. For the treatment of sample 1 in 0.2 mol l^{-1} $NaNO_3$ see text.

aggregated CMC. In 0.1 mol l^{-1} KOH we obtain ν=0.59, which indicates that in KOH CMC may be considered as a linear polymer in a good solvent [34,35]. As ν is rather sensitive to the presence of aggregates [35] we conclude that in 0.1 mol l^{-1} KOH no (or very little) aggregated CMC is present. The value ν=0.59 is preserved in the $NaNO_3$ solutions. Hence, measurements carried out in 0.1 mol l^{-1} KOH yield results similar to those in 0.1 mol l^{-1} $NaNO_3$, albeit the sample is somewhat degraded (depolymerised) due to presence of oxygen in the alkaline solution. The agreement between ν in KOH and in $NaNO_3$ indicates that aggregated CMC can be present in our samples, only in very small amounts. Cryotransmission electron microscopy supports this conclusion.

As can be seen from figure 2.8, the degree of substitution does not affect the relation between R_g and N_K. This is found in 0.1 as well as in 0.02 mol l^{-1} $NaNO_3$. According to Odijk, the lack of dependence on ds indicates that at pH=7, CMC is above the threshold for the onset of counterion condensation. At pH=7, CMC is fully dissociated. Indeed, the value of the effective charge parameter λ exceeds the limiting value 1 for a fully dissociated CMC sample with ds=0.75 (λ=ds L_B/L_{mon}=1.04, if L_{mon}=0.52 nm [26] is substituted for the monomeric length of a glucose unit). Since the other samples have even higher charge densities, they will also exceed the limiting value. In evaluating R_g versus N_K, we used the wormlike chain model as presented by Davis [8]. Therefore, in the calculation of λ_{eff} we used the model of the uniformly charged cylinder rather than putting λ_{eff}=1 for all experiments. The calculated relation between R_g and N_K for the three electrolyte concentrations is represented by the solid curves. As will be shown in the discussion regarding the potentiometric titrations, the cross-section of the cylinder shows a dependence on the degree of substitution. Taking into account this ds dependence, the calculated relation between R_g and N_K shows only a slight dependence on the degree of substitution. For this reason, in figure 2.8 only the calculated curve for ds=0.91 is shown. Any dependence on ds is too weak to be deduced from our experimental data. Qualitatively, both Davis's and Odijk's approaches give good agreement with experimental results. Best fits to the experimental data were obtained using Davis's approach when L_{p0} was set to 17 nm (0.02 mol l^{-1} $NaNO_3$) or 15 nm (0.1 and 0.2 mol l^{-1}). The bare persistence length using the Odijk model is lower than that obtained by the Davis model. Using Odijk's approach we obtain 13 nm (0.02 mol l^{-1} $NaNO_3$) and 11 nm (0.1 and 0.2 mol l^{-1} $NaNO_3$), respectively.

Why do the models of Odijk and Davis give different quantitative results? As stated before, in Odijk's approach the function $K(N_K)$ in equation 2.4 is assumed to have a fixed value of 4/3, which is valid for chains consisting of many (infinite number of) Kuhn segments. For our samples with the highest molar mass, this assumption is reasonable. For L_p=15 nm (L_K=30 nm) the number of Kuhn segments for CMC with L_c=10000 nm equals 330 and $K(N_K)$ reaches the value of about 1.2 [16]. Thus, for the highest molar mass fraction the error in Odijk's assumption is small. However for L_c=600 nm, which covers the range of the

Table 2.2 Electrostatic excluded volume β_e, expansion factor α_{ev}, and electrostatic persistence length L_{pe} calculated for CMC with ds=0.75 according to the models of Odijk [9] and Davis [8]. The intrinsic persistence length is set at 13 nm. In Odijk's approach $K(N_K)$ has a constant value of 1.33.

c_{NaCl} (mol l^{-1})	N_K	$K(N_K)$	β_e (nm^3)		α_{ev}		L_{pe} (nm)	
			Odijk	Davis	Odijk	Davis	Odijk	Davis
0.02	20	0.839	10700	8000	1.237	1.141	1.62	1.37
0.02	100	1.171	10700	8000	1.293	1.297	1.62	1.37
0.02	200	1.223	10700	8000	1.455	1.370	1.62	1.37
0.10	20	0.839	3100	1900	1.156	1.053	0.32	0.31
0.10	100	1.171	3100	1900	1.198	1.132	0.32	0.31
0.10	200	1.223	3100	1900	1.324	1.224	0.32	0.31

smallest molecules, $K(N_K)$ reaches a value of only about 0.8. Consequently, putting $K(N_K)$ equal to the limiting value is only valid for a fraction of our samples. With $K(N_K)=4/3$, z is overestimated, yielding a higher number for the expansion factor. Furthermore, the assumption that a CMC molecule may be considered as a line charge tends to overestimate the electrical contribution to the excluded volume. This can be demonstrated as follows. The parameter ω in equation 2.7 reads [16]

$$\omega = \frac{2\pi}{L_B\kappa}\left(\frac{\lambda_{eff}}{a\kappa K_1(a\kappa)}\right)^2 e^{-2a\kappa} \qquad (2.14)$$

with K_1 a modified Bessel function of the second kind of order one. For values $\omega > 5$ in equation 2.7, $R(\omega)$ may be approximated by $\pi / 4\,(\ln(\omega) + \ln(2) + \gamma - \frac{1}{2})$. Inserting $\ln(\omega)$ into the expression for $R(\omega)$ and putting $a\kappa$ equal to zero, Odijk obtains the following expression for the electrostatic excluded volume:

$$\beta_e = 2\pi L_p^2 \frac{1}{\kappa}\left(-\ln(L_B\kappa) + \ln(\lambda_{eff}^2) + \ln(4\pi) + \gamma - \frac{1}{2}\right) \qquad (2.15)$$

where γ is Euler's constant (0.57722). The expression between brackets divided by κ, is Odijk's effective diameter of a Kuhn segment [9]. To evaluate the consequences of setting $a\kappa$ to zero and taking $K(N_K)=4/3$, we have calculated the expansion factor α for different situations, i.e. different chain lengths and ds values, at two different salt concentrations, using both Odijk's and Davis's approach. The results are presented in tables 2.2 and 2.3. The data illustrate that the assumption of setting $K(N_K)$ at 1.33 is not legitimate for the whole range of the CMC samples. Comparing the electrostatic excluded volume according to the two models, it can be seen that Odijk's approach in general gives a higher number than Davis's. The origin for this difference lies in the fact that in Odijk's expression for $\ln(\omega)$ all terms including $a\kappa$ are omitted. It can be shown that the sum of these terms has a negative value, so

Table 2.3 Electrostatic excluded volume β_e, expansion factor α_{ev}, and electrostatic persistence length L_{pe} calculated for CMC with ds=1.25 according to the models of Odijk [9] and Davis [8]. The intrinsic persistence length is set at 13 nm. In Odijk's approach $K(N_K)$ has a constant value of 1.33.

c_{NaCl} (mol l^{-1})	N_K	$K(N_K)$	β_e (nm^3)		α_{ev}		L_{pe} (nm)	
			Odijk	Davis	Odijk	Davis	Odijk	Davis
0.02	20	0.839	10700	12200	1.237	1.157	1.62	2.93
0.02	100	1.171	10700	12200	1.293	1.323	1.62	2.93
0.02	200	1.223	10700	12200	1.455	1.401	1.62	2.93
0.10	20	0.839	3100	2900	1.156	1.073	0.32	0.77
0.10	100	1.171	3100	2900	1.198	1.173	0.32	0.77
0.10	200	1.223	3100	2900	1.324	1.144	0.32	0.77

Davis arrives at a lower value for $R(\omega)$ than does Odijk.

The magnitude of β_e is also determined by the magnitude of L_p (see equation 2.7), which in turn depends on λ_{eff} (equation 2.6). In figure 2.9 the relation between λ_{eff} and the bare charge density λ is given for two salt concentrations (0.02 and 0.1 mol l^{-1}) and two CMC radii (0.95 and 1.15 nm). These radii correspond, as will be elucidated in the following section, to CMC with ds=0.75 and 1.25, respectively. The relation according to Manning's counterion condensation theory is also included (dotted line). If fully dissociated, CMC with ds values of 0.75 and 1.25 corresponds to λ=1.1 and 1.7 respectively. At λ=1.1 the difference between λ_{eff}

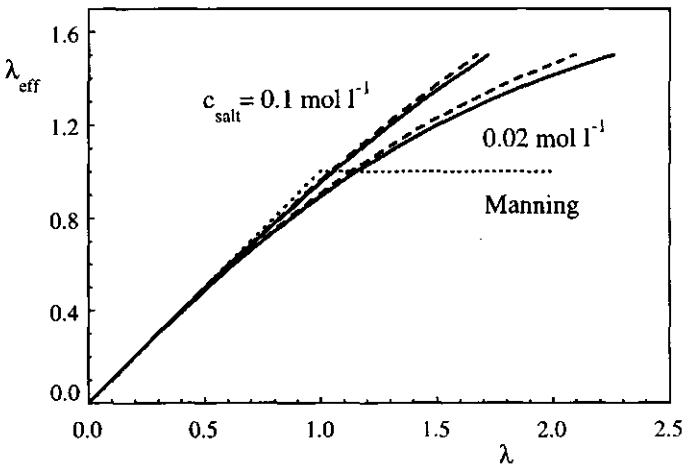

Figure 2.9 Effective charge parameter λ_{eff} as a function of the charge parameter λ. The curves were calculated from the numerical solution of the Poisson-Boltzmann equation for a charged cylinder. The dashed curves refer to a cylinder with radius 0.95 nm, the solid curves with radius 1.15 nm. The relation according to Manning's counterion condensation theory is also included (dotted curve).

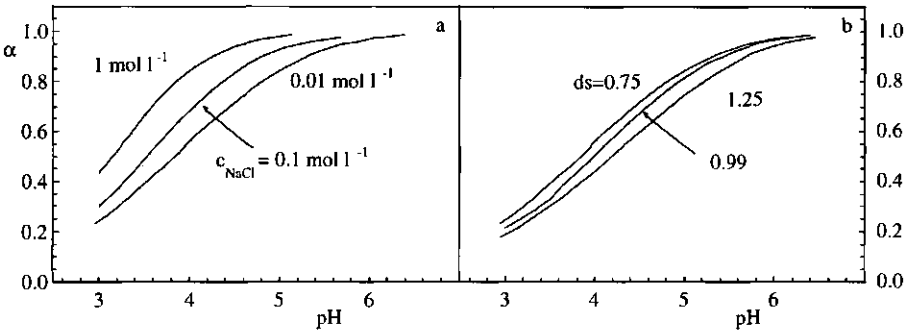

Figure 2.10 pH-dependence of degree of dissociation (α) of CMC in aqueous solution. Figure a shows the dependence on the electrolyte concentration (NaCl) for CMC ds=0.75, figure b shows the dependence on ds at fixed electrolyte concentration (0.01 mol l^{-1} NaCl).

according to Manning and λ_{eff} as obtained from the solution of the full PB equation is rather small, consequently L_{pe} according to Odijk and Davis is comparable (see table 2.2). As in Odijk's approach the line charge approximation tends to overestimate β_e, its value for CMC ds=0.75 calculated according to Davis will be lower as compared to Odijk's approach. In the case of CMC ds=1.25 (λ=1.7) λ_{eff} is higher when calculated from the PB equation, thereby increasing the value of β_e compared to CMC ds=0.75. So for CMC ds=1.25 the difference in β_e between both approaches is less than for CMC ds=0.75. As shown in table 2.3 β_e according to Davis may even exceed β_e as obtained by Odijk. In the evaluation of our data we used L_{p0} as an adjustable parameter, L_{p0} was not determined in an absolute manner (e.g. by neutron scattering). Therefore we cannot judge on basis of the outcome of our analysis which approach (Davis's or Odijks) is most suitable to determine L_{p0} from the relation between R_g and M. With respect to electrostatics differences between Davis and Odijk will show up when $\lambda > 1$ (see figure 2.9). So, the electrostatic persistence length of chains having a low charge density can be described adequately according to Odijk (see, for instance, de Nooy et al. [36]). As the Davis model gives a more complete description of electrostatics and takes molecular properties (such as chain length and cross-section of the molecule) into account we prefer to use Davis's approach for highly charged polyelectrolytes.

2.4.3 Potentiometric titrations

In figure 2.10 the dissociation behaviour of CMC in aqueous solution is given as a function of electrolyte concentration and ds. The curves refer to experiments that were carried out with sample 1. Titrations with depolymerised CMCs (up to sample 5) yield identical results; i.e., no dependence on the molar mass has been observed. As can be seen, the dissociation behaviour clearly exhibits polyelectrolyte character. As an increasing number of

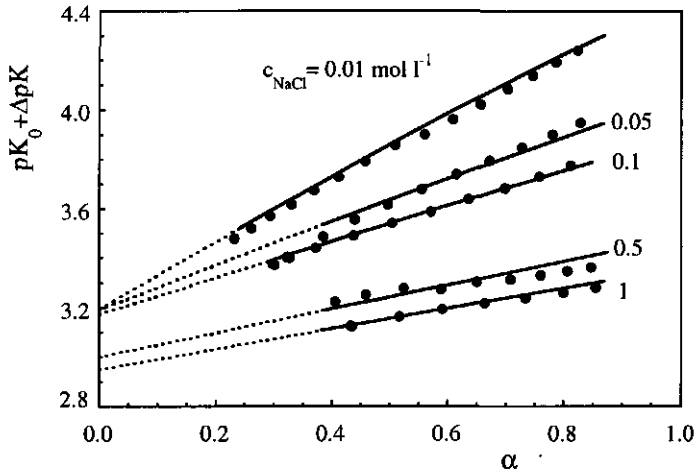

Figure 2.11 Apparent dissociation constant ($pK_a=pK_0+\Delta pK$) for CMC ds=0.75 as a function of the degree of dissociation α at various NaCl concentrations (indicated in figure). The solid curves were calculated from the numerical solution of the Poisson-Boltzmann equation for a charged cylinder (radius 0.95 nm).

carboxylic groups becomes dissociated, the increased charge on the chain will hamper subsequent dissociation of nondissociated groups. Salt screens the charges, thereby facilitating the dissociation, which results in a higher degree of dissociation at a given pH. As the dissociation is affected by the charge density, the dissociation constant (and thereby pK_a) will not be a constant but will depend on α. This dependence is demonstrated in figure 2.11 for CMC (ds=0.75) at various NaCl concentrations. As expected, pK_a is not constant but increases with charge density. The polyelectrolyte character is most pronounced at low salt concentrations but is still noticeable at high concentration (1 mol l^{-1}).

The solid curves refer to pK_a as calculated from the uniformly charged cylinder model (equation 2.10). In all calculations, the radius of a solvated Na^+ ion (0.25 nm [37,40]) was chosen for the thickness of the Stern layer. Best fits to the experimental data were obtained using a cylinder radius of 0.95 nm, irrespective of the salt concentration. Extrapolating the calculations to α=0 yields the pK of the intrinsic dissociation constant (pK_0) of about 3.2 (see table 2.4), which is in reasonable agreement with data reported in the literature (3.0 [38], 3.4, 3.3 [41]). The procedure used for the sample with ds=0.75 was also applied to the other samples. It turns out that pK_0 does not depend on ds, provided the radius of the cylinder is taken as dependent on ds. Best fits were obtained using radii of 1.0, 1.05 and 1.15 nm for CMC with ds=0.91, 0.99 and 1.25, respectively. This is not unreasonable, taking into account the size of a carboxymethyl group (which is estimated at 0.4 nm from atomic bond lengths) and the diameter of a glucose unit (0.50 nm [26]). Furthermore, the effective diameter of a cellulose chain is somewhat larger because a glucose molecule does not lie in line but is

Table 2.4 Intrinsic dissociation constant pK_0 for CMC in solutions with different NaCl concentrations. The radii of the chain and pK_0 were obtained by fitting experimental data to the model of a uniformly charged cylinder.

ds	radius (nm)	electrolyte concentration (mol l^{-1})				
		0.01	0.05	0.1	0.5	1
0.75	0.95	3.22	3.22	3.20	3.00	2.95
0.91	1.00	3.18	3.20	3.20	3.00	2.94
0.99	1.05	3.15	3.22	3.18	3.00	2.95
1.25	1.15	3.23	3.30	3.20	3.10	2.95

somewhat tilted with respect to its adjacent unit. Our conclusion that the cross-section of CMC increases with ds is corroborated by findings reported by Koda et al. [39]. From density measurements on aqueous CMC (ds=0.56 to 2.85) solutions with different concentrations they calculated the apparent molar volume. Extrapolation of these data to zero concentration yields the partial molar volume of CMC. The measurements in ref. 39 reveal an increase of the partial molar volume with increasing ds, which is related to an increase in the dimension of the CMC backbone.

At this point we should comment on the validity of smearing-out discrete charges on the chain to a uniformly charged cylinder. Concerning the rigidity of the backbone the assumption is probably reasonable. As inferred from the SEC measurements, the polymer has a bare persistence length of about 15 nm. Hence, the polymer can be considered as stiff over a length of about 30 monomers. Thus, the assumption of a rigid backbone (cylinder) holds, even at high salt concentrations. An indication for the validity of the smearing-out can be

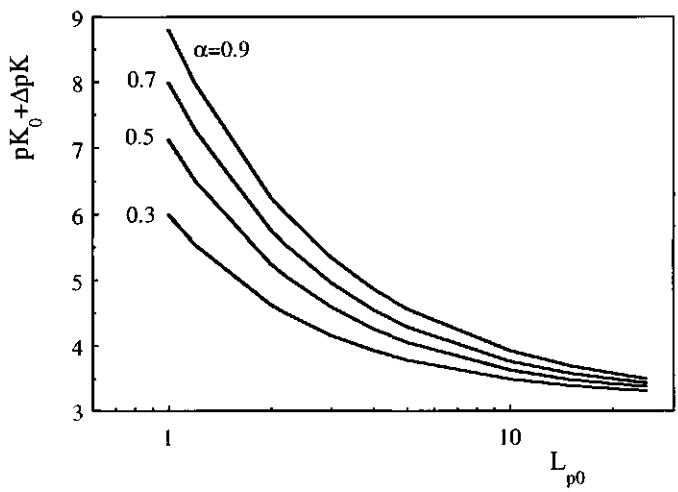

Figure 2.12 Calculated dissociation constant ($pK_0+\Delta pK$) of CMC ds=0.75 in 0.01 mol l^{-1} 1-1 electrolyte as a function of L_{p0}. The curves were calculated for different degrees of dissociation α, using equation 2.12.

Table 2.5 Intrinsic persistence length determined according to Katchalsky et al.[10,11]. For all ds values, pK_0 was set to 3.2.

ds	L_{p0}
0.75	5.6±0.3
0.91	5.9±0.5
0.99	6.1±0.2
1.25	6.1±0.3

found by comparing the distance between two charges with the radius of the Debye-Hückel ionic atmosphere around a charge on the chain. As stated by Muroga et al. [40] the assumption of a uniform charge density is not valid if the distance between two charged groups exceeds κ^{-1}. For CMC, the average distance between to charged groups is given by $b/(\alpha ds)$. So the assumption maintains its validity as long as the degree of dissociation exceeds a critical value given by $\alpha_c=b/(\kappa^{-1}ds)$. In 0.01 mol l^{-1} NaCl (κ^{-1}=3.04 nm) α_c=0.23 and 0.14 for ds=0.75 and 1.25, respectively. At this salt concentration experimental values always exceeds the critical value. In 0.05 mol l^{-1} NaCl α_c is situated at 0.51 (ds=0.75) and 0.30 (ds=1.25), whilst α_c has values 0.71 (ds=0.75) to 0.43 (ds=1.25) in 0.1 mol l^{-1} salt solution. For the higher salt concentrations the average distance is always below κ^{-1} (even for α=1) so the second requirement is not fulfilled. Thus we conclude that the model gives a satisfactory description of the polyelectrolyte if the salt concentration is in the range 0.01-0.1 mol l^{-1}. Indeed, the model predicts values of pK_0 in 0.5 and 1 mol l^{-1}, which differs considerable from the results obtained at lower salt concentrations.

In figure 2.12 for CMC ds=0.75, $pK_0+\Delta pK$ calculated according to equation 2.12 (hence, by introducing discrete charges) is given as a function of the intrinsic persistence length at four degrees of ionisation (α=0.3, 0.5, 0.7 and 0.9) in 0.01 mol l^{-1} NaCl. The curves demonstrate that ΔpK decreases with the intrinsic persistence length. The origin of this dependence lies in the fact that in the model of Lifson and Katchalsky the charges are situated at the end of a Kuhn segment. As the intrinsic persistence length takes larger values, the average distance between two charges increases, eventually becoming infinite when L_{p0} goes to infinity. At very large separation the charges will not feel each other and, just like the change in electrostatic free energy, ΔpK converges to zero. From titration experiments, $pK_0+\Delta pK$ at different degrees of dissociation is known. By comparing $pK_0+\Delta pK$ calculated for fixed L_{p0}, but at different degrees of dissociation, with experiment, the plots in figure 2.12 can be used to determine the value of L_{p0}. The result is given in table 2.5, from which it can be seen that L_{p0} is not affected by ds. This result was also obtained from the SEC analyses. The magnitude of L_{p0}, however, is substantially lower than according to the SEC analyses.

In figure 2.13 $pK_0+\Delta pK$ is given as a function of the degree of ionisation for CMC with

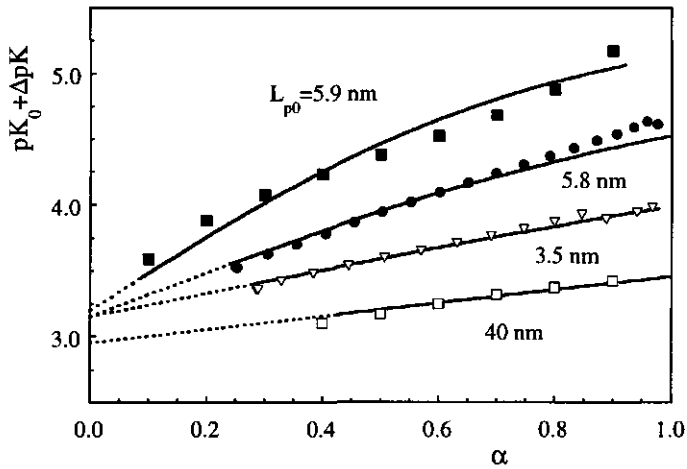

Figure 2.13 Apparent dissociation constant $pK_0+\Delta pK$ as a function of degree of dissociation for CMC ds=0.91 in 0.01 and 0.1 mol l^{-1} NaCl (symbols: ● and ▽). The top curve (■) relates to CMC ds=0.81 in salt free solution [41]. The lowest curve (□) is for xanthan in 0.01 mol l^{-1} NaCl [24]. Solid curves were calculated according to Katchalsky et al. [10,11]. Best fits for L_{p0} are indicated in the figure.

ds=0.91 in 0.01 and 0.1 mol l^{-1} NaCl. Solid curves refer to the calculated ΔpK using equation 2.12 and taking L_{p0}=5.8 and 3.5 nm for CMC in 0.01 and 0.1 mol l^{-1} NaCl, respectively. For comparison, data on xanthan in 0.01 mol l^{-1} NaCl [24] and CMC with ds=0.81 in a salt free solution [41] are also given. The low salt concentration data are derived from CMC titrations in the absence of salt, so the ionic strength (0.002 mol l^{-1}) is determined by the sodium counterions of NaCMC only. The figure shows that for the lower salt concentrations (0.002 and 0.01 mol l^{-1} NaCl) L_{p0} is predicted rather satisfactorily by Katchalsky's model at 5.8 nm. The same value is obtained at 0.05 mol l^{-1} NaCl. For higher salt concentrations L_{p0} is strongly underestimated. In 0.1 mol l^{-1} NaCl the model yields a value of L_{p0}=3.5 nm, lower values were found at the highest salt concentrations. Probably this is caused by the assumption that charge interactions are accounted for by a Debye-Hückel interaction, which is not justified at high salt concentrations. For xanthan the best fit is obtained for L_{p0}=40 nm, which corresponds to the bare persistence length of the single-helix conformation of the polymer.

In the derivation of equation 2.11, Katchalsky and Lifson evaluated the average value of $\exp(-\kappa r)/r$ using the probability function for the random configuration of an uncharged chain. For a charged molecule, compact configurations will occur less frequently than according to the random-chain probability function, which is a crude approximation. Thus, in the approach of Katchalsky and Lifson the electrostatic energy is overestimated. This probably causes a lower value of L_{p0} to be obtained with their model. Since the charges are assumed to be situated at the end of a Kuhn segment, increasing L_{p0} tends to decrease the electrostatic

energy. Evaluating L_{p0} from potentiometric titrations by Katchalsky's theory cannot be considered an absolute method. However, it can be used satisfactorily for a reasonable estimate of L_{p0}.

2.5 Conclusions

CMC is characterised by means of SEC-MALLS and potentiometric titrations. The former method reveals information about the distribution of the molar mass and radius of gyration. R_g increases with decreasing electrolyte concentration, reflecting the influence of electrostatics on the dimension of the polymer. The dimension of CMC is described adequately with the electrostatic wormlike chain model [8]. Applying the model to the relation between M and R_g, an intrinsic persistence length of 16 nm is found for CMC, indicating that CMC can be seen as a semiflexible polymer. Odijk's model [9] for the swelling of polyelectrolytes yields a somewhat lower value (L_{p0}≈12 nm). The Davis theory [8] gives a more complete description as it takes molecular properties (such as the length and cross-section of the molecule) into account.

SEC-MALLS experiments show that the degree of substitution does not affect the relation between M and R_g. According to Odijk, this observation points to counterion condensation. Counterion condensation occurs when the average distance between charges becomes less than 0.714 nm (Bjerrum length); then counterions are kept in proximity of the polymer chain so that the effective average distance between charges equals the Bjerrum length. For fully dissociated CMC counterion condensation takes place for ds > 0.75. In the Davis theory the charge density on the chain is calculated from the Poisson-Boltzmann equation for a uniformly charged cylinder. So, the relation between M and R_g is expected to depend on ds. However, if the cross-section of the backbone is taken into account, only a slight dependence is observed.

The cross-section (radius) of the CMC backbone was obtained from potentiometric titrations. Considering CMC as a uniformly charged cylinder radii of 0.95 nm (ds=0.75) up to 1.15 nm (ds=1.25) were inferred. L_{p0} was also obtained from potentiometric titrations. Using Katchalsky's theory for the dissociation behaviour as a function of the polymer stiffness, L_{p0} was found to be 5.9 nm. That this value is lower than that inferred from SEC-MALLS is probably due to an incorrect evaluation of the electrostatic energy in the Katchalsky model. Potentiometric titrations are experimentally less time consuming than SEC-MALLS. However, taking into account the shortcomings of the model, they can serve at best as a suitable technique to estimate the persistence length of a polyelectrolyte.

Appendix

In this appendix we briefly outline the numerical procedure that is used for the calculation of the potential at the surface of the polyelectrolyte chain. Besides ψ_0 the procedure yields the relation between λ and λ_{eff}.

The Poisson-Boltzmann equation for a uniformly charged cylinder in a solution containing a 1-1 electrolyte in cylindrical coordinates, is given by:

$$\frac{1}{r}\frac{d}{dr}\,r\,\frac{d\psi(r)}{dr} = -\frac{\rho_c(r)}{\varepsilon_0\varepsilon_r} = \kappa^2\,\frac{kT}{q_e}\sinh\left(\frac{q_e}{kT}\,\psi(r)\right) \qquad \text{(A1)}$$

where $\rho_c(r)$ is the charge density and $\psi(r)$ is the potential at distance r from the centre of the cylinder. Introducing dimensionless variables u and Ψ by means of $u=\ln(\kappa^{-1}r)$ and $\Psi=q_e\psi/kT$, we can rewrite equation A1 in terms of two coupled first-order differential equations [23]:

$$\frac{d\Psi}{du} = z \qquad \text{(A2)}$$

$$\frac{dz}{du} = e^{2u}\sinh(\Psi) \qquad \text{(A3)}$$

This set of equations is solved numerically via a fourth order Fehlberg algorithm [42]. First, a value is assigned to λ_{eff}. The integration starts at large distance from the surface (ρ=10) where the linearised solution (i.e. at large distance where Ψ is low) of the PB equation is applicable:

$$\Psi = 2\lambda_{eff}K_0(e^u)/(a+d)\kappa K_1((a+d)\kappa) \qquad \text{(A4)}$$

$$z = -2\lambda_{eff}e^uK_1(e^u)/(a+d)\kappa K_1((a+d)\kappa) \qquad \text{(A5)}$$

K_0 and K_1 are modified Bessel functions of the second kind of order zero and one, respectively. The integration proceeds inward until r=a+d. The potential and charge density at the boundary of the Stern layer are determined as $\psi_{a+d}=\psi$ and $\lambda=-½z$ at r=a+d [23]. In this manner, one can calculate for each value of λ_{eff} a corresponding value of λ, so that a relation between the charge density and the effective charge density is obtained. Finally, with the use of the expression for the capacitance of a cylindrical capacitor, the surface potential is calculated, yielding the relation between λ and ψ_0.

References

1. G.J. Fleer, M.A. Cohen Stuart, J.M.H.M. Scheutjens, T. Cosgrove, B. Vincent, *Polymers at Interfaces*, Chapman & Hall, London (1993) p 33.

2. M. Yalpani, *Polysaccharides*, Elsevier, New York (1988).
3. M. Rinaudo, In *Cellulose and cellulose derivatives: Physico-chemical aspects and industrial applications*, J.F. Kennedy, G.O. Phillips, P.O. Williams, L. Piculell, Eds., Woodhead Publishing Limited, Cambridge (1995) p 257.
4. H. Yamakawa, M. Fujii, *Macromolecules* **7** (1974) 128.
5. K. Kamide, M. Saito, H. Suzuki, *Makromol. Chem., Rapid Commun.* **44** (1983) 33.
6. H. Benoit, P.M. Doty, *J. Phys. Chem.* **57** (1953) 958.
7. P.N. Lavrenko, O.V. Okatova, V.N. Tsvetkov, H. Dautzenberg, B. Philipp, *Polymer* **31** (1990) 348.
8. R.M. Davis, *Macromolecules* **24** (1991) 1149.
9. T. Odijk, *Biopolymers* **18** (1979) 3111.
10. A. Katchalsky, N. Shavit, H. Eisenberg, *J. Polymer Sci.* **13** (1954) 69.
11. A. Katchalsky, S. Lifson, *J. Polymer Sci.* **13** (1954) 43.
12. A. Katchalsky, S. Lifson, *J. Polymer Sci.* **11** (1951) 409.
13. W. Kuhn, *Kolloid Z.* **68** (1934) 2.
14. H. Yamakawa, *Modern Theory of Polymer Solutions*, Harper & Row, New York (1971) (a) p56, (b) p108.
15. H. Yamakawa, W. Stockmayer, *J. Chem. Phys.* **57** (1972) 2843.
16. R.M. Davis, W.B. Russel, *J. Polym. Sci. Polym. Phys.* **24** (1986) 511.
17. T. Odijk, *Macromolecules* **12** (1979) 688.
18. J. Skolnick, M. Fixman, *Macromolecules* **10** (1977) 944.
19. T. Odijk, A.C. Houwaart, *J. Polym. Sci. Polym. Phys. Ed.* **16** (1978) 627.
20. M. Fixman, J. Skolnick, *Macromolecules* **11** (1978) 863.
21. G.S. Manning, *J. Chem. Phys.* **51** (1969) 924.
22. M. Fixman, *J. Chem. Phys.* **70** (1979) 4995.
23. W.B. Russel, *J. Polym. Sci.* **20** (1982) 1233.
24. L. Zhang, T. Takematsu, T. Norisuye, *Macromolecules* **20** (1987) 2882.
25. B. Zimm, *J. Chem. Phys.* **16** (1948) 1093.
26. E. Ott, H.M. Spurlin, M.W. Grafflin, *High Polymers Vol. V Cellulose and Cellulose Derivatives part II*, Interscience Publishers, Inc., New York (1954) p 676.
27. J. Reuben, H.T. Connor, *Carbohydr. Res.* **115** (1983) 1.
28. F.A. Buytenhuys, R. Bonn, *Papier (Darmstadt)* **31** (1977) 525.
29. Z. Ma, Z. Wiebang, Z. Li, *Chinese J. Polymer Sci.* **7** (1989) 45.
30. D.W. Shortt, *J. Liq. Chromatogr.* **16** (1993) 3371.
31. W.H. Beyer (Ed)., *CRC Standard Probability and Statistics, Tables and Formulae*, CRC Press Boston (1991) p 231.
32. P.F. Mijnlieff, D.J. Coumou, *J. Colloid Interface Sci.* **27** (1968) 553.
33. H. Struszczyk, K. Wrzesniewka-Tosik, D. Ciechanska, E. Wesolowska, In *Cellulose and Cellulose derivatives: Physico-chemical aspects and industrial applications*, J.F. Kennedy, G.O. Phillips, P.O. Williams, L. Piculell, Eds., Woodhead Publishing Limited, Cambridge (1995).
34. P.G. de Gennes, *Scaling Concepts in Polymer Physics*, Cornell University Press New York (1979).
35. L. Schulz, W. Burchard, *Das Papier* **42** (1993) 1.
36. A.E.J. de Nooy, A.C. Besemer, H. van Bekkum, J.A.P.P. van Dijk, J.A.M. Smit, *Macromolecules* **29** (1996) 6541.
37. F.J. Millero, *Chem. Rev.* **71** (1971) 147.
38. M. Rinaudo, In *Charged and Reactive Polymers Vol I Polyelectolytes*; E. Sélégny, M. Mandel, U.P. Strauss (Eds.), D. Reidel Publishing Company, Dortrecht (1994) p 163.
39. S. Koda, S. Hasegawa, M. Mikuriya, F. Kawaizumi, H. Nomura, *Polymer* **29** (1988) 2100.

40. Y. Muroga, K. Suzuki, Y. Kawaguchi, M. Nagasawa, *Biopolymers* **11** (1972) 137.
41. F.H. Crowdhury, S.M. Neale, *J. Polym. Sci. A* **1** (1963) 2881.
42. W.H. Press, S.A. Teukolsky, W.T. Vetterling, *Numerical Recipes*, Cambridge University Press, New York (1989) p 552.

Chapter 3

Kinetics of polyelectrolyte adsorption

Abstract

The kinetics of polyelectrolyte adsorption has been investigated theoretically. Analogous to Kramers' rate theory for chemical reactions we present a model which is based on the assumption that a polyelectrolyte encounters a barrier in its motion towards an adsorbing surface. The height of the barrier, which is of electrostatic origin, is calculated with a self-consistent-field (SCF) model. The salt concentration strongly affects the height of the barrier. At moderate salt concentrations (~0.2 mol l^{-1}) the equilibrium in the adsorption is attained, at low salt concentration (~0.01 mol l^{-1}) equilibrium is not reached on the time scale of experiments. The attachment process shows resemblances with the classical DLVO theory.

3.1 Introduction

In the context of polymer adsorption, the question of reversibility is posed time and again. In the past, many experimental results have been taken as evidence for the existence of non-equilibrium states, and various explanations have been forwarded [1,2]. Some observations could be explained without taking irreversibility into account, e.g., sample polydispersity effects [3,4a]. However, it is obvious that kinetic barriers cannot be ignored, and that slow processes should be expected. Recent experimental work has therefore focused on kinetic aspects of adsorption and desorption, and various interesting slow surface processes were identified [5-8]. Also, quite general arguments were forwarded that can explain the apparent absence of desorption by solvent rinsing [9]. From the theoretical point of view, the problem of adsorption kinetics was recently studied in detail by Semenov and Joanny [10]. These authors made estimates of the rate of adsorption of a neutral polymer. An important aspect of their theory is a calculation of the barrier experienced by an incoming chain for which they apply a variant of Kramers' theory for reaction rates [11].

It is somewhat surprising, however, that adsorption kinetics of polyelectrolytes has not yet been considered theoretically. Polyelectrolytes experience not only short-range interactions between their segments and the adsorbent surface, but also rather strong electrostatic interactions. In particular, when short range attraction competes with electrostatic

repulsion, one may anticipate a situation in which a strong electrostatic barrier impedes adsorption that would be thermodynamically allowed. This situation is very akin to that of charged colloidal particles that remain stable despite of the lower free energy of the aggregated state, simply because of an insurmountable kinetic barrier of electrostatic origin [12].

Strong hysteresis effects have indeed been observed in several experimental studies of polyelectrolyte adsorption. For example, polyelectrolytes with weakly dissociating groups can be adsorbed to substantially higher amounts if, instead of adsorbing at a fixed pH, one goes through a pH cycle, i.e., the polymer is first adsorbed at a pH where it has (very) little charge, after which the polymer is charged up by a shift in pH; this has been termed "enhanced adsorption" [13]. Another observation pointing to the presence of a kinetic barrier is the interaction between two mica surfaces covered with (positively charged) polylysine, as measured by Luckham and Klein in the surface-force apparatus [14]. Upon first approach, these authors found a long range repulsion, which disappeared once the two surfaces were brought close in. This strongly suggested the presence of long dangling ends that needed to be pushed through a barrier in order to adsorb. With neutral polymer, such behaviour has never been found.

Recently we have studied the adsorption of carboxymethyl cellulose (CMC) on inorganic oxide particles (TiO_2, α-Fe_2O_3) as a function of pH, ionic strength, and polymer structure (degree of carboxylate substitution, chain length). The results showed features similar to the ones discussed above. In particular, the effect of a pH cycle was very pronounced [15].

In connection with the above mentioned features we wondered to what extent electrostatic repulsion played a role in the adsorption kinetics, and we decided to tackle this problem theoretically. This chapter is organised as follows. We first briefly review the basic rate equation which is solved using the approach introduced by Joanny and Semenov in combination with a self-consistent field (SCF) theory for (polyelectrolyte) adsorption. Then the SCF method is described by which the height of the adsorption barrier as a function of coverage is obtained. In the results section we first discuss equilibrium adsorption of polyelectrolytes which have an additional non-Coulombic ('specific') interaction with the substrate. This is followed by a set of numerical results for the rate of adsorption under a variety of experimental conditions. In particular kinetic adsorption curves are calculated. These curves are used to determine the extent of reduction of the adsorbed amount due to kinetic factors assuming realistic experimental time scales. Finally, we discuss our kinetic model bearing in mind relevant experimental data.

3.2 Theory

A polymer molecule, moving to an adsorbent surface, meets a number of resistances. At large distance from the surface there is the resistance due to transport in solution, where the

mechanisms of convection and diffusion operate. Next, there can be a barrier in the proximity of the surface, e.g., due to the presence of a layer of adsorbed polymer molecules, or due to an electrical field. We assume that this barrier operates over short distances as compared to the transport contribution. We now suppose that shortly after starting an experiment, a stationary state is established, where the concentration profile in the solution changes only very slowly with time. One can then write for the mass transport of polymers towards the surface J_t:

$$R_t J_t = c_b - c_s(\Gamma) \tag{3.1}$$

Here J_t is expressed in mol m^{-2} s^{-1}, c_b is the bulk concentration far from the interface and c_s is the subsurface concentration (mol m^{-3}) at adsorption Γ, i.e., the concentration of free polymer molecules that find themselves just near the adsorption barrier. R_t is the transport resistance in s m^{-1}, which depends on the hydrodynamic conditions and on the diffusion coefficient [16]. For example, in an impinging-jet geometry, R_t is given by [17]:

$$R_t^{-1} = 0.776\left(v\bar{\alpha}\right)^{1/3}(D/r)^{2/3} \tag{3.2}$$

where v is the fluid velocity, $\bar{\alpha}$ a dimensionless streaming intensity parameter, r the radius of the inlet tube and D the diffusion coefficient of the polymer. The molecules that have reached the barrier can pass in both directions (adsorption and desorption). The forward flux of adsorbing molecules $(d\Gamma/dt)_{fw}$ must obey first order kinetics with respect to the subsurface concentration:

$$R_b(\Gamma)\left(\frac{d\Gamma}{dt}\right)_{fw} = c_s(\Gamma) \tag{3.3}$$

where R_b is the barrier resistance including the effect of a partial coverage of the surface. In order to obtain the backward flux, we note that in equilibrium backward and forward flux must be balanced. Hence, the backward flux $(d\Gamma/dt)_{bw}$ (desorption of polymers) equals:

$$R_b(\Gamma)\left(\frac{d\Gamma}{dt}\right)_{bw} = -c_{eq}(\Gamma) \tag{3.4}$$

where c_{eq} is the equilibrium concentration corresponding to a particular value of Γ. The net flux $(d\Gamma/dt)$ is given by the sum of the forward and backward contributions. For not too short times, the flux reaches a steady state situation, and J_t equals $d\Gamma/dt$ [7]. Obtaining the net flux from equations 3.3 and 3.4 after elimination of c_s we arrive at:

$$\left[R_b(\Gamma) + R_t\right]\frac{d\Gamma}{dt} = c_b - c_{eq}(\Gamma) \tag{3.5}$$

where both R_b and c_{eq} are functions of Γ. The dependency is such that R_b increases with adsorption, c_{eq} and Γ are related by means of an adsorption isotherm. Equation 3.5 suffices to calculate the rate of the adsorption process, provided the equilibrium adsorption isotherm

$\Gamma(c_{eq})$ and the barrier resistance $R_b(\Gamma)$ are known. Finally, integration leads to the time-dependent adsorption $\Gamma(t)$.

In order to obtain the barrier resistance, we use, like Joanny et al. [10], the Kramers' equation:

$$R_b(\Gamma) = \int \frac{1}{D'} e^{u(\Gamma,z^*)/kT} dz^* \tag{3.6}$$

In this equation, $u(\Gamma,z^*)$ is a potential energy felt by an adsorbing molecule which is at a distance z^* from the point where it first touches the surface. Since the potential is a function of the charge at the surface u is a function of the adsorbed amount. D' is an effective diffusion coefficient for the adsorption event, and kT has its usual meaning. The integral is taken over the entire path where the potential differs from the bulk value. In our approach we assume that as soon as one segment makes contact with the surface the chain is adsorbed. We neglect the resistance that the chains meets in the process of spreading out, i.e. motion towards the surface is the rate determining step in the attachment process.

At this point it is important to realise that the potential energy experienced by an entering polymer chain depends on the polymer conformation, since the chain potential energy is a sum over the potential energies of all the monomers, and these feel different energies at different distances from the wall. Chains having one monomer at distance z^* whilst other segments are positioned at distances $z > z^*$ will experience less resistance than a chain having more than one segment at z^*. We now suppose that, for each z, the polymer explores all possible configurations (with appropriate Boltzmann weighting) with one segment at $z=z^*$ and all other segments at $z > z^*$. Hence, $\exp(u(\Gamma,z^*)/kT)$ is actually a partition function (with respect to large distance) which therefore will be denoted as $Q_\infty/Q(z^*)$ [10], where $Q(z^*)$ and Q_∞ are partition functions of a chain with its closest monomer at $z=z^*$ (in the proximity of the surface) or at large distance from the surface (in the bulk) respectively.

Such a partition function is readily evaluated using the numerical procedure first proposed by Scheutjens and Fleer [18,4c]. In this method, endpoint probabilities G(z;s) are calculated for walks on a lattice consisting of s steps and ending at z. This can be done such that the walks are restricted to the half space $z \geq z^*$; we denote these end point probabilities as $G^{z^*f}(z;s)$. The walks are generated taking into account the interactions of segments with their surroundings, i.e. they take place in the "field" which represents these interactions. Obviously, $z^* = 1$ corresponds to tails belonging to an adsorbed chain; we therefore restrict the calculation to $z^* > 1$. If two such walks, one of length s, and one of length N-s+1, are connected at z^*, one obtains a polymer chain with length of N segments which is just at a distance z^* from the touching point. The associated probability is $G^{z^*f}(z;s)G^{z^*f}(z;N-s+1)$. Summing this probability over all values of s from 1 to N, (and correcting by a factor G^{z^*} for the double counting of segment s which occurs in both walks), we obtain the required

partition function Q(z*):

$$Q(z^*) = \frac{\sum_{s=1}^{N} G^{z^*f}(z; s)\, G^{z^*f}(z; N-s+1)}{G^{z^*}} \tag{3.7}$$

A similar expression for Q_∞ can be obtained. In the lattice model $\exp(u(z^*)/kT)$ is not a continuous function but it has discrete values in each lattice layer. Thus $R_b(\Gamma)$ is expressed in the lattice model as :

$$R_b(\Gamma) = \int \frac{1}{D'} \frac{Q_\infty}{Q(z^*)}\, d(z^*/l) \equiv \frac{1}{D'} \sum_{z^*=2}^{z_\infty} \frac{Q_\infty}{Q(z^*)} \tag{3.8}$$

where z_∞ defines the layer where $Q_\infty/Q(z^*)$ equals unity. Further more is assumed that D' does not depend on the position of the moving chain. The model employed to generate $u(z^*)$ profiles was the multi-Stern layer approach first discussed by Böhmer et al [19]. The polyelectrolyte solution, containing as basic units (charged) polymer segments, solvent molecules, and free ions fills a lattice, such that each lattice cell contains exactly one unit. Short range (contact) interactions, such as occurring between various units, or between units and the substrate, are taken into account by means of Flory-Huggins type interaction parameters. Electrostatic energies are incorporated by including an electrostatic Boltzmann term in the probability for each charged species (polymer segments and salt ions [19]), and calculating the electrostatic potential by a discrete version of the Poisson equation. All densities and potentials are averaged in planes of lattice sites parallel to the surface (mean field approximation); correlations in the parallel directions are ignored. As discussed in ref. 19, this is an acceptable description for sufficiently high polymer densities (where lateral interaction between the chains becomes important) and monovalent ions in aqueous solution. The equilibrium density profiles along z (the normal to the adsorbent plane) for each of the components is calculated in a self-consistent manner, using the field to generate the conformations, and deriving a density profile, hence a field from the weighted sum over all conformations. In this way, equilibrium polyelectrolyte density profiles, and their associated adsorbed amount Γ, can be calculated for any imposed equilibrium concentration, so that the adsorption isotherm is known. Using the density profiles, the barrier height can be immediately calculated as prescribed by equation 3.8.

It should be no surprise that the resistance is largely of electrostatic origin. Indeed, the resistance R_b calculated by the method described above is for neutral molecules almost negligibly small when compared to realistic values of R_t. Hence, we are dealing with an electrostatic double layer repulsion between two particles of like charge. Because we have assumed a homogeneous density parallel to the surface, the repulsive interaction energy u_{el} (per unit area) calculated is that for two charged flat plates approaching each other. According

to standard double layer theory [12], u_{el} can be expressed in the minimum dimensionless potential y_m between the two plates in a 1-1 electrolyte solution:

$$u_{el} = -2c_{salt}kT\int_{\infty}^{z^*}\left[\cosh(y_m(z^*)) - 1\right]dz^* \tag{3.9}$$

where c_{salt} is the particle concentration of a 1-1 electrolyte.

3.3 Results

3.3.1 Choice of parameters

SCF calculations were performed for a cubic lattice with a spacing l=0.5 nm. All interaction parameters, except the interaction between polymer segments and the surface (χ_s) were chosen zero. Relative permittivities ε_r were set to 80 for all components. Calculations were done for polymers with a chain length of 100 segments, and the total number of lattice layers in the system was also set equal to 100. Our numerical calculations are restricted to χ_s= 5; in the analytical model we used various values of χ_s.

Numerical integrations of equation 3.5 were obtained by use of a stepsize-adapted fourth order Runge-Kutta algorithm [20]. In each step the solution is calculated for two intervals with stepsize h and one interval using stepsize 2h. If the relative difference between the solutions is less than 10^{-5}, the stepsize is doubled. The value of R_t^{-1} was taken to be 10^{-6} m s^{-1}, in accordance with typical experiments in an impinging jet flow cell. The diffusion coefficient D was chosen as 10^{-12} m^2 s^{-1}, which is a typical value for a polymer of about 100 segments.

In the following, the adsorbed amount will be represented in terms of the surface coverage in mono layers θ, i.e. the number of segments in adsorbed chains per lattice site. For comparison with experiment, θ can be readily converted into Γ [4b]. The salt concentration is given as a volume fraction (ϕ_{salt}). The conversion of ϕ_{salt} to c_{salt} depends on lattice spacing and Avogadro's number [21]; for a cubic lattice with l=0.5 nm one obtains c_{salt}=13ϕ_{salt} (c_{salt} in mol l^{-1}).

3.3.2 Adsorption equilibrium

Before paying attention to the kinetics of adsorption, we first consider adsorption at equilibrium (θ_{eq}). In our discussion we will restrict ourselves to adsorption of strong (quenched) polyelectrolytes. A possible approach is to use the numerical self-consistent field model as proposed by Böhmer et al. [19]. However, for our discussion of trends it is just as

instructive to use the analytical approximation proposed by Fleer [22]. Fleer considers the adsorption of polyelectrolytes on a neutral surface under the action of a non-electrostatic ("specific") interaction, the strength of which is given by the parameter χ_s. The crucial assumption of the theory is that the polymer chains adsorb in flat conformations, i.e., all segments are in contact with the wall, and the contribution of loops and tails to the adsorbed amount is negligible. Comparisons with numerical calculations using the full Böhmer theory have shown that this assumption is justified for cases where the electrostatic interactions are dominant, i.e. where the polyelectrolyte are strongly charged and the salt concentration is not extremely high [22]. In order to preserve electroneutrality, the charge of the adsorbed segments, which is given by the product of the segment charge z_p and the amount of adsorbed segments θ_{sp}, must be compensated by a diffuse layer of countercharge. According to the Gouy-Chapman theory, the total charge in such a layer is proportional to $\varepsilon_r \kappa \sinh(y/2)$, where κ is the inverse Debye length, and ε_r the relative dielectric constant. Since we are dealing with lattice calculations, we rewrite this as $0.67\sqrt{\phi_{salt}}\sinh(y/2)$, where y is the dimensionless potential of the adsorbed layer at the surface, normalised with respect to kT, and the proportionality constant of 0.67 [22] takes the properties of the lattice and the dielectric properties of water at room temperature into account.

The adsorbed amount θ_{sp} can be expressed in y and the non-electrostatic affinity χ_s for the surface: $\theta_{sp} = 1 - 3/2 \exp(z_p y - \chi_s)$. Hence, θ_{sp} must be solved from the following implicit expression :

$$z_p\theta_{sp} = z_p\left(1 - \frac{3}{2}e^{z_p y - \chi_s}\right) = 0.67\sqrt{\phi_{salt}}\sinh(y/2) \qquad (3.10)$$

For $z_p > 0.5$ the surface potential y attains a value of about 4. For such high values $\sinh(y/2)$ may be approximated as $(1/2)\exp(y/2)$. In the special case where $z_p=1$ the surface potential can be immediately calculated from a quadratic equation in $\exp(y/2)$, yielding:

$$e^{y/2} = \frac{1}{3}e^{\chi_s}\left(-\frac{1}{3}\sqrt{\phi_{salt}} + \sqrt{\frac{1}{9}\phi_{salt} + 6e^{-\chi_s}}\right) \qquad (3.11)$$

which gives, in combination with equation 3.10, an explicit expression for the adsorption as a function of the salt concentration.

Assuming that the total adsorption at a charged surface can be written as the sum of a charge compensation contribution ($\theta_{cc} = -z_s/z_p$) and a specific contribution θ_{sp} as described above, the total adsorption, as a function of surface charge and salt concentration, can be readily obtained from the analytical model. In figure 3.1 the adsorbed amount at $\phi_{salt}=10^{-3}$ is shown as a function of the segment charge for four values of χ_s. For comparison, the adsorbed amount calculated with the lattice model at $\chi_s = 5$ is also given (dashed curve). All curves

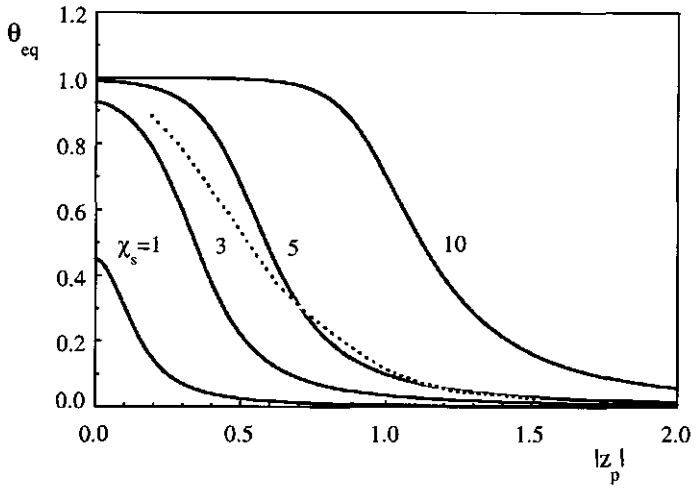

Figure 3.1 Adsorbed amount as a function of the segment charge for four values of χ_s and $\phi_{salt}=10^{-3}$. The dashed curve shows the adsorption calculated with the Böhmer SCF lattice model for a chain with r=100.

show a decrease in the adsorbed amount as the segment charge increases. Because χ_s determines the potential and, hence, the charge at the surface, a higher affinity for the surface will allow more charges in the surface layer, resulting in a higher adsorption. As can be seen from the curves for $\chi_s = 5$ the results obtained with the one-layer model agree reasonably with the full numerical calculations with the Böhmer theory. In figure 3.2 we show the adsorption of a polyelectrolyte (z_p=1) as a function of the surface charge density (z_s) at various salt concentrations. It is not our purpose to discuss the discrepancies between both models but merely to illustrate that general trends can easily be obtained with the analytical model. In our discussion on the kinetics we will use the data calculated with the original Böhmer model.

3.3.3 Kinetics

As pointed out in the previous section, charged polymer chains approaching the surface will feel a repulsion that increases as the surface charge due to adsorbed polymers builds up. In figure 3.3, the ratio $Q_\infty/Q(z^*)$ is shown as a function of the distance from the surface for a neutral surface covered with polyelectrolyte up to a coverage of 0.1 and for five volume fractions of 1-1 electrolyte. Of course, at large distance from the surface the incoming chain does not feel the presence of charged segments at the surface, $Q(z^*)=Q_\infty$. As the polymer approaches the surface the presence of adsorbed segments hampers the motion towards the surface. As can be seen, the resistance increases strongly with the distance to the surface (note the logarithmic scale), in particular if the salt concentration is low.

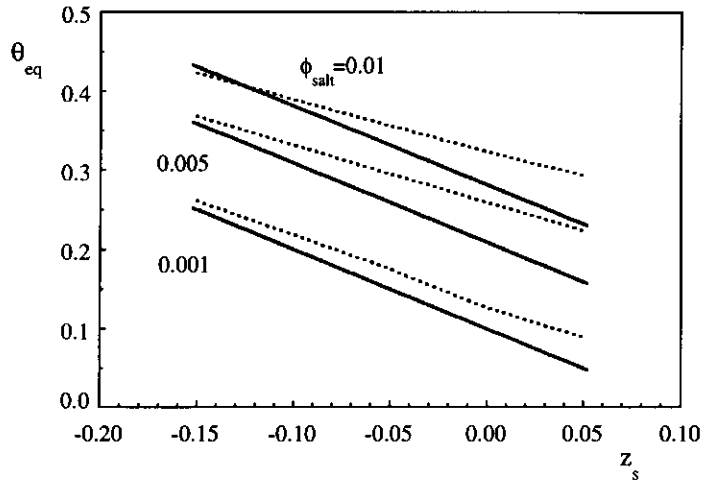

Figure 3.2 Adsorption at equilibrium of a strong polyelectrolyte (z_p=1) as a function of the surface charge for three volume fractions of 1-1 electrolyte. Solid curves are calculated with the analytical model, dashed curves with the Böhmer SCF model.

At relatively large separation, the potential in the region where the double layers of surface and incoming polymer overlap are low, so that a Debye-Hückel approximation makes sense. Hence, we can write in the overlap region for the electrical potential of the surface layer ~exp(-κz)) and for the approaching polymer ~exp(-κ(z*-z)). The dimensionless electric potential in the overlap region (y_t) can reasonably be approximated by the sum of the two individual potentials [23]. The distance where the minimum in y_t (y_m) is situated is easily obtained from minimising y_t with respect to z. Realising that for small y_m $\cosh(y_m)$ can be approximated as $1 + y_m^2/2$ one can easily show from equation 3.8 that u_{el} is proportional to $(\phi_{salt}/\kappa)\exp(-\kappa z^*)$. When the logarithm of u_{el}/kT is plotted against z*, a straight line is indeed observed for small double layer overlap (figure 3.4).

The shape of the potential profiles as given in figure 3.3 shows resemblance with the interaction curve of colloidal particles. In fact, the processes of coagulation and polyelectrolyte adsorption are quite comparable. The classical Fuchs theory [24] for the rate of slow coagulation considers diffusion of a particle in a force field produced by the other particle. The force field has a repulsive part which comes from the overlap of the double layers of the coagulating particles. In addition, there is an attractive part arising from the Van der Waals' interaction between the particles. In a similar way, there is a short range attraction between the polyelectrolyte and the surface which shows up as a break in the resistance curve at z* = 1. When the profiles given in figure 3.3 are plotted semi logarithmically (as done is in figure 3.4) straight parallel lines are found, which shows once more that we are dealing with double layer overlap of two flat plates. The effect of increasing adsorption on the resistance is

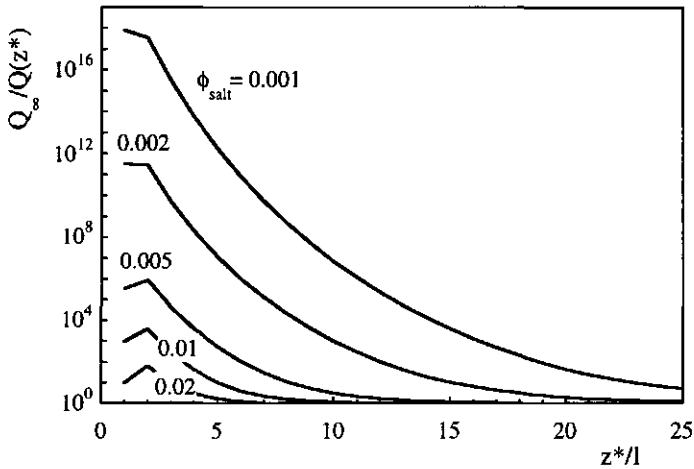

Figure 3.3 Resistance for polyelectrolyte (z_p=-1) approaching an equally charged surface. The bare surface is uncharged. Curves are calculated for θ_{eq}=0.10 for five volume fractions of 1-1 electrolyte.

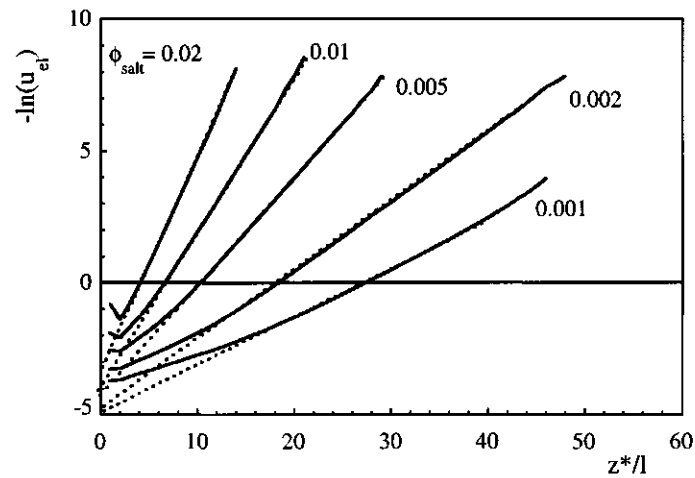

Figure 3.4 Logarithm of repulsive potential as a function of the separation distance z* between polyelectrolyte and surface. The meaning of the dotted lines is explained in the text.

illustrated in figure 3.5. As more charges accumulate at the surface, diffusion towards the surface will become less likely.

As pointed out above the curves in figures 3.3 and 3.5 can be considered as resistances that a polyelectrolyte meets on its way to the surface. By adding the resistances in all layers, the barrier for adsorption is obtained (equation 3.6). In figure 3.6, R_b is given as a function of the adsorbed amount, i.e. in different stages of the adsorption process, for 5 volume fractions

of 1-1 electrolyte. As anticipated, R_b is an increasing function of θ_{eq}.

In the SCF model $Q(z^*)$ is calculated by means of a walk on a lattice. The weight of a step in a layer is a function of the volume fraction of the components in that layer, i.e. the potential in the Boltzmann factor depends on volume fractions introducing the self consistency in the lattice model [4c]. As a lattice layer becomes more occupied with a component, the probability of making a step towards that layer decreases. When a layer is completely filled with a component stepping towards that layer is not allowed. Applied to the surface layer this means that motion a polymer towards the surface layer is not allowed as the surface layer is completely filled with polymer segments (i.e. at saturation of the surface). The manner in which R_b is calculated takes saturation of the surface layer automatically into account, i.e. R_b will diverge to infinity as the volume fraction of segments at the surface approaches unity.

At high salt concentrations a gradual increase in the barrier is observed. Due to the large screening, repulsion only manifests itself at short distances from the surface. Decreasing the salt concentration increases the adsorption barrier dramatically. At low surface coverage there is a moderate barrier for adsorption; as more segments adsorb, the barrier increases very steeply (note the logarithmic scale for R_b). Again, we note the similarity with coagulation kinetics. The effectiveness of collision (W) leading to coagulation is determined by the potential barrier of the process. It turns out that W is almost entirely determined by the value of the potential at the maximum of the interaction curve of the coagulating particles, i.e. the contributions at short distances dominate the barrier resistance. A similar observation can be made from figures 3.3 and 3.6. Particularly for low salt concentrations the main contributions

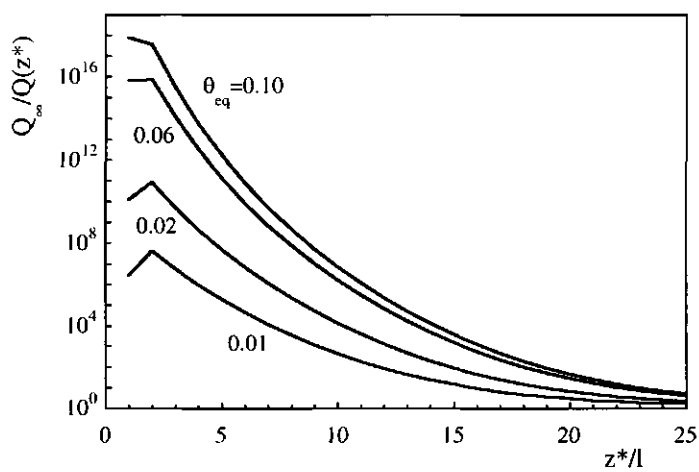

Figure 3.5 Resistance for a polyelectrolyte (z_p= -1) approaching a polymer covered surface for $\phi_{salt}=10^{-3}$. The bare surface is uncharged, curves are calculated for several values of θ_{eq} (i.e. for different stages in the adsorption process).

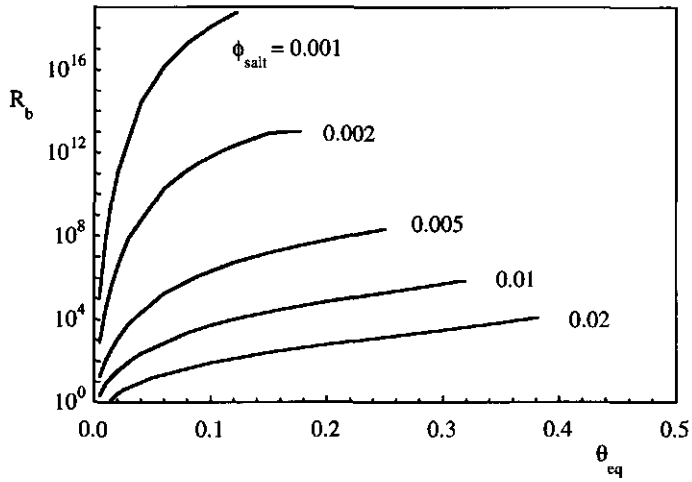

Figure 3.6 Potential barrier R_b for the adsorption of a polyelectrolyte (z_p=-1, r=100) on an uncharged surface in different stages of the adsorption process. Volume fractions of 1-1 electrolyte are indicated in the figure.

to R_b originate from layers close to the surface.

Once the barrier for the adsorption is known one can calculate the adsorption as a function of time. In figure 3.7 the adsorption on an uncharged surface as a function of time is calculated for five volume fractions of salt. At low surface coverages the adsorption increases surface is the rate determining step in the adsorption process. In this stage the adsorption is

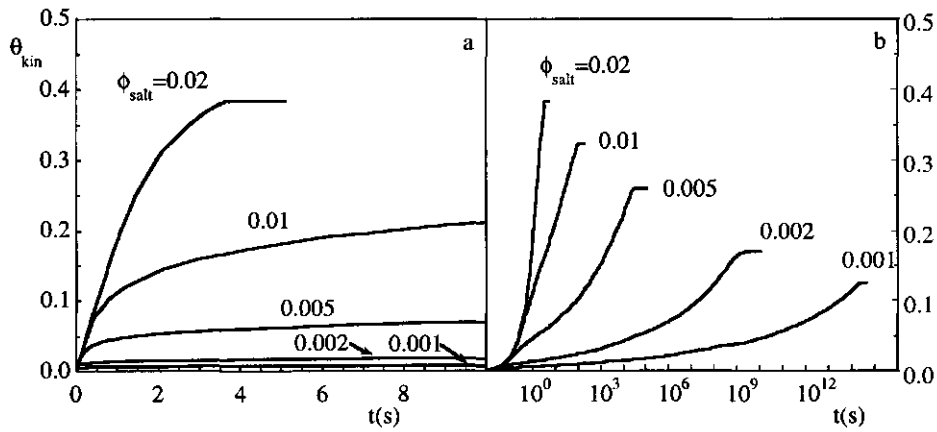

Figure 3.7 Adsorption of a polyelectrolyte (z_p= -1) on an uncharged surface as a function of time for five volume fractions of 1-1 electrolyte. Figure a shows the adsorption on a short time scale, in figure b the adsorption is plotted for long times (note the logarithmic scale). Endpoints in figure b are for equilibrium adsorption and a polymer concentration of 300 mg l^{-1} (volume fraction 10^{-4}).

linearly in time. This is the regime where mass transport from the bulk solution towards the surface is not determined by salt concentration since the adsorption barrier is too small to have any effect on the adsorption rate. As more segments become attached to the surface, the barrier for adsorption increases. When the barrier exceeds the resistance R_t for the transport process the increase in adsorption is no longer linear in time. Now the attachment step determines the adsorption rate. On relatively short time scales, a levelling off in the adsorption is observed for all salt concentrations, as if saturation had been obtained. However, this not true for all curves. In the case of $\phi_{salt} = 0.02$ the adsorption corresponding to equilibrium is indeed reached. The curves for $\phi_{salt} = 0.002$ and lower reach pseudo plateau levels which do not correspond to equilibrium. This is seen more clearly from figure 3.7b where the adsorption is plotted against the time on a logarithmic scale. The endpoints of the curves correspond to the adsorption at equilibrium for a polymer concentration of 300 mg l^{-1} (volume fraction 10^{-4}). As the figure clearly illustrates, the time needed to reach equilibrium depends strongly on the salt concentration. In the case of moderate salt concentration ($\phi_{salt} = 0.005$ to 0.02) the equilibrium in the adsorption is reached within a time scale comparable to that used in adsorption experiments (10^3 - 10^5 seconds). Adsorption equilibrium is not reached for low salt concentrations.

The features that are observed for the adsorption on an uncharged surface also show up for an oppositely charged surface (z_s=0.15). Figure 3.8 shows R_b for a positively charged surface onto which a negative polyelectrolyte adsorbs. At $\theta_{eq} < 0.15$, the surface charge is incompletely compensated by adsorbed polyelectrolyte, so that the net charge seen by

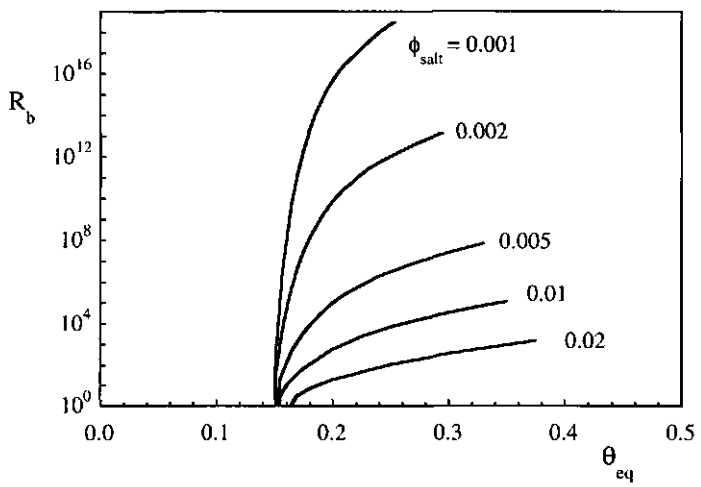

Figure 3.8 Potential barrier R_b for the adsorption of a polyelectrolyte (z_p=-1, r=100) on an oppositely charged surface as a function of surface coverage θ_{eq}. Salt concentrations (1-1 electrolyte) are indicated in the figure.

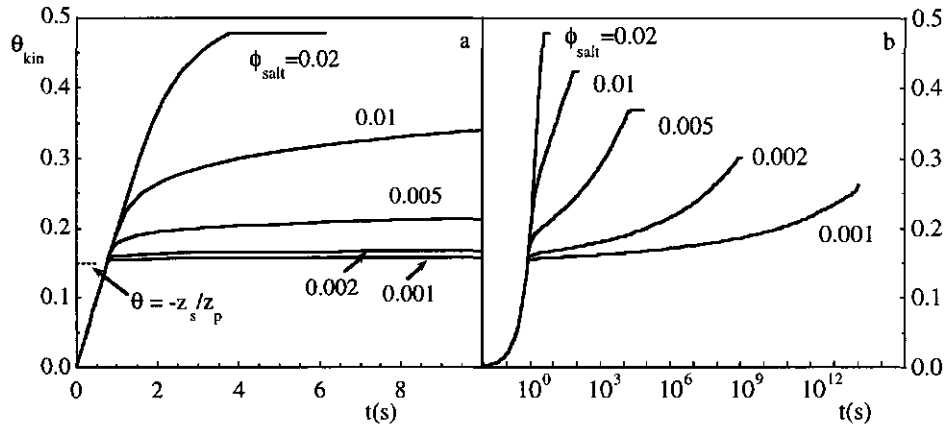

Figure 3.9 Adsorption of a polyelectrolyte (z_p= -1) on a charged surface (z_s=0.15) as a function of time for five volume fractions of 1-1 electrolyte. The point where surface charge is compensated by the adsorbed polyelectrolyte is indicated. Figure a shows the adsorption on a short time scale, in figure b the adsorption is plotted for long times (note the logarithmic scale). Endpoints in figure b are for equilibrium adsorption and a polymer concentration of 300 mg l^{-1} (volume fraction 10^{-4}).

incoming segments is opposite to the charge of the segments, and there is no barrier. As soon as the surface charge is compensated, a repulsive potential is felt by the incoming chains, which shows up in an increase in the adsorption barrier. Comparing the curves in figures 3.6 and 3.8 it appears that the curves for the charged surface at $\theta_{eq} = 0.15$ nearly coincide the ones for θ_{eq} at the uncharged surface, indicating that the net charge at the surface is an important parameter that determines the potential barrier.

The calculated time dependent adsorption on the oppositely charged surface is given in figure 3.9. The region where mass transport determines the adsorption rate is almost entirely restricted to $\theta_{eq} < 0.15$ (surface charge is not yet compensated by polyelectrolyte). As soon as the surface charge is compensated the adsorption reaches a pseudo plateau for low salt concentrations. Equilibrium is reached for moderate salt concentrations (ϕ_{salt} = 0.005 to 0.02), but not for low salt concentrations. The abrupt ending of the time dependent adsorption curves stems from the shape of the adsorption isotherm. The calculated isotherms (not shown in this chapter), i.e. θ_{eq} as a function of the equilibrium concentration, are of the high affinity type. At (very) low concentrations the adsorption increases steeply. The adsorbed amounts corresponding to the endpoints in the time dependent adsorption curves are nearly reached for low concentrations (~ 0.3 mg l^{-1}). The high affinity character of the isotherm implies that c_{eq}-c_b in equation 3.5 only equals zero when θ_{kin} approaches θ_{eq} very closely. Since c_{eq} approaches c_b so abruptly the adsorption also ends abruptly.

In the previous paragraphs we have mainly considered the influence of the salt concentration on the adsorption. The influence of the surface charge is illustrated by means of

figure 3.10. In this figure the adsorption is given as a function of z_s. The full curves represent the adsorption calculated at t=1000s. For comparison we show the corresponding adsorption at equilibrium, as calculated with the lattice model (dashed curves). For $\phi_{salt} = 0.005$ the kinetically limited adsorption is rather close (~75%) to its equilibrium value. For the two highest salt concentrations θ_{kin} coincides with the equilibrium adsorption. However, for $\phi_{salt} = 0.001$ and 0.002, θ_{kin} is much smaller than θ_{eq}, in particular if the bare surface charge becomes small. Hence figure 3.10 illustrates again the pronounced influence of the salt concentration on the adsorption kinetics. Comparing θ_{kin} with the amount θ_{cc} corresponding to charge compensation, it turns out that θ_{kin} is simply the sum of θ_{cc} and a non-electrostatical contribution, which for $z_s \geq 0$ does not depend on the surface charge. This is because R_b depends on the net charge of the surface layer (figure 3.6 and 3.8). The large divergence between kinetically limited adsorption and equilibrium adsorption with decreasing surface charge can now easily be understood. The relative contribution of θ_{cc} increases as the surface charge increases. Eventually, charge compensation will have the main contribution to the adsorption and θ_{kin} will approach θ_{eq}. At decreasing surface charge θ_{cc} also decreases so the influence of the barrier on the total adsorbed amount becomes more important, thereby increasing the difference between θ_{kin} and θ_{eq}.

In figure 3.11 the ratio between the adsorption after 1000 s and the adsorption at equilibrium is given as a function of the polymer charge. For a polyelectrolyte with a small z_p, the adsorption approaches that of an uncharged polymer. Since effects of electrostatics are small, the adsorption is not hampered by an electrostatic barrier, hence the ratio θ_{kin}/θ_{eq}

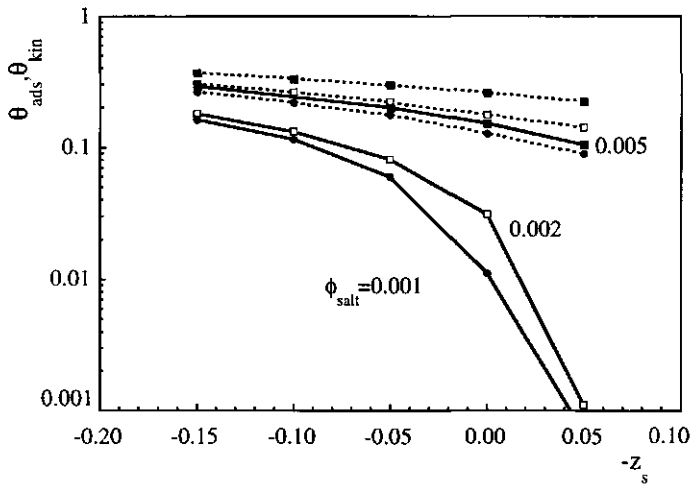

Figure 3.10 Influence of surface charge z_s on polyelectrolyte adsorption (z_p = -1) at three salt concentrations (indicated). The full curves represent the adsorption calculated at t=1000 s (θ_{kin}), dashed curves represent the equilibrium adsorption calculated with lattice model (θ_{ads}).

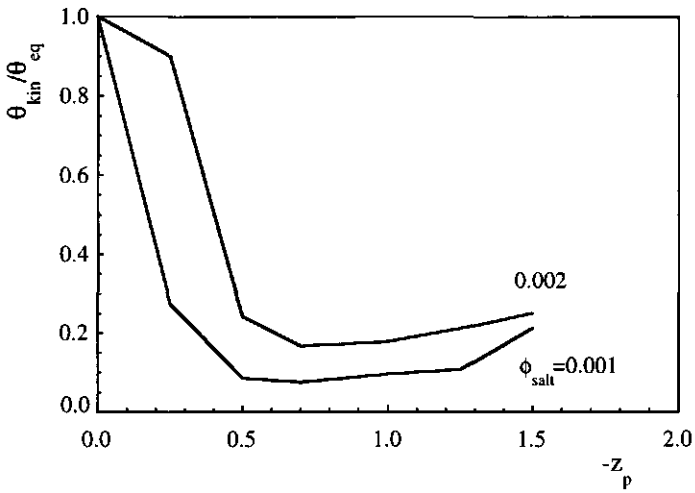

Figure 3.11 Influence of the segment charge z_p on the kinetically limited adsorption θ_{kin}, as determined at t=1000 s.

approaches unity. As the segment charge increases the adsorption will be increasingly affected by an electrostatic barrier, thereby increasing the difference between θ_{kin} and θ_{eq}. Upon increasing the segment charge, both θ_{kin} and θ_{eq} will decrease, however not to the same extent. Initially the former decreases more strongly, at larger z_p the decrease in θ_{eq} dominates. Consequently, beyond about z_p=0.7 the ratio θ_{kin}/θ_{eq} increases again. For high segment charge it is obvious that only small adsorption, even at equilibrium, is possible.

3.4 Discussion

Our results show very convincingly the large effect that an electrostatic barrier has upon the rate of adsorption. Qualitatively, most of the results could be anticipated using arguments from the DLVO theory for the stability of lyophobic colloids which treats the interaction between two rigid charged particles. The present theory deals explicitly with flexible chain molecules with many internal degrees of freedom. From the results it seems that this does not change the interaction in a qualitative way. To what extent the molecular flexibility has a quantitative influence remains to be studied.

In our model, the attractive part of the polymer-surface interaction has a very short range. As a consequence, the adsorption kinetics depends exclusively on the electrostatic part of the interaction. The equilibrium adsorbed mass, however, is strongly influenced by χ_s. As a result, the discrepancy between the equilibrium and the kinetically limited adsorption becomes larger as χ_s increases. This implies that reversibility is most likely to be found for

systems where χ_s is small or even zero; this seems to be supported by experiments [25].

All our calculations have been performed for the case of a polyelectrolyte and a surface with a fixed charge density (quenched system). In literature equilibrium adsorption for annealed systems (with a pH dependent charge) has also been considered [22,26]. In terms of DLVO interactions, the former case can be compared to the case of constant charge, whereas the latter case corresponds to a constant potential. It is well known, that the constant potential case leads to weaker repulsion at short distances, but that coagulation rates are qualitatively very similar for both cases. We therefore expect that the present calculations are also relevant for the adsorption kinetics of annealed polyelectrolytes.

In our approach we have used a mean field model, i.e. discrete charges are smeared out in a layer. In real systems, charges are often localised so that discrepancies of our model with experiments can be expected. The localisation of charges will manifests itself mostly at low adsorption where the surface coverage is rather heterogeneous. At large distance from the surface the smearing out of charges is a reasonable approximation. As a polymer approaches a surface more closely the electric field generated by adsorbed molecules becomes inhomogeneous. If a chain approaches locally a surface with bare spots it can pass more easily through the barriers raised by adsorbed chains. Hence, the barrier for adsorption is expected to be less than when the charges are smeared out; at low ϕ_{salt} our model tends to overestimate the adsorption barrier, i.e. the adsorption is underestimated. As the surface coverage increases the approximation of smearing out of charges is more plausible; the adsorption is less underestimated for higher ϕ_{salt}. On the other hand our model tends to overestimate the adsorption since the process of spreading is not taken into account.

We finally comment on the experiments with carboxymethyl cellulose (CMC) presented in ref. 15. Clearly, these data show a large difference in adsorbed amounts between a case where the pH is kept fixed during adsorption and a case where a pH cycle (high/low/high) is applied. It is therefore tempting to conclude that the adsorption at fixed pH is kinetically blocked, and that the cycle leads to an adsorbed amount closer to equilibrium. However, this is at variance with the observation that even at an ionic strength as high as 0.5 M there is still a substantial effect of cycling the pH. According to our calculations, the barrier resistance should be negligible under such conditions so that equilibrium is reached. Evidently, the CMC/oxide system has features not covered by the present treatment.

To our opinion the discrepancies with our model and experiment can be attributed to an incomplete description of the desorption step. It is beyond the scope of this chapter to discuss the desorption step in detail, we limit ourselves to a small remark. It is likely that localised interactions, e.g. ion pairs between polyelectrolyte and charged surface sites or the formation of strong (chemical) bonds [27] play an important role in the desorption process. Due to the interaction with the surface, a barrier will be present for the desorption, which is high in case of ion pairs or strong chemical bonds. As soon as surface bonds are broken desorption becomes possible. Flexible chains can desorb their segments one by one. Experimentally, this

may show up as an increase of the (hydrodynamic) layer thickness of the adsorbed layer. Complete desorption will take place if the number of segments in contact with the surface is below some critical value. The critical number decreases as the interaction with the surface becomes stronger. Desorption of semi-flexible or rigid chains will occur less gradually as compared to flexible chains. The rigidity of the chain does not permit a desorption of segments one by one. Each desorption step involves a number of segments roughly given by the persistence length. The barrier for the desorption of rigid chains will therefore be higher than for flexible chains.

3.5 Conclusions

Adsorption of polyelectrolytes at low ionic strength on surfaces providing a short-range, non-electrostatic attraction is kinetically blocked by an adsorption barrier of electrostatic origin. The height of this barrier, and its effect on the adsorption kinetics was generally calculated by combining an argument based on the Kramers' theory of reaction rates with the Scheutjens-Fleer-Böhmer self-consistent field theory for polyelectrolyte chains near a charged interface. The theory explains why the adsorbed amounts found in experiments always corresponds closely to charge neutralisation, as if specific interactions with the substrate do not exist, and why hysteresis should be expected upon cycling the pH, i.e., the polymer charge density.

References

1. G. Kraus, J. Dugone, *Ind. Eng. Chem.* **47** (1955) 1809.
2. W.H. Grant, L.E. Smith, and R.R. Stromberg, *Faraday Discussions Chem. Soc.* **59** (1975) 209.
3. M.A. Cohen Stuart, G.J. Fleer, and J.M.H.M. Scheutjens, *J. Colloid Interface Sci.* **97** (1984) 526.
4. G.J. Fleer, M.A. Cohen Stuart, J.M.H.M. Scheutjens, T. Cosgrove, B. Vincent, *Polymers at Interfaces*, Chapman & Hall, London (1993), (a) Ch. 5, (b) pp. 472, (c) Ch. 4.
5. P. Frantz, D.C. Leonhardt, and S. Granick, *Macromolecules* **24** (1991) 1868.
6. H.E. Johnson, J.F. Douglas, and S. Granick, *Phys. Rev. Lett.* **70** (1993) 3267.
7. J.C. Dijt, M.A. Cohen Stuart, and G.J. Fleer, *Macromolecules* **27** (1994) 3219.
8. J.C. Dijt, M.A. Cohen Stuart, and G.J. Fleer, *Macromolecules* **27** (1994) 3229.
9. J.C. Dijt, M.A. Cohen Stuart, and G.J. Fleer, *Macromolecules* **25** (1992) 5416.
10. A.N.Semenov, J.F. Joanny, *J. Phys. II (Paris)* **5** (1995) 859.
11. H.A. Kramers, *Physica* **7** (1940) 284.
12. E.J.W Verweij, J.Th.G. Overbeek, *Theory of Stability of Lyophobic Colloids*, Elsevier, Amsterdam (1948).
13. J. Meadows, P.A. Williams, M.J. Garvey, R.A. Harrop, and G.O. Phillips, *Colloids Surfaces* **32** (1988) 275.
14. P.F. Luckham, J. Klein, *J. Chem. Soc. Faraday Trans I* **80** (1984) 865.
15. C.W. Hoogendam, A. de Keizer, M.A. Cohen Stuart, B.H. Bijsterbosch, J.G. Batelaan, and P.M. van der Horst, *Langmuir* **14** (1998) 3825; chapter 4 in this thesis.
16. M.A. Cohen Stuart, G.J. Fleer, *Ann. Rev. Mat. Sci.* **26** (1996) 463.

17. T. Dabros, Th. G.M. van de Ven, *Colloid Polym. Sci.* **261** (1983) 694.
18. J.M.H.M. Scheutjens, G.J. Fleer, *J. Phys. Chem.* **83** (1979) 1619; *ibid.* **84** (1980) 178.
19. M.R. Böhmer, O.A. Evers, and J.M.H.M. Scheutjens, *Macromolecules* **23** (1990) 2288.
20. W.H. Press, S.A. Teukolsky, W.T. Vetterling, B.P. Flannery, *Numerical Recipies*, Cambridge University Press, New York (1992).
21. R. Israels, *Adsorption of charged diblock copolymers*, Wageningen Agricultural University, (1994) thesis pp. 58.
22. G.J.Fleer, *Ber. Bunsenges. Phys. Chem.* **100** (1996) 936.
23. R.J. Hunter, *Foundations of Colloid Science (Vol. I)*, Clarendon Press, Oxford (1987).
24. N. Fuchs, *Z. Physik* **89** (1934) 736.
25. N.G. Hoogeveen, M.A. Cohen Stuart, and G.J. Fleer, *J. Colloid Interface Sci.* **182** (1996) 146.
26. I. Borukhov, D. Andelman, and H. Orland, *Europhys. Lett.* **32** (1995) 499.
27. Q.I. Liu, J.S. Laskowski, *J. Colloid Interface Sci.* **130** (1989) 101.

Chapter 4

Adsorption mechanisms of carboxymethyl cellulose on mineral surfaces

Abstract

The adsorption behaviour of carboxymethyl cellulose (CMC) on inorganic surfaces (TiO_2 and α-Fe_2O_3) in aqueous solution has been studied systematically. The general trends are that the adsorbed amount decreases with increasing pH, whereas increasing the electrolyte (NaCl) concentration causes the adsorption to increase. The actual values, however, are influenced by the kinetics of the adsorption process. Near the point of zero charge of the oxidic surfaces the adsorption depends linearly on pH. This linearity is interpreted in terms of a molecular condenser, which is composed of the surface layer and the polyelectrolyte in the first layer near the surface. Adsorption is independent of the number of carboxylic groups per glucose unit (degree of substitution, ds). Neither at low (0.01 mol l^{-1}) nor at high (1 mol l^{-1}) electrolyte concentration does the adsorption depend on the chain length which indicates a (rather) flat conformation of the adsorbed polymer. The apparent hydrodynamic thickness of the adsorbed layer is found to be substantial.

Strong hysteresis is observed with respect to the pH dependence of adsorption: as compared to the adsorption measured directly at specified fixed pH values, at high pH values a substantially higher adsorbed amount can be obtained by initially adsorbing at low pH and subsequently increasing the pH value. Desorption of CMC only takes place after initially low pH values are increased substantially. The arduous desorption originates from a strong interaction with the surface and is enhanced by the chain rigidity of the CMC backbone.

4.1 Introduction

In many (industrial) processes polymers have found successful applications. For instance, they are well-known as an effective thickening agent in paints, preventing settling of pigment. The rheological properties of polymer solutions also allow a uniform spreading of the paint. In papermaking, polymers are used as additives to improve the retention of fibers and pigments or to increase the paper strength. Water soluble polymers have practical importance in cosmetics, coatings, and in wastewater purification [1-3]. Some applications are a consequence of the rheological properties of polymer solutions while others are due to

adsorption at a solid-liquid interface. Nowadays the relevance of understanding the adsorption behaviour of polymers at solid-liquid interfaces is generally recognised. A detailed understanding of this behaviour is needed to develop new or to improve current applications.

For the purposes mentioned above one can use either synthetic polymers or chemically modified natural polymers. Within the group of chemically modified natural polymers polysaccharides, in particular cellulose derivatives, have proven to be important components. Cellulose is one of the world's most abundant polymers, it is non-toxic and biodegradable, whereby its derivatives are widely applied. An important representative of the cellulose derivatives is carboxymethyl cellulose (CMC). CMC is used as an additive in papermaking, in pharmaceuticals and cosmetics, and in food products [1-3]. For pelletisation of iron ore the addition of an inorganic binder such as bentonite has proven to be very effective. However, inorganic binders have the disadvantage that they cause serious contamination in the final product. Organic binders (polymers) are combusted in the pellet melting process, thereby strongly reducing the amount of contamination. Especially CMC has been successfully applied as an alternative for inorganic binders in the pelletisation process [4]. This application is a consequence of its adsorption behaviour at a solid-liquid interface. In this chapter we will focus on the adsorption behaviour of CMC.

Although the applications are numerous and CMC is one of the world's largest produced polymers, to our knowledge systematic studies on the effects of molecular mass, degree of substitution (ds), pH and salt concentrations have not been carried out. Often the effect of only a few of these parameters is investigated simultaneously.

Since CMC is a highly charged polyelectrolyte, its adsorption behaviour is strongly affected by electrostatics. This clearly shows up in the adsorption dependence on pH and electrolyte concentration. For instance, for the adsorption of CMC with ds=0.7 on $BaSO_4$ Nag et al. [5] observed an increase with decreasing pH, at fixed electrolyte concentration. At fixed pH an increase with increasing salt concentration was observed. Qualitative agreement with those experiments was found by Williams et al. [6]. In addition, these authors investigated the influence of ds on adsorption. A slight difference was found between CMCs having ds=0.78 and ds=1.25, respectively, CMC with ds=0.45 showing a considerably higher adsorption. The effect of the chain length was studied by both Bain et al. [7] and Arêas and Galembeck [8]. The last mentioned authors observed for adsorption on hydroxylapatite slightly lower values for high molecular mass CMC (M_w=80 kg mol^{-1}) than for CMC with M_w=10 kg mol^{-1}. The opposite was found by Bain et al. [7] from a comparison of the molecular weight distribution before and after adsorption on $BaSO_4$. The fact that often commercially available samples are used, prepared from different cellulose sources, obfuscates comparison between different studies. In our study we used a set of CMCs with ds ranging from 0.75 to 1.25 and of varying molar mass (30 to 1 10^3 kg mol^{-1}). All our samples were prepared on a small scale from the same cellulose source (cotton linters having a small degree of polydispersity).

Polymer adsorption at large has been studied intensively, theoretically as well as

experimentally [9]. In particular the adsorption of neutral polymers is now well understood. The field of polyelectrolyte adsorption however is less explored. Modern theories assume equilibrium in the processes of adsorption. It is our opinion that in case of polyelectrolyte adsorption also kinetics affect the adsorption behaviour. In this chapter we present data on CMC adsorption on inorganic oxides (TiO_2 and α-Fe_2O_3), emphasising the effects of ds, chain length, pH, electrolyte concentration, and the aforementioned kinetics on the adsorbed amount.

4.2 Experimental

4.2.1 Materials

4.2.1.1 Preparation and characterisation of hematite and rutile

Rutile has been synthesised according to Bérubé and de Bruyn [10], by dropwise addition of liquid $TiCl_4$ to demineralised water. A precipitate of amorphous TiO_2 was obtained after boiling a small fraction (10 %) of the solution for two hours. The solid particles were applied as nuclei in the remaining non-boiled $TiCl_4$ solution, whereafter the suspension was aged for 3 weeks at 373 K (boiling under reflux). Upon addition of NaOH the suspension flocculated at the expected pzc (point of zero charge) of the particles (pH≈5). The aged sample was washed with demineralised water until the conductivity of the supernatant did not exceed 10 µS. Synthesis of TiO_2 by adding $TiCl_4$ to an aqueous solution of NH_3 followed by ageing the precipitate for three weeks at 373 K in alkaline medium, as described by Ragai et al. [11], yielded anatase rather than rutile.

Hematite (α-Fe_2O_3) has been prepared according to Breeuwsma [12]. Amorphous Fe_2O_3 was obtained by dropwise addition of a concentrated KOH solution to a ferric nitrate solution at 373 K. The precipitate was aged in an autoclave during 2 days, at about 420 K. After ageing, the sample was coagulated at the expected pzc (pH≈8) and washed with demineralised water until the conductivity of the supernatant did not exceed 10 µS.

X-ray analyses indicated that no crystallographic modifications other than rutile or hematite were present in the TiO_2 and α-Fe_2O_3 samples, respectively.

The specific surface area (A_s) was determined by BET N_2 adsorption. Prior to the surface area analyses the samples were freeze dried and degassed. The specific surface areas were found to be 47 and 48 $m^2\,g^{-1}$ for rutile and hematite, respectively. Information about the porosity of the samples was obtained from adsorption and sequential desorption. On account of the shape of the adsorption isotherms and the existence of a hysteresis loop, the isotherms may be characterised as type IV isotherms in the classification of Brunauer, Deming, Deming and Teller (BDDT) [13]. The hysteresis loop indicates that the solid particles are mesoporous

(pore radius 1-10 nm).

The surface charge of rutile and hematite can be attributed to dissociation of surface hydroxyl groups or association of hydroxyl groups with protons [14,15]. The surface charge densities (σ_0) at different salt concentrations were obtained by means of potentiometric titrations. The number of titrated surface groups follows from depletion of protons or hydroxyl ions from solution. It can be calculated from the volume of titrant KOH or HCl (V_t) and the pH change due to the addition of titrant. The relation between the activity and the concentration of free protons or OH^- ions was established through a titration of a HCl solution with the same electrolyte concentration as used in the titration of the samples (blank). After subtraction of the blank, the surface charge is calculated as

$$\sigma_0 = \frac{1}{m_{sp}A_s}\left[(V_t\ c_t)_{susp} - (V_t\ c_t)_{blank}\right]F \qquad (4.1)$$

where F is the Faraday constant, c_t the concentration of the titrant, and m_{sp} the dry mass of the solid. Points of zero charge of the bare surfaces were identified as the common intersection points of the respective charge-pH curves at different ionic strengths [12]. The points of zero charge were found to be 5.8 and 8.3 for the rutile and hematite sample, respectively. For both rutile and hematite the pzc is not affected by the electrolyte concentration which indicates that there is no specific adsorption of Na^+ or Cl^- ions.

4.2.1.2 Preparation and characterisation of carboxymethyl cellulose

Small batches of carboxymethyl cellulose were prepared by Akzo Nobel in a homogeneous reaction, by treating alkali cellulose (cotton linters) in iso-propanol with sodium monochloroacetate ($ClCH_2COONa$) in nitrogen atmosphere. During the reaction hydrogen atoms are substituted by CH_2COONa groups. Samples differing in degree of substitution (ds), that is, the average number of substituted hydroxyl groups per glucose unit, were synthesised by addition of different amounts of sodium monochloroacetate to the cellulose. A part of each batch with a given ds was treated with hydrogen peroxide, which cleaves the cellulose chain at random position. By addition of different amounts of hydrogen peroxide, a series of CMCs varying in molecular mass were obtained. The molecular mass of the samples, as obtained from SEC-MALLS, ranged from 10^3 kg mol^{-1} (non-depolymerised CMC) to 30 kg mol^{-1} [16]. The polydispersity ratio M_w/M_n ranged from 1.8 to 2.5 [16] and is comparable to M_w/M_n for cotton linter cellulose which is about 2.2 [17], but is substantially lower compared to the majority of commercial CMC types derived from wood cellulose, which show polydispersities from 6 to even 20. After purification the NaCMC was freeze dried and stored in dry form. Though differences in chain length were accomplished by depolymerisation rather than by a polymerisation reaction, we will denote the chain length of CMC by its degree of polymerisation (dp).

The monomeric composition (mole fractions of non-, mono-, di-, and tri-substituted glucose) of our samples, each with a given degree of substitution, was determined by means of HPLC. The samples had ds=0.75, 0.99, and 1.25, respectively. The ds values of the depolymerised samples were somewhat lower (ds=0.74, 0.97, and 1.23, respectively). From Spurlin's statistical model [18] for a substitution reaction at random position the monomeric composition of the samples was calculated. Relative reaction rates for the substitution were taken from Reuben [19]. Good agreement was found between the experimental and calculated composition [16]. On basis of this agreement we concluded that the substituents are randomly distributed over the chain [16].

Stock solutions of about 1 g l^{-1} CMC with different ds, dp, and c_{salt} were prepared by agitation of solid CMC in demineralised water at room temperature during 15 hours. Afterwards NaCl was added as a solution except for the 1 mol l^{-1} NaCl solutions where the salt was added in solid form. Addition of solid high molecular mass CMC to a NaCl solution leads to undissolved fractions of about 2% at 0.01 mol l^{-1} NaCl and 15-30% for $c_{NaCl} \geq 0.1$ mol l^{-1}. Thess undissolved fractions, which do not depend on ds, contain scaly particles that disappear upon heating at 353 K. When the solution was cooled to room temperature no undissolved particles reappeared. Probably depolymerised CMC also yields scaly particles when added to a NaCl solution. This was not investigated, but to be on the safe side we always added salt after preparing a CMC solution.

4.2.2 Determination of the adsorbed amount of CMC

4.2.2.1 Depletion measurements

The adsorbed amount of CMC on suspended particles was obtained by depletion from solution, as carried out according to the following procedure. A particle suspension (Fe_2O_3 or TiO_2) of known concentration was added to solutions with different CMC concentrations but having the same pH and electrolyte (NaCl) concentration. The mixtures were shaken for 16 hours in an orbital shaker, at 298 K. Before the mixtures were centrifuged, their ultimate pH was determined. Finally, the CMC concentration in the supernatant was determined using a general method for analysing carbohydrates introduced by Dubois et al. [20]. A volume of 2 ml of CMC solution was added to 80 µl of reagent (80% phenol, 20% water w/w), followed by 5 ml of concentrated sulphuric acid. After homogenisation the mixture was allowed to stand for 30 minutes and then the absorbance was determined at 486 nm.

The adsorbed amount (Γ) follows from the difference in CMC concentration before (c_0) and after adsorption (c_e)

$$\Gamma = \frac{1}{m A_s} (c_0 - c_e) V \qquad (4.2)$$

where m is the mass of the substrate and V the total volume of the solution.

4.2.2.2 Reflectometry

Adsorption experiments were also carried out on a flat surface using a reflectometer with a stagnation-point flow cell. We will outline the method only briefly, for a detailed description of the experimental set-up the reader is referred to Dijt et al. [21,22].

A polymer solution is transported under well-defined hydrodynamic conditions towards an adsorbing surface. The polymer flux depends on the experimental set-up, the viscosity of the solution, the diffusion coefficient of the polymer and the polymer concentration. As substrate we used a silicon wafer that was coated with a TiO_2 layer. The wafer was obtained from Philips Laboratories, Eindhoven (The Netherlands). Streaming potential measurements indicated a pzc of about pH=4, which indicates that the TiO_2 layer is probably not rutile but amorphous TiO_2 [23].

The adsorbed amount is measured on-line and is obtained from changes in reflectivities of the parallel and perpendicular components of a laser beam (wavelength 632.8 nm). The adsorption is proportional to the reflectometer signal. The latter is converted into an adsorbed amount according to Abeles' method [24]. The conversion factor depends among other parameters (such as the thickness and the refractive index of the TiO_2 layer, the index of refraction of the solution and the wavelength of the laser beam) on the refractive index increment (dn/dc) of the polymer. This parameter was determined by measuring the refractive index as a function of the CMC concentration and amounted to 0.163 $cm^3\ g^{-1}$[16]. As also observed by Rinaudo et al. [25], dn/dc was found to be independent of ds. By comparison of the change in reflectivities of our wafer with those of wafers with known TiO_2 layer thickness (as determined by ellipsometry), the thickness of the TiO_2 layer was determined at 25 nm.

4.2.2.3 Dynamic light scattering

The hydrodynamic layer thickness of adsorbed CMC was obtained by dynamic light scattering. As a start, fluctuations in the intensity of light scattered by a nearly monodisperse spherical hematite sol (concentration 2.5 ppm w/w) without any CMC being present were measured as a function of time. These fluctuations are a consequence of the Brownian motion of the particles. By means of an ALV 5000 digital correlator the fluctuations were processed into an intensity auto-correlation function. We used the method of cumulants [26,27] for data analysis. By fitting the natural logarithm of the intensity auto-correlation function to a second order polynomial, the average translational diffusion coefficient (D_0) of the hematite particles can be obtained. For spherical particles D_0 is related to their radius (R) according to the Stokes-Einstein equation ($R=kT/6\pi\eta D_0$), where kT has its usual meaning and η is the viscosity of the solvent. Subsequently, the reduction in the diffusion coefficient as caused by

the adsorbed polymer layer is assessed. For low polymer concentrations the viscosity of the solution can be taken equal to the solvent viscosity. Now the thickness of the adsorbed layer (δ_h) can be readily calculated according to

$$R + \delta_h = \frac{kT}{6\pi\eta D} \tag{4.3}$$

where D is the diffusion coefficient in the presence of adsorbed CMC.

Applying equation 4.3 requires the use of spherical particles to obtain δ_h. For this reason, in the light scattering experiments we used a different hematite sol (spherical particles) than that used for the adsorption measurements (these particles were non-spherical). Spherical, nearly monodisperse hematite particles were prepared according to Penners [28] by nucleation in a $FeCl_3/HClO_4$ solution at 373 K. The radius of these bare particles amounted to 42 nm. Analysis by means of the method of cumulants showed a slight difference (about 2%) in the radii of the bare particles between using a first or second order polynomial. This indicates that the hematite sample is slightly polydisperse. The preparation of hematite according to Penners has a low yield. In depletion measurements much higher amounts of substrate are needed in comparison to the light scattering experiments. Therefore, we used spherical hematite particle only for light scattering experiments ant the non-spherical hematite for depletion experiments.

All experiments were carried out using a He-Ne laser (wavelength 632.8 nm) at a constant scattering angle of 90°. Low polymer concentrations were used in order to avoid difficulties in the interpretation of the measured diffusion coefficient [29,30], so the viscosity of the polymer solution may be taken equal to the solvent viscosity.

4.2.2.4 Electrophoretic mobility

Electrophoretic mobilities of (CMC-covered) rutile particles were measured in a cylindrical cell using a Malvern Zetasizer III. A rutile dispersion (0.018 % w/w) in 0.01 mol l^{-1} NaCl was added to an equal volume of CMC solution (300 mg l^{-1} in 0.01 mol l^{-1} NaCl). Prior to addition both the dispersion and the CMC solution were set to the same pH by addition of HCl or NaOH.

4.3 Results and discussion

4.3.1 Adsorption on α-Fe_2O_3 (depletion experiments)

Figure 4.1 shows typical adsorption isotherms of CMC (M_w=1100 kg mol^{-1}, ds=1.25) on hematite in 0.01 mol l^{-1} NaCl at two pH values. The isotherms have a high affinity character and a well-defined plateau value. Similar results are obtained for CMC with lower ds and

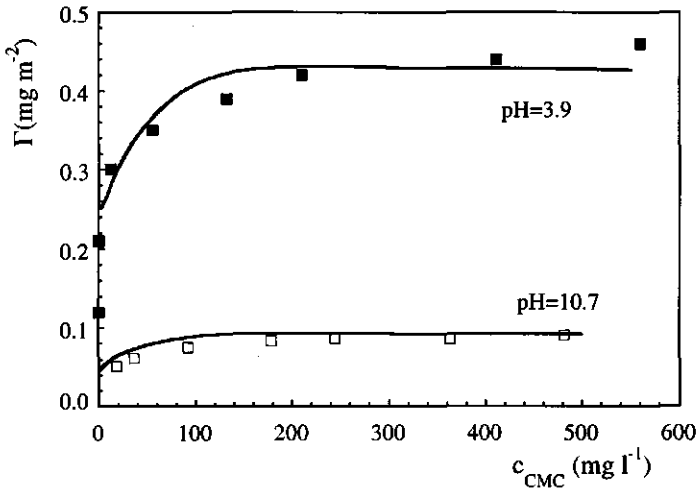

Figure 4.1 Adsorption isotherms of CMC (ds=1.25, M_w=1100 kg mol^{-1}) on hematite in 0.01 mol l^{-1} NaCl, pH indicated in figure.

lower M_w, i.e. the adsorbed amount does neither depend on ds nor on M_w in the ranges we used.

For a polydisperse system, at low polymer concentration both short and long chains adsorb. With an increase of the concentration, the absolute number of long chains that can adsorb then increases, thereby displacing shorter chains. Because the loss of translational entropy per unit mass is smaller for long chains than for short chains, whereas the gain in adsorption energy is the same (i.e. the number of segments per chain in contact with the adsorbing surface is comparable), long chains will adsorb preferentially [31]. If tails and long loops have a significant contribution to the adsorbed amount, the adsorption will depend on the molar mass. As the number and the size of the loops increases with the chain length the adsorption increases with molar mass of the polymer [9]. On account of the large difference in molar mass (45 kg mol^{-1} for the lowest and about 1000 kg mol^{-1} for the highest molecular mass CMC) a pronounced effect of the chain length on the plateau value of adsorbed amount would then be expected. If the contribution of loops and tails to the adsorbed amount is small, i.e. if the segments are mainly situated in trains, the conformation of the adsorbed layer is flat. Such a flat conformation manifests itself in an adsorption that is independent of the chain length [9]. There may be preferential adsorption of long chains over short ones, but this does not affect the plateau value in the adsorbed amount. So, in conclusion the absence of a pronounced chain length dependence of the plateau values points to a (rather) flat conformation of adsorbed CMC.

At pH=3.9 CMC is only partly (about 40 %) dissociated whereas the hematite surface has a high positive charge density resulting in a high adsorption. At pH=10.7 the hematite surface

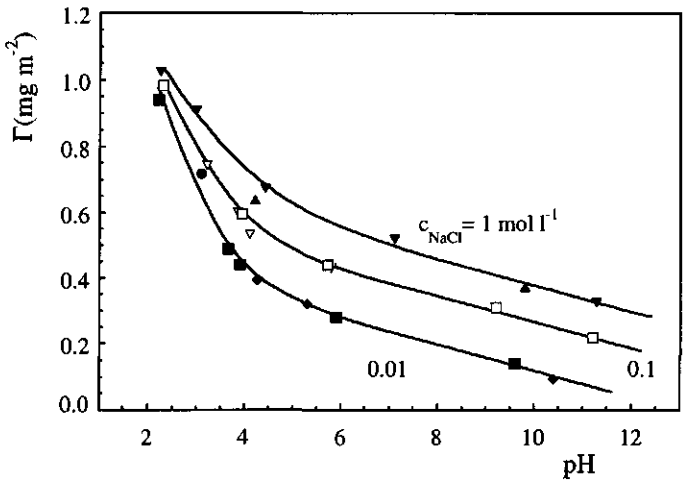

Figure 4.2 Plateau values in the adsorption of CMC on hematite as a function of pH. The dependence is given for various electrolyte (NaCl) concentrations (indicated in figure). c_{NaCl}=0.01 mol l^{-1} : ●:ds=0.75, ■:ds=0.99, ◆:ds=1.25; c_{NaCl}=0.1 mol l^{-1} : ∇: ds=0.75, □: ds=0.99; c_{NaCl}=1 mol l^{-1} : ▼: ds=0.75, ▲: ds=0.99. The adsorption is independent of the molar mass.

is negatively charged resulting in a low plateau value for the strongly charged (fully dissociated) CMC. Despite the considerable difference in charge density between CMCs with different ds, the adsorption (if expressed in mg m^{-2}) is not affected by ds. Taking into account the difference in the molar mass of a monomeric unit, which is given by 162+80ds, the adsorption at pH=3.9 amounts to 1.8 and 1.6 μmol m^{-2} for ds=0.75 and ds=1.25, respectively. So, in spite of the rather large difference in polymeric charge density, its effect on the adsorption is small.

Mineral surfaces often contain pores [13]. If the size (radius) of a pore is (much) less than the dimension of a polymer, the latter cannot enter the pore. Hence, part of the surface will be excluded from adsorption (pore size exclusion). No effect of pore size exclusion was observed for the hematite sample that we used. This was confirmed by the following experiment. We determined the adsorption on hematite starting with a concentration of 970 mg l^{-1} CMC (M_w = 1100 kg mol^{-1}). When the supernatant (570 mg l^{-1}) was subsequently brought into contact with an equal amount of bare hematite, the same adsorbed amount was found. In the first experiment any low molecular mass fraction can adsorb inside the pores. Since this fraction is absent in the supernatant, a lower adsorption is expected for the second experiment if pore size exclusion is of any importance. Despite the large difference in initial concentration a lower adsorption is not observed, which indicates that exclusion effects do not play a role for this sample.

The plateau values in the adsorption on hematite as a function of pH in the presence of

different amounts of electrolyte (NaCl) are shown in figure 4.2. Plateau values are given for CMC with different molar mass and ds. Neither the molar mass nor ds affects the adsorbed amount. A monotonic increase in adsorption with decreasing pH is observed. For a qualitative explanation we have to consider the following aspects. At pH=8.3 (point of zero charge, pzc) the bare hematite surface carries no net charge. At pH < pzc the bare surface carries a positive charge that increases with decreasing pH. Besides the substrate surface charge, the charge of CMC is also a function of pH. At pH > 5.5 CMC is fully dissociated [16,32], at lower pH the degree of dissociation decreases. Consequently, below pH=8.3 CMC and the hematite surface attract each other. At pH > 8.3 the net surface charge of hematite is negative, adsorption can then only be accomplished when the electrostatic repulsion between hematite and CMC is compensated by non-electrostatic attraction. Actually, even at pH values considerably above the pzc adsorption is observed. Considering the high surface charge density it may be concluded that the non-electrostatic interactions are strong. Moreover, as oxidic surfaces have the possibility to (locally) adjust their charge, thereby reducing the negative charge, adsorption is facilitated. Lateral repulsion between charged segments at the surface also hampers the adsorption. Since the repulsion between segments is screened, increasing the salt concentration facilitates higher adsorption.

Polyelectrolyte adsorption on an equally charged surface is not uncommon. Girod et al. [33] reported adsorption of partially hydrolysed polyacrylamide (HPAM) on TiO_2 up to pH=12. Despite the rather high polymer charge (0.16 charges per segment) the adsorption at pH=12 in the absence of salt is substantial (0.13 mg m^{-2}). Comparing the adsorption of HPAM at high electrolyte concentration (2 mol l^{-1} NaCl) with neutral (i.e. non-hydrolysed) PAM the adsorption of HPAM (0.5 mg m^{-2}) is found to be almost twice that of PAM (0.28 mg m^{-2}). At such high electrolyte concentrations charges are almost completely screened, so if HPAM and PAM would have the same non-electrostatic interactions with the surface the same amount of adsorption should be expected. Girod et al. [33] conclude that not only (smeared out) electrostatics play a role in the adsorption, but that a difference in specific binding of HPAM and PAM to the surface (binding to localised sites) is also important. Hoogeveen et al. [23] reported adsorption of cationic AMA (polydimethylaminoethyl methacrylate) on TiO_2 below the pzc. At high pH, where the polymer is uncharged, no adsorption is observed. So the adsorption below the pzc cannot be attributed to a non-electrostatic interaction; adsorption at localised sites (ion pairs between carboxylic groups and positive surface sites) seems to be a more appropriate mechanism for the observed adsorption. With respect to CMC Williams et al. [34] also observed adsorption at pH > pzc on $BaSO_4$. At low electrolyte concentration (10^{-3} mol l^{-1} NaCl) the adsorption at pH=6.5 (which is 2.5 pH units above the pzc) amounts to 0.2-0.5 mg m^{-2}, depending on the ds of the CMC sample. As stated by these authors the adsorption is facilitated by desorption of SO_4^{2-} ions, which reduces the negative charge of the $BaSO_4$ particles. Furthermore, they observe a significantly lower adsorption at pH=2 when the adsorption is carried out in H_2SO_4 rather

than in HCl, which suggests a competition between polymer segments and sulphate ions for surface sites [34]. Binding between charged polymer groups (carboxylic groups) and positively charged surface groups may also apply to CMC adsorption on hematite.

At pH < pzc, where the bare surface (without adsorbed CMC) and CMC are oppositely charged, the adsorption increases with decreasing pH. Such a dependence has been observed before and is usually explained in terms of charge interaction between polyelectrolyte and substrate surface. With decreasing pH, the bare surface charge increases. On the other hand, the dissociation of the carboxylic groups decreases, thereby decreasing the charge on the polymer. Despite this decreasing charge with decreasing pH, the polyion still retains a relatively high charge density. At pH=3 the degree of dissociation is about 0.25 and 0.3 for CMC with ds=1.25 and ds=0.75, respectively, so on average the polyion carries about 0.3 charges per segment [16]. Considering charge compensation as the mechanism for adsorption, such highly charged polymers will adsorb to such an extent as to compensate the surface charge. Since the charge per segment becomes less at lower pH, more segments are needed to compensate the surface charge, which shows up in increasing adsorption with decreasing pH. Upon further pH decrease the charge density of the macromolecule also decreases further. Since the also present small counterions gradually become more effective in compensating the surface charge than the macromolecules with the low charge density, the latter cannot sufficiently compete with the small ions any more, leading to a decrease in the adsorption. A maximum in the adsorption of a weak polyacid at low pH, which arises in this manner, has been observed previously, both theoretically [35] and experimentally [36,37]. Furthermore it was shown by van de Steeg et al. [38] that the position of the maximum in the adsorption shifts to higher polymer charge density with increasing electrolyte concentration. For weak polyacids the position of the maximum is situated at about 1.5 pH units below $pK_{½}$ (i.e. the pH were the polyelectrolyte has a degree of dissociation of 0.5) [35]. The $pK_{½}$ value for CMC ranges from about 4.0 (in 0.01 mol l^{-1} NaCl depending on ds) to about 3.2 (1 mol l^{-1} NaCl), so that the maximum is expected to be situated at pH≈2.5 (in 0.01 mol l^{-1} NaCl) and pH≈1.5 (1 mol l^{-1}). Whether such a maximum exists for CMC cannot be concluded from figure 4.2. However, experiments at low pH were not carried out due to the low solubility of CMC at pH < 2.5 [39].

Plateau values of the adsorption isotherms at different pH values as a function of the logarithm of the electrolyte concentration are represented in figure 4.3. As figure 4.3 shows, the slope of the straight lines is independent of pH for pH > 4.5, but decreases at lower pH. Once more this figure illustrates the influence of electrostatics on the adsorption. However, the observed logarithmic dependence cannot be explained straightforwardly. Previously, theoretical considerations have led to the conclusion that for a strong polyelectrolyte adsorbing on an uncharged surface, the adsorption is linear in $\sqrt{c_{salt}}$ [40]. Furthermore, these calculations give the same slope for the electrolyte dependence (i.e. straight parallel lines) for different surface charges. In ref. 40 the adsorption was calculated for a strong polyelectrolyte

with moderate non-electrostatic affinity for the surface (U_{ads} = 1 kT). We used the same model to calculate the adsorption of a strong polyelectrolyte as a function of the electrolyte concentration for different values of U_{ads}. Our calculations show that the square root dependence is not preserved when U_{ads} is increased. In fact, a logarithmic dependence is observed for c_{salt} in the range from 0.01 to 1 mol l^{-1} for U_{ads} = 5 kT. Moreover, parallel lines are found when the electrolyte dependence is calculated for different surface charge densities. As U_{ads} is further increased, the logarithmic dependence disappears. So, the calculations suggest that a logarithmic dependence is obtained for a more or less unique value of U_{ads}. The fact that the choice of one unique value of U_{ads} yields a logarithmic dependence indicates, in our opinion, that the qualitative agreement between calculations and our experiments is fortuitous.

4.3.2 Desorption from α-Fe_2O_3

A common property in the adsorption of polymers is the (apparent) slow desorption after adsorption has taken place. Dijt et al. [21,22] investigated the kinetics of adsorption and subsequent desorption of neutral polymers on silica. Using a reflectometer with a stagnation point flow cell, they studied the effect of rinsing with polymer-free solvent after adsorption. The general finding is a small decrease in the adsorbed amount with time, i.e. desorption is a very slow process. Dijt et al. applied the local equilibrium concept to explain the low desorption rate in their kinetic experiments. In this approach it is assumed that the adsorbed layer is at equilibrium with the solution adjacent to this layer, which has a polymer

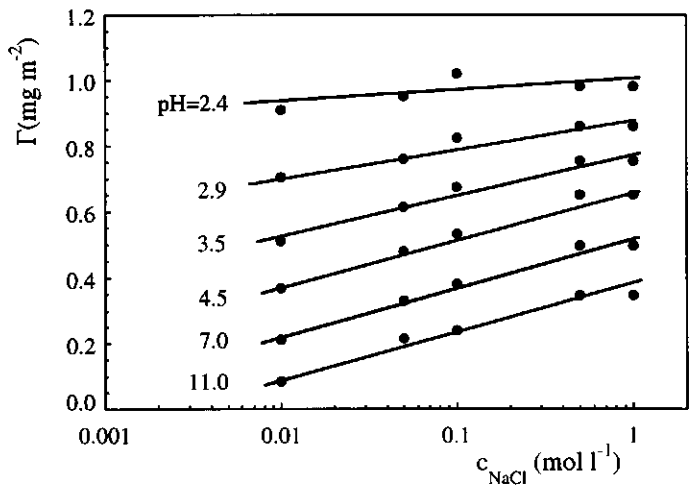

Figure 4.3 Plateau values in the adsorption of CMC on hematite as a function of the logarithm of the electrolyte (NaCl) concentration at fixed pH (indicated in figure).

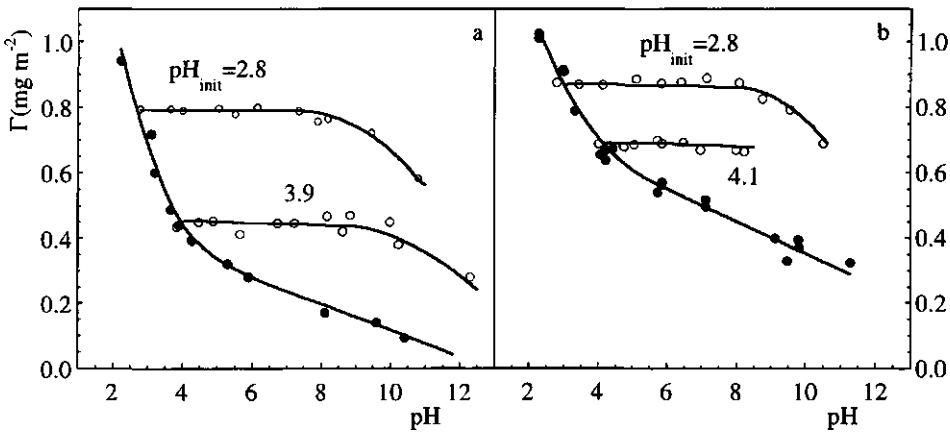

Figure 4.4 The effect of successive pH increments after adsorbing CMC on hematite at two low initial pH values (indicated in figure). Figure a relates to 0.01 mol l^{-1} NaCl, Figure b to 0.5 mol l^{-1} NaCl.

concentration c_s. The rate of desorption is related to the difference between the concentration at the subsurface region and that in the bulk (c_s-c_b), where c_b=0 in Dijt's experiments. The dependence between c_s and the adsorption is dictated by the polymer adsorption isotherm. Initially, c_s is in the plateau region of the adsorption isotherm. As c_s is large with respect to the bulk, desorbed polymers can easily diffuse to the bulk, thus initially the process of desorption is fast. Since polymer adsorption isotherms exhibit a high affinity character, c_s decreases very strongly when the adsorbed amount decreases. Diffusion of polymer from the subsurface layer to the bulk solution then becomes very slow making it the rate determining step in the desorption process [21]. In case of polyelectrolyte adsorption the desorption step can often be accelerated by changing the surface charge of the substrate. Hoogeveen [23] adsorbed cationic polyvinylpyridine on TiO_2 at pH=8 (negatively charged surface). When the pH is decreased to 4, a rapid decrease in the adsorbed amount was observed. The pH change results in a surplus of positive charge and consequently a high opposing electrical potential. As a consequence of the developed potential, detachment of polyelectrolyte takes place. So, the potential provides the driving force for the desorption process.

We attempted a similar forced desorption by increasing the surface charge after adsorbing CMC on hematite at low pH. In our experiments solutions are agitated continuously, which implies that the desorption process is not limited by diffusion. In figure 4.4 the curve corresponding with the closed symbols represents the directly measured adsorption of CMC as a function of pH (i.e. the same data as given in figure 4.2). The curves corresponding to the open symbols refer to experiments where CMC was initially adsorbed at low pH (indicated in figure), after which the pH was increased stepwise. After each step the mixture was shaken for 24 hours, after which the solution pH and CMC concentration were

determined. No significant change in pH (within 0.1 pH unit) could be observed after 24 hours. From the CMC concentration the adsorbed amount is calculated according to equation 4.2. Figure 4.4 shows that the adsorbed amount does not change as long as the pH is below the pzc of the bare surface. As we pointed out in the previous paragraph, an increase in the pH gives rise to a more negative electric potential that may eventually lead to desorption. A high pH increase is needed to accomplish desorption both in 0.01 and 0.5 mol l^{-1} NaCl.

Adsorption-desorption hysteresis was also observed for, e.g., hydrolysed polyacrylamide on cationic polystyrene latex by Meadows et al. [41]. These authors determined the extent of desorption as a result of increasing the pH to 6.5 after initial adsorption at pH=3.0. It turned out that the extent of desorption depends on the initially adsorbed amount; at low surface coverage (i.e., in the initial stage of the adsorption isotherm) no desorption was observed, whereas at a surface coverage corresponding to the plateau value in the isotherm, about 35% desorption took place. By means of electron spin resonance (ESR) they investigated the configuration changes occurring upon pH increase. These ESR measurements indicated that for the molecules remaining behind desorption is accompanied by an increase of segments situated in loops and tails. Hackley [42] observed adsorption-desorption hysteresis for poly(acrilic acid) (PAA) on silicon nitride (Si_3N_4). PAA is first adsorbed at pH=3 whereafter the pH is increased stepwise. With an increase of the pH, the adsorbed amount is constant up to the pzc of the bare surface (pzc=6.4). At pH > pzc the adsorbed amount decreases but is still higher compared to the amount as measured directly at specified fixed pH values.

For our system the effect of a pH increase was further investigated by studying the effect on the hydrodynamic layer thickness (δ_h) by means of dynamic light scattering. CMC

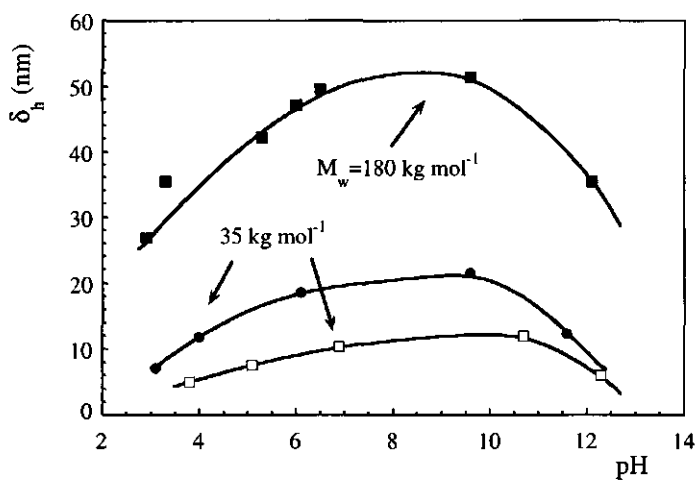

Figure 4.5 Hydrodynamic layer thickness of adsorbed CMC (ds=0.99) on hematite at 0.01 mol l^{-1} NaCl. CMC was initially adsorbed at low pH (■,●; pH_{init}=2.8, □: pH_{init}=3.7), whereafter the pH was increased stepwise.

(ds=0.99, M_w=35 and 180 kg mol^{-1}) was initially adsorbed on nearly monodisperse spherical hematite particles at low pH in 0.01 mol l^{-1} NaCl, after which the change in the layer thickness was obtained from the change in diffusion coefficient due to adsorption. The result is given in figure 4.5 for two initial values of pH. Unfortunately, we were not able to measure δ_h for systems where CMC was adsorbed at pH > 4 or from electrolyte solutions with concentrations higher than 0.01 mol l^{-1} (the hematite sol is only stable at low pH and low electrolyte concentration). At pH_{init}=3.7, δ_h is lower than that at pH_{init}=2.8. As shown in figure 4.2, the adsorbed amount at pH=3.7 is less than at pH=2.8, which allows a more unfolded (flat) conformation. Adsorbing CMC with higher molar mass gives rise to a substantially higher hydrodynamic layer thickness. This is expected for neutral polymers, where the higher adsorption of larger molecules is accompanied by the formation of larger loops and tails. However, for CMC no effect of the molar mass on the adsorption on hematite is observed. The hydrodynamic layer thickness is mainly determined by tails [9,31]. Therefore the higher layer thickness is attributed to a few longer tails protruding into the solution. Although these tails determine δ_h, the contribution to the total adsorbed amount is negligible.

With an increase of the pH from its initial value an increase in the hydrodynamic layer thickness is observed. A possible explanation could be that aggregation of particles takes place, which would result in a decrease in the average diffusion coefficient. However, the decrease in D (and with that the inferred increase in δ_h) is not accompanied by a change in the intensity of the scattered light. As the scattered intensity is proportional to the sixth power of the size of the scattering particle, the decrease in D can rather be attributed to an increase in δ_h rather than to aggregation. This is confirmed by the fact that addition of salt up to 1 mol l^{-1} does not change the scattered intensity (i.e., no aggregation takes place). It has been shown theoretically [9] as well as experimentally (see for instance ref. 43) that for polyelectrolytes the thickness of the adsorbed layer increases with the adsorbed amount. If a pH increase would lead to a situation that corresponds to equilibrium at higher pH, a decrease in the adsorbed amount accompanied by a decrease in δ_h should be expected. In case of the CMC-hematite system another trend is observed; i.e., δ_h increases with increasing pH at constant adsorption.

We interpret the data in figure 4.5 as follows. Initially CMC is adsorbed in a relatively flat conformation (no influence of the molar mass is observed in the adsorption). Subsequently, increasing the pH has two effects. In the first place, the degree of dissociation of both non-adsorbed (loops and tails) and adsorbed (trains) segments increases. A higher degree of dissociation results in an increase of the charge density on the chain, which causes a stretching of the few tails. Secondly, the electric potential at the surface gradually becomes more negative, which causes a detachment of adsorbed segments leading to the formation of larger loops. The increased repulsion between charged segments puts a strain on the loops (i.e. the size of the loops tends to increase), which causes further detachment of segments

from the surface. Since at pH=4 CMC is already dissociated to a large extent (≈50% dissociation [16]) the stretching of the tails is assumed to play a minor role in the increase of δ_h for pH > 4. Due to the rigidity of the CMC backbone [16] (we will touch upon this later on) and its relatively flat adsorption, it is more likely that desorption of segments results in the formation of (larger) tails rather than of loops. This mechanism explains the pronounced increase in δ_h at constant adsorbed amount. Above pH=8 more and more segments lose contact with the surface, ultimately leading to complete desorption of chains and a decrease in δ_h. Adsorption at pH=2.8 gives a higher adsorbed amount than adsorption at pH=3.7. As a consequence of the higher segment density near the surface, there will be more repulsion between charged segments, resulting in a higher probability for detachment of tails and a relatively high value of δ_h.

4.3.3 Adsorption on TiO_2 (depletion experiments)

In figure 4.6 plateau values for the adsorption of CMC on rutile at different salt concentrations are shown as a function of pH. Qualitatively, there is a resemblance with the adsorption on hematite. Again no dependence of the adsorbed amount on the molar mass or the degree of substitution is observed. With decreasing pH the adsorbed amount increases, but since the pzc of rutile is at a lower pH, the curves are shifted correspondingly. As observed for the adsorption on hematite, the adsorbed amount depends logaritmically on the

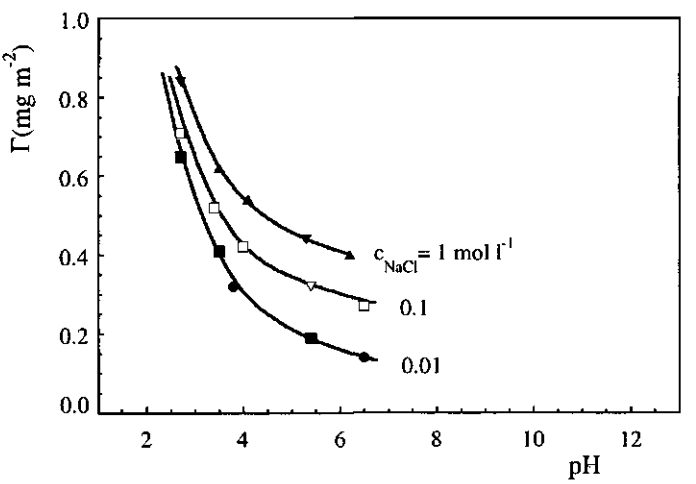

Figure 4.6 Plateau values in the adsorption of CMC on rutile as a function of pH. The dependence is given for various electrolyte (NaCl) concentrations (indicated in figure). c_{NaCl}=0.01 mol l^{-1} : ●:ds=0.75, ■:ds=0.99; c_{NaCl}=0.1 mol l^{-1} : ∇: ds=0.75, □: ds=0.99; c_{NaCl}=1 mol l^{-1} : ▼: ds=0.75, ▲: ds=0.99. The adsorption is independent of the molar mass.

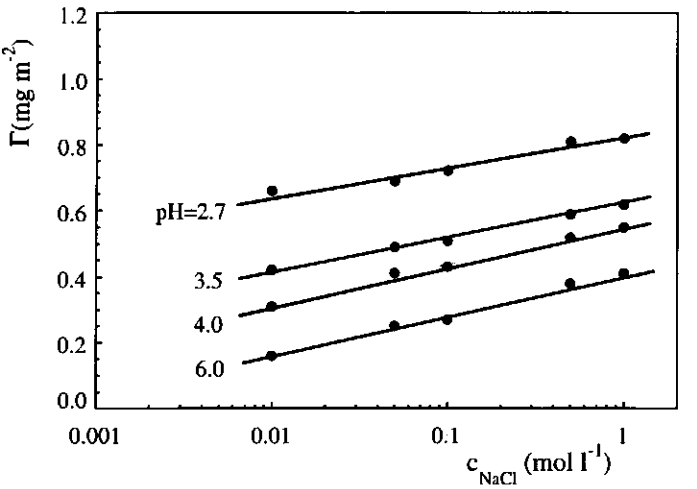

Figure 4.7 Plateau values in the adsorption of CMC on rutile as a function of the logarithm of the electrolyte (NaCl) concentration at fixed pH (indicated in figure).

electrolyte concentration (figure 4.7), albeit the slope at low pH is higher than that on hematite. The fact that for both the adsorption on hematite and rutile a logarithmic dependence on c_{salt} is observed would imply that on both surfaces $U_{ads} \approx 5$ kT. As we are dealing with different surfaces it is highly unlikely that the adsorption energy has the same value on these surfaces, which again illustrates that the qualitative agreement with the calculated adsorption is fortuitous. The effect of increasing the pH after initially adsorbing

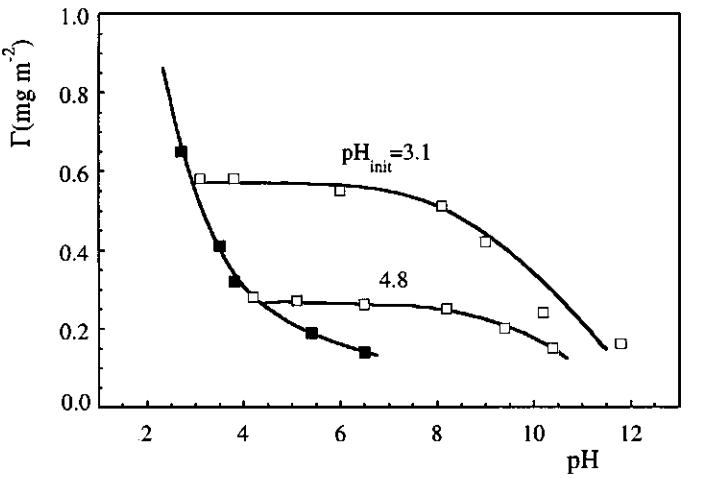

Figure 4.8 The effect of successive pH increments after adsorbing CMC on rutile in 0.01 mol l^{-1} NaCl at two low initial pH values (indicated in figure).

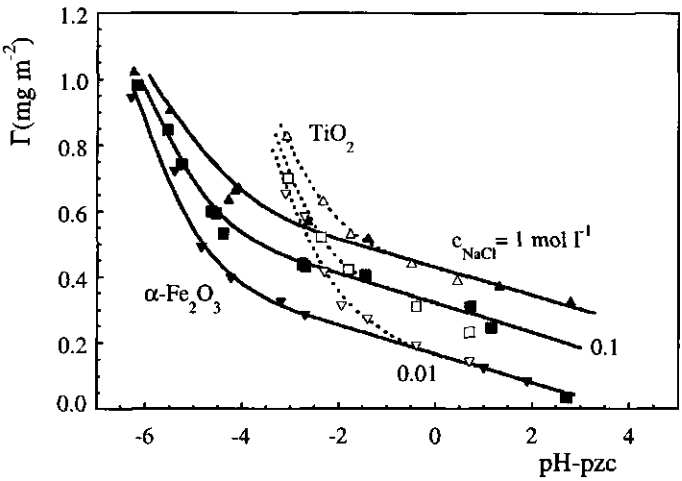

Figure 4.9 Plateau values in CMC adsorption on rutile and hematite as a function of the pH relative to the point of zero charge of the bare surface.

CMC at low pH was also investigated for rutile in 0.01 mol l^{-1} NaCl (figure 4.8). As observed for the hematite surface a substantial pH increase is needed to facilitate desorption of CMC.

Also for rutile the question arises to what extent the surface area as determined by N_2 gasadsorption is accessible for CMC. In order to establish if porosity of the rutile surface affects the adsorption, measurements are performed for two molar masses (130 and 1100 kg mol^{-1}) and two solid-solution ratios (differing by a factor 5). It follows that the adsorbed amounts are equal, for both molar masses and solid-solution ratios. Since small molecules canenter pores more easily than large ones, a higher adsorption is expected for the low molecular CMC if pore size exclusion is of any importance. Because such a dependence is not observed, it can be concluded that the pore sizes are outside the range of the applied polymers.

For both hematite and rutile the adsorption increases with salt concentration for pH < pzc as well for pH > pzc. Van de Steeg et al. [38] investigated the adsorption of a polyelectrolyte on an oppositely charged surface. Depending on thenon-electrostatic contribution to the adsorption, they distinguish a regime where the adsorption is decreased upon increasing the electrolyte concentration (so called screening-reduced adsorption) and a regime where an increase in the adsorption is found when the electrolyte concentration is increased (screening-enhanced adsorption). The former regime is characterised by domination of electrostatical interactions between segments and the surface. In the latter regime the adsorption is determined by non-electrostatic interactions with the surface and lateral repulsion between charged segments. If the affinity for the surface is high enough, adsorption exceeding surface charge compensation can take place. On the other hand a surplus of

polymer charge causes lateral repulsion, which hampers the adsorption. Salt screens the lateral repulsion thereby facilitating higher adsorption. For low U_{ads} (0.3 kT) the adsorption is mainly screening-reduced, the screening-enhanced adsorption occurring at high U_{ads} (4 kT) [38]. In our experiments we always find an increase in the adsorption when the electrolyte concentration is increased. In van de Steeg's nomenclature the adsorption of CMC on rutile and hematite is thus of the screening-enhanced type, indicating a high affinity of CMC for both surfaces. A high affinity for the surfaces facilitates adsorption at pH > pzc where electrostatics work against the adsorption.

A comparison of the adsorption as a function of pH relative to the bare pzc (pH-pzc) for both oxides is given in figure 4.9. As shown, the adsorption on both oxides coincides for pH-pzc > -1, whereas below pH-pzc = -1 the curves diverge. From pH=5.5 on, CMC is fully dissociated, i.e. it behaves like a strong polyelectrolyte. As the pzc of rutile is situated at pH=5.8, the adsorption on rutile for pH-pzc > -1 (pH > 4.5) can be seen as the adsorption of a strong polyelectrolyte. It was shown by Fokkink et al. [44] that around pH=pzc the surface charge-(pH-pzc) curves of hematite and rutile coincide for different electrolyte concentrations. Potentiometric titrations reveal that such a behaviour also exists for the samples that were used in our experiments. For the hematite surface pH-pzc = -1 corresponds to pH=7.3, so to complete dissociation of CMC. Hence, with respect to electrostatics the conditions are comparable for both surfaces for pH-pzc > -1. The coincidence of the adsorption for pH-pzc > -1 indicates either that electrostatics dominate the adsorption or that the adsorption energy is identical for both surfaces. Though the adsorption energy has to be high in order to establish adsorption at pH, above pzc it is not likely that the adsorption energy for different surfaces is identical. So domination of electrostatics (mainly intramolecular repulsion) seems a more reasonable explanation for the observed adsorption behaviour. At pH-pzc < -1, CMC no longer behaves as a strong polyelectrolyte. Since the pzc's of both oxidic surfaces are situated at different pH values, the adsorption curves diverge due to a different degree of dissociation of CMC.

4.3.4 Kinetics of adsorption on TiO_2 (reflectometry)

The kinetics of CMC adsorption on TiO_2 was studied by reflectometry. The time dependent adsorption of CMC (ds=0.99) with different chain lengths (M_w=35 and 1200 kg mol^{-1}) is presented in figure 4.10. The pH was set at 3.5 and the concentrations of the NaCl solutions were 0.01 and 0.5 mol l^{-1}, respectively. In the adsorption process one can distinguish three stages. Initially the adsorption increases linearly in time. In this stage the rate of adsorption is solely determined by mass transfer from solution to the interface. For molecules with identical molar mass the initial adsorption rate appears to be slightly higher in the solutions with the highest electrolyte concentration. The diffusion coefficient is somewhat higher in 0.5 mol l^{-1} NaCl (molecules are less extended), thereby causing the flux of polymers

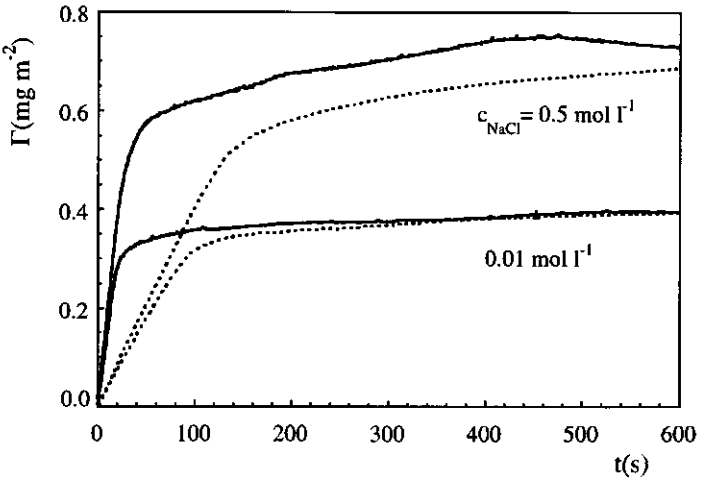

Figure 4.10 Time dependent adsorption of CMC ds=0.99 (10 mg l^{-1}) on TiO_2 at pH=3.5 (reflectometry). Electrolyte concentration indicated in figure. Solid curve: M_w=35 kg mol^{-1}, dashed curve: M_w=1200 kg mol^{-1}.

towards the surface to be somewhat higher. As the adsorption increases molecules approaching the surface will experience a gradually increasing hindrance. In this stage molecules are not able to adsorb directly after arriving in the proximity of the surface; the adsorption is no longer linear in time. The hindrance is caused by loops and tails of already adsorbed molecules, obstructing the approach towards the surface. In a previous paper [45] we paid attention to electrostatic hindrance in the adsorption process of a polyelectrolyte. Since we are dealing with highly charged molecules, an electrostatic hindrance is also likely to play a role in the kinetics of CMC adsorption, especially in 0.01 mol l^{-1}. The last stage in the adsorption process is characterised by flattening of the adsorption curve. Due to the high surface coverage the resistance to adsorption has increased to such an extent that the rate of adsorption becomes so low that the adsorbed amount hardly increases any more.

In order to assess to what extent electrostatics play a role in the kinetics we have applied our model [45] for the adsorption of a charged polymer on a (charged) surface. In this model we consider the resistance that a charged molecule encounters when approaching a (charged) surface. This quantity is composed of the resistance to motion in solution and to repulsiveelectrostatic forces that act in the proximity of the surface where adsorption takes place. The former can be obtained experimentally from reflectometry experiments, the latter is calculated numerically with the use of a lattice model [40]. In this way we can calculate the barrier for adsorption at different stages of the adsorption process (i.e. as a function of the adsorbed amount). Finally the adsorption as a function of time is obtained by solving the differential equation for the rate of adsorption numerically [45]. All interaction parameters,

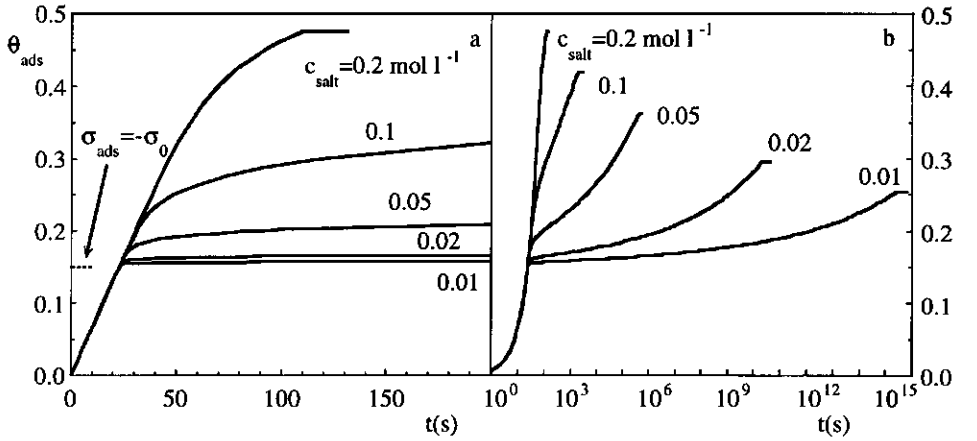

Figure 4.11 Calculated time dependent adsorption of a polyelectrolyte (10 mg l^{-1}) with a fixed charge density (one charge per segment) on an oppositely charged surface (230 mC m^{-2}). In figure a the adsorption is given on a time scale comparable with adsorption experiments, figure b shows the complete curve (i.e. time needed to reach equilibrium). The adsorption is expressed in equivalent monolayers.

except the interaction between polymer segments and the surface, were chosen zero. Relative permittivities were set to ε_r=80 for all components. Non-electrostatic interactions between polymer and interface were taken into account by incorporating an adsorption energy. As argued in the previous sections, CMC has a strong interaction with oxidic surfaces, therefore a high value (U_{ads}=5 kT) is used for the adsorption energy.

In figure 4.11 we show the calculated time-dependent adsorption of a strong polyacid (100 segments with each segment having a fixed charge -1) on an oppositely charged surface (constant charge density σ_0=230 mC m^{-2}) for five values of the ionic strength (0.01 to 0.2 mol l^{-1}) at 30 mg l^{-1} polymer concentration. Calculations were carried out for a cubic lattice, the adsorbed amount (θ_{ads}) is expressed in equivalent monolayers. The three stages mentioned above also show up in the calculated adsorption curves (figure 4.11a). An initial linear increase in the adsorption with time is observed for $\theta_{ads} \leq 0.15$ for all electrolyte concentrations. The surface coverage $\theta_{ads} = 0.15$ corresponds to compensation of the surface charge by adsorbed polyelectrolyte. As long as the surface charge is not compensated, the barrier for adsorption is low, repulsive forces between surface and polymer approaching the surface being absent. Beyond surface charge compensation, an electrostatic barrier builds up, which manifests itself in a (strong) decrease in the adsorption rate (i.e. adsorption is no longer linear in time). In the case of low electrolyte concentrations the adsorption rate changes rather abruptly, in 0.1 and 0.2 mol l^{-1} solutions a gradual increase in the adsorption is observed above surface charge compensation. Thus the presence of electrolyte reduces the barrier for

adsorption. This is further demonstrated by means of figure 4.11b where adsorption is plotted logarithmically as a function of time. In figure 4.11b endpoints refer to the adsorbed amount when full equilibrium is reached between adsorbed polymer and polymer in solution at 30 mg l^{-1}. For the highest electrolyte concentration, equilibrium is reached on a time scale that is comparable with experiments ($\approx 10^5$ s), at low concentrations extremely long periods are needed to reach equilibrium.

The adsorption curves given in figure 4.10 show a qualitative resemblance with our calculations. In case of 0.01 mol l^{-1} NaCl mass transport is the rate determining step up to 0.25 mg m^{-2} both for the high and the low molecular mass polymer. At high salt concentration the adsorption is transport limited up to 0.45 mg m^{-2} irrespective of the molar mass. As argued by Dijt et al. [46] mass transport is the rate determining step provided molecules are able to come very close to the surface without being disturbed by the adsorbed layer. If the barrier for adsorption would be solely determined by steric hindrance (as for neutral molecules), the divergence is expected to show up at the same adsorbed amount for different salt concentrations. As the layer thickness increases with the molecular mass (figure 4.5), already adsorbed high M CMC will obstruct the adsorption to a higher extent than low M CMC. So, if only steric hindrance plays a role, deviation from the initial adsorption rate is expected to occur at a higher adsorbed amount for the low M CMC. Though both CMCs differ considerably in M, this is not observed clearly. Hence we can conclude that steric hindrance is not the dominant factor determining the kinetics of CMC adsorption. Furthermore, from figure 4.10 it can be seen that the adsorption rate is diminished to a lower extent for the high salt concentration. This is also observed from the model calculations,

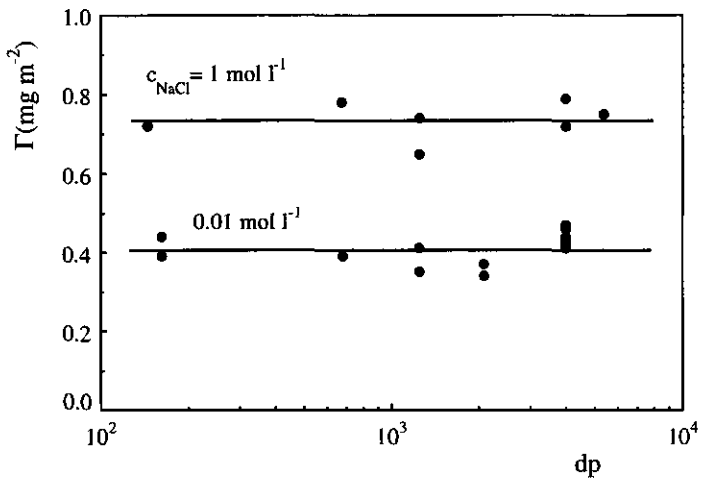

Figure 4.12 Chain length dependence of the plateau adsorption of CMC (ds=1.25) on TiO_2 at pH=4 and two concentrations NaCl (indicated in figure). The length is represented by the degree of polymerisation (dp). Adsorption is determined by reflectometry.

which again illustrate that electrostatics are important in the adsorption kinetics of CMC.

In the previous paragraphs we have already mentioned that the adsorbed amount is not affected by the molar mass of CMC. An overall summary of plateau values as determined by reflectometry is shown in figure 4.12, where the adsorption is given as a function of the chain length (degree of polymerisation, dp) at pH=4 for two salt concentrations. Figure 4.12 clearly corroborates that the adsorption is not affected by the chain length over a broad range. Since all experiments were obtained by reflectometry, exclusion of polymers by surface pores cannot influence the adsorption behaviour. For low salt concentration no chain length dependence is expected; mutual repulsion between charged segments can only be compensated by gaining adsorption energy in the first layer. By doing so molecules will adsorb in a flat conformation. However at 1 mol l^{-1} NaCl charges are highly screened, so repulsion between segments is small. Considering CMC at high salt concentration as a neutral polymer, a dependence on the dp is expected. However, such a dependence is missing, indicating a flat conformation of the adsorbed layer. Assuming close packing of adsorbed chains (chains lying precisely next to each other), using 0.52 nm [39] and 0.5 nm as the length and the radius of a monomeric unit, respectively, the adsorbed amount corresponding to a close packed monolayer is estimated at 0.8 mg m^{-2}. In 1 mol l^{-1} NaCl the adsorption amounts to 0.76 mg m^{-2}, which would correspond to a close packed monolayer. In reality such a situation cannot be reached, which means that the conformation of adsorbed CMC in 1 mol l^{-1} NaCl includes some loops and tails. On account of the non-dependence of the adsorption on the molecular mass we conclude that CMC adsorbs in a relatively flat conformation; the surface is highly covered and the majority of segments is situated close to the surface in trains and short loops. The size of the loops is not affected by the chain length.

4.3.5 Electrophoretic mobility of CMC covered TiO_2

In figure 4.13 the electrophoretic mobility u of CMC (ds=1.25, M_w=130 and 1100 kg mol^{-1}) covered and bare rutile particles in 0.01 mol l^{-1} NaCl is shown as a function of the pH. Though the thickness of the adsorbed layer increases with the molar mass, thereby increasing the friction of the covered particles, the electrophoretic mobility increases with molar mass. The electrophoretic mobility is determined by the charge within the slip plane (surface of shear). For bare particles this plane coincides with the Stern plane [47]. For particles covered with polymer the surface of shear will be beyond the Stern plane due to loops and tails protruding into the solution. Reasoning that also the rutile charge, like that of hematite, is completely screened by the polyelectrolyte and small counterions, it is clear that the charge of the loops and tails has to determine the electrophoretic mobility of the CMC covered particles. This is corroborated by the following. Similar experiments as with CMC ds=1.25 have been carried out with CMC ds=0.75 M_w= 190 and 1100 kg mol^{-1} (not shown in figure 4.13). Qualitatively the dependence of the mobility on pH resembles that of CMC

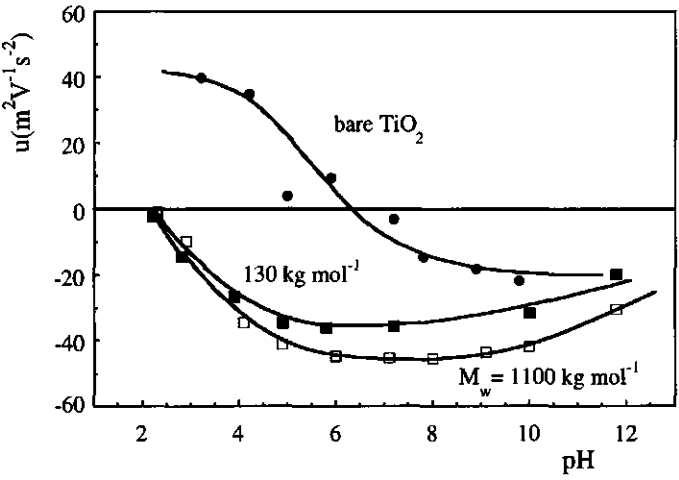

Figure 4.13 Electrophoretic mobility of CMC (ds=1.25, molar mass indicated in figure) covered and bare rutile particles as a function of pH in 0.01 mol l^{-1} NaCl.

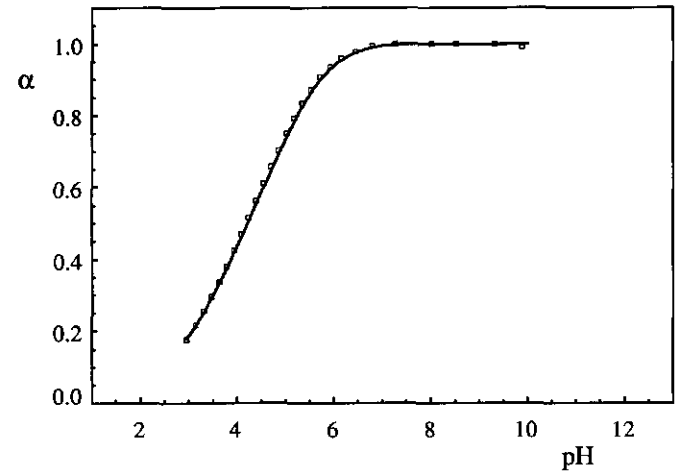

Figure 4.14 Degree of dissociation (α) of CMC ds=1.25 in 0.01 mol l^{-1} NaCl.

ds=1.25, but the mobility is somewhat lower (i.e., less negative). As the charge density of CMC ds=0.75 is lower, the mobility of the covered rutile particles is also lower. Though the thickness of the adsorbed layer increases with the molar mass, thereby increasing the friction of the covered particles, the electrophoretic mobility increases with molar mass (i.e., with the length of the chain). As we argued in the previous section that the size of the loops is not affected by the chain length, we can conclude that the tails determine differences in mobility.

The corresponding pH dependence of the degree of dissociation (α) of CMC ds=1.25 in 0.01 mol l^{-1} NaCl is shown in figure 4.14 (the dissociation does not depend on M_w) [16]. As

shown in this figure, at pH=6 CMC is fully dissociated, i.e. the charge of the polymer does not increase upon a pH increase anymore. Reasoning that the mobility is determined by both tails and loops, the increase in the mobility from pH=2 to 6 is due to increasing dissociation of tails and loops. In the pH range from 6 to 8 the mobility reaches a steady value. Increasing the pH above 8 causes CMC to desorb and accordingly the mobility to decrease. At high pH the mobility equals that of the bare particles, indicating that at high pH no adsorbed CMC is present at the rutile surface anymore.

4.3.6 Adsorption of CMC on variable charged surfaces

On both hematite and rutile a linear dependence of the adsorption on pH is observed for pH-pzc > -1 (figure 4.9). With respect to this linear dependence, in this section we will separate generic features in the adsorption mechanism due to charge compensation from those that cause higher adsorption than surface charge compensation. In general, electrostatics are a very complicated factor, both in the kinetics as well as in the equilibrium properties of polyelectrolyte adsorption. Characteristic for adsorption of a weak polyelectrolyte on a variable charged surface is that additional charges are induced on the surface as well as on the polyelectrolyte, that is, the presence of a negative polyelectrolyte near the surface leads to an increase of positively charged groups on the surface and a positive surface increases the degree of dissociation of the polyelectrolyte. The effect of polyelectrolyte adsorption on the surface charge is illustrated in figure 4.15. In this figure the charge density of a variable charged surface (σ_{0p}) is given as a function of the adsorbed amount of a strong polyelectrolyte

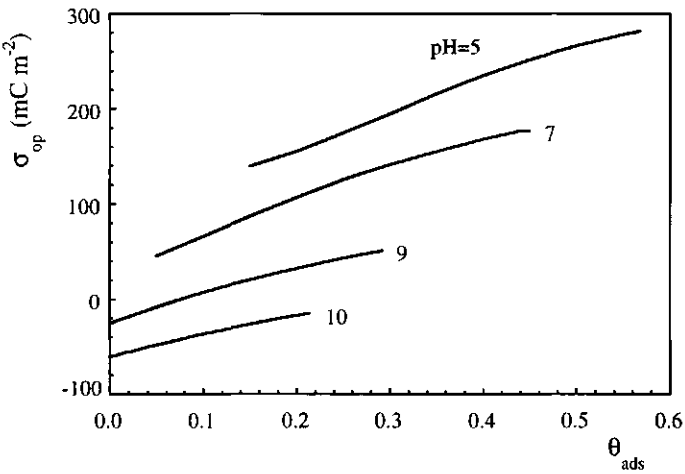

Figure 4.15 Calculated surface charge density of a variable charged surface (pzc=8) in 0.05 mol l^{-1} 1-1 electrolyte solution as a function of the adsorption of a strong polyelectrolyte. The adsorption is expressed in equivalent monolayers.

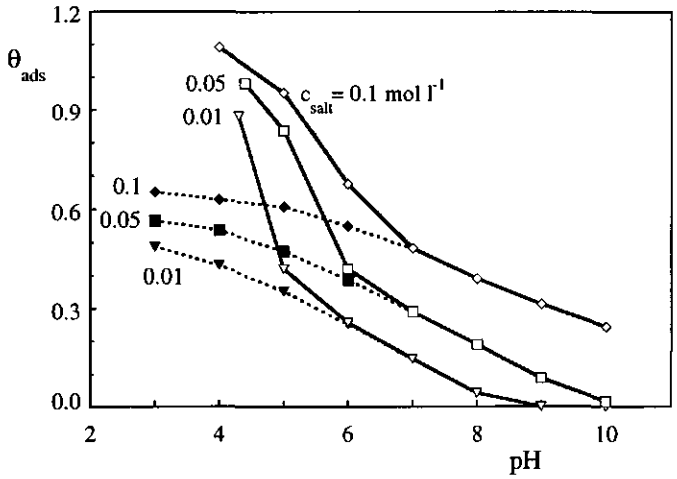

Figure 4.16 Calculated adsorption at 10^5 s of a strong polyelectrolyte (dotted curves) and a weak polyacid ($pK_{½}$=4, solid curves) on a variable charged surface (pzc=8). The adsorption was calculated for a polymer concentration of 10 mg l^{-1} as a function of pH at three 1-1 electrolyte concentrations (indicated in figure).

at 0.05 mol l^{-1} 1-1 electrolyte for four pH values. All data were calculated with the use of a lattice model [9,40]. Surface sites were modelled as segments with pK=8, that is, the pzc of the surface is at pH=8. The polyelectrolyte is modelled as a chain consisting of 100 segments, each segment having a constant charge of -1 and an adsorption energy of 5 kT. Clearly, figure 4.15 shows that the surface charge can adjust itself to adsorption, i.e. an increase of charge is observed when the bare surface charge is positive (pH=5 and pH=7). Above the pzc the surface becomes less negative (pH=10) or even changes in to a positive value (pH=9).

Vermeer et al. [48] theoretically investigated the adsorption of a weak polyelectrolyte on a surface with variable charge. Their calculations show a linear pH dependence of the adsorbed amount for pH values above $pK_{½}$ of the polyelectrolyte (i.e. where the weak polyelectrolyte behaves as a strong polyelectrolyte). The adsorbed amount is only slightly dependent on the electrolyte concentration. With respect to CMC adsorption, however, a distinct dependence on the electrolyte concentration is observed. The calculations of Vermeer et al. relate to the condition where the adsorbed polymer is at equilibrium with polymer in solution. However, as we demonstrated in a previous paragraph the time to reach such an equilibrium may be considerable. We therefore applied the model of ref. 45 to calculate the time dependent adsorption of both a polyelectrolyte with fixed charge (-1 per segment) and a polyelectrolyte that has dissociable groups ($pK_{½}$=4) on a surface with pzc=8, at a concentration of 10 mg l^{-1}. Both polyelectrolytes were modelled as chains consisting of 100 segments, where for each segment U_{ads}= 5 kT. From the model calculations the adsorption on the time scale of an experiment (10^5 s) is obtained. Adsorption at 10^5 s as a function of pH for

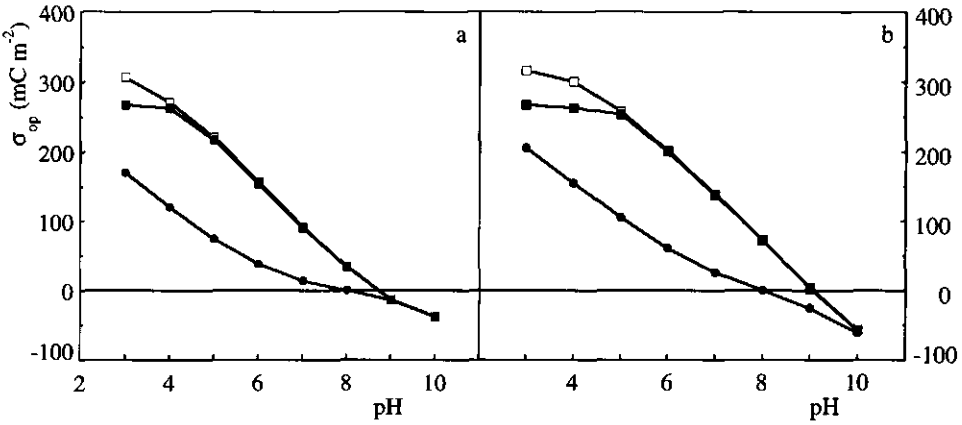

Figure 4.17 Calculated surface charge density of a variable charged surface as a function of pH in 0.01 mol l^{-1} (figure a) and 0.05 mol l^{-1} (figure b) 1-1 electrolyte solution. The lower curve (●) refers to the bare surface charge, the upper curves relate to the charge density when a strong polyelectrolyte (□) or a weak polyacid (■) is adsorbed. The adsorbed amounts correspond with those in figure 4.16.

three 1-1 electrolyte concentrations (0.01-0.1 mol l^{-1}) is given in figure 4.16. As shown, the adsorption decreases nearly linearly with pH for pH > 7. The slope has a slight dependence on the electrolyte concentration, the adsorbed amount itself being salt dependent. To understand the observed linear dependence, we will first explore the surface charge in the presence of adsorbed polyelectrolyte. In figure 4.17 we have plotted the surface charge in the presence of adsorbed polyelectrolyte after 10^5 s (i.e. corresponding to an adsorbed amount as given in figure 4.16) as a function of pH for two electrolyte concentrations. For comparison the bare surface charge, i.e. without adsorbed polyelectrolyte, is also given. Again, figure 4.17 illustrates that adsorption significantly influences the surface charge. The bare surface charge is not linear in pH. However, in the presence of adsorbed polyelectrolyte the surface charge depends linearly on pH for pH > 6. Our model calculations show $d\sigma_{0p}/dpH$ to be equal to 56 mC m^{-2}, irrespective of the electrolyte concentration. The magnitude of σ_{0p}, however, depends on the electrolyte concentration. On comparison of the charge of the adsorbed amount with the surface charge it turns out that the former is composed of the surface charge, σ_{0p} plus an excess amount. Comparing the data in figures 4.16 and 4.17 it appears that for the strong polyelectrolyte the excess adsorbed charge does not depend on pH over the whole pH range but increases with the electrolyte concentration. As the charge density of the strong polyelectrolyte is constant, the excess adsorbed amount is also non-dependent on pH. The charge density of the weak polyacid, however, depends on pH and the distance from the surface [9]. Therefore, the excess adsorbed amount is not constant for low pH (i.e., it increases with pH). For simplicity we will restrict our discussion to the linear region, where the polyacid acts as a strong polyelectrolyte.

Table 4.1 Characteristic slope of the adsorbed charge with pH at fixed 1-1 electrolyte concentration in pH region near pzc of the bare surface. Comparison of data.

system			
polyelectrolyte	substrate	$(\partial\sigma_{ads}/\partial pH)_c$ (mC m^{-2})	Ref.
weak polyacid (calculated)	Nernstian surface	56	this work
CMC	TiO_2 and α-Fe_2O_3	17	this work
AMA [(1)]	TiO_2	73	23
AMA$^+$ [(2)]	TiO_2	22	23
polyacrylic acid	TiO_2	20	49
polyacrylic acid	α-Fe_2O_3	58	49
HPAM [(3)]	TiO_2	10	33
HPAM [(3)]	Fe_2O_3	7	37

(1) AMA: polydimethylaminoethyl methacrylate; (2): AMA+: polytrimethylammoniumethyl methacrylate; (3) HPAM: hydrolysed polyacrylamide.

As stated in one of the previous paragraphs, polyelectrolytes approaching an equally charged surface experience an electrostatic repulsion. This barrier slows down the adsorption process. Parameters that affect the height of the barrier are the net charge at the interface (i.e., the sum of the surface charge σ_{0p} and the adsorbed charge) and the charge density of the chain that approaches the surface [45]. As long as the net charge is positive, i.e. the surface charge is not compensated, there is no electrostatic barrier for adsorption. Our calculations indicate that the time needed to accomplish surface charge compensation is short compared to the time of an adsorption experiment (see figure 4.11). Upon increasing adsorption the surface charge becomes overcompensated, thereby strongly reducing the rate of adsorption. Now the net charge at the interface regulates the adsorption rate, i.e. the excess adsorption determines the amount of overcompensation in time. Although the surface charge adjusts itself to adsorption (which lowers the barrier) model calculations (not shown here) indicate that the amount of excess charge increases with adsorption. Thus, the barrier for adsorption increases with adsorption. Because salt lowers the barrier, adsorption will increase more rapidly in time with increasing electrolyte concentration. This mechanism explains why the excess adsorption is constant in pH (i.e. it is not determined by the bare surface charge) but increases with electrolyte concentration. As the surface charge depends linearly on pH and the excess adsorbed amount is not affected by pH the adsorption becomes also linear in pH for pH > 7. Unlike the calculations of Vermeer et al. [48] (which relate to equilibrium), our model calculations show a reasonable qualitative agreement with CMC adsorption. The former show a slight dependence of the adsorbed amount on the electrolyte concentration, whereas the latter show a clear dependence. With respect to the adsorption of CMC we conclude that in the linear region the adsorbed amount is very likely not at equilibrium with polymer in solution. The electrostatic barrier prevents reaching equilibrium on the time scale of an experiment. At low pH the charge on the CMC chain is lower, hence the electrostatic barrier

is less high. So, in our opinion, at low pH equilibrium is reached on the time scale of an experiment. Thus, the pH dependence can be explained satisfactorily by our calculations. The logarithmic dependence of the electrolyte concentration, however, is not correctly described. The origin is possibly related, as we argued in a previous paper [45], to the smearing out of charges. In the lattice model charges are smeared out, whereas in real systems this is not the case. The smearing out will be a reasonable approximation for high coverages. At low adsorption domains on the surface exist that are not covered with polyelectrolyte. Approaching such a domain may lead to adsorption, whereas in the mean field approximation it can not. So, the model tends to underestimate the adsorption, especially for low concentrations of electrolyte.

4.3.7 Capacitor properties applied to CMC adsorption

For the surfaces discussed in this paper a linear dependence of Γ on pH in the pH region near the bare surface pzc has also been found for other polyelectrolytes. Some relevant data are summarised in table 4.1. In order to compare these data the slope $d\Gamma/dpH$ is converted to $d\sigma_{ads}/dpH$, where σ_{ads} is the adsorbed charge of the polyelectrolyte. As the data in table 4.1 show, no unique number is found for the slope $d\sigma_{ads}/dpH$. The linearity between σ_{0p} and pH indicates that the surface and the compensating charge of the polyelectrolyte in the first layer behave as a capacitor. The analogy with capacitor properties was used by Hoogeveen et al. [23] to interpret their adsorption data. In their approach the interface with adsorbed polymer is divided into two Stern layers, each treated as a condenser. The surface charge in the presence of adsorbed polymer (σ_{op}) is assigned to the inner condenser. The outer condenser has a charge $\sigma_{op}+\sigma_{ads}$, where σ_{ads} is the adsorbed polymer charge given by $-\Gamma F ds\alpha/M_0$, M_0 representing the molar mass of a monomeric unit. If both Stern-layers are assumed to be free of charge the potential difference between the potential at the surface (ψ_{0p}) and the outer Stern-layer (ψ_s) can be expressed in terms of two molecular condensers in series, with thicknesses d_1 and d_2 and permittivities ε_1 and ε_2 [23]

$$\psi_{0p} - \psi_s = \sigma_{op}\frac{d_1}{\varepsilon_1} + \left(\sigma_{op} + \sigma_{ads}\right)\frac{d_2}{\varepsilon_2} \qquad (4.4)$$

Using this equation we can quantify the slope $d\Gamma/dpH$. The adsorbed charge σ_{exc} that overcompensates the surface charge is counterbalanced by the charge in the diffuse double layer (σ_d) which in first approximation is related to ψ_s by $\psi_s=-\sigma_d/\varepsilon\kappa=\sigma_{exc}/\varepsilon\kappa$, where ε is the permittivity of the solution and κ the inverse Debye length. Using this relation and realising that $\sigma_{ads}=-\sigma_{op}+\sigma_{exc}$ one can write for σ_{ads}

$$\sigma_{ads} = \frac{\varepsilon_1}{d_1}\left(\frac{\kappa^{-1}}{\varepsilon} + \frac{d_1}{\varepsilon_1} + \frac{d_2}{\varepsilon_2}\right)\sigma_{exc} - \frac{\varepsilon_1}{d_1}\psi_{0p} \qquad (4.5)$$

Assuming that close to the pzc ψ_{0p} is related to the pH by Nernst's law (ψ_{0p}=(2.3RT/F)(pzc-pH)) one can easily show that the change in the adsorption at constant electrolyte concentration is given by

$$\left(\frac{\partial\Gamma}{\partial pH}\right)_\kappa = -\frac{2.3\,RT}{F^2}\,\frac{M_0}{ds\alpha}\,\frac{\varepsilon_1}{d_1} \qquad (4.6)$$

In the derivation of equation 4.6 we have used the relation $\sigma_{ads} = -\Gamma F ds\alpha/M_0$ and the fact that σ_{exc} does not depend on pH, but is influenced by c_{salt}. Furthermore it is assumed that the degree of dissociation (α) does not depend on the pH or the electrolyte concentration, which is reasonable for pH > 5.5 (see figure 4.14). Equation 4.6 predicts the change in adsorption with pH to be independent of the electrolyte concentration. As can be seen from figure 4.9 this is observed indeed from our depletion experiments. From figure 4.9 it follows that $(\partial\Gamma/\partial pH)_\kappa$ equals -0.044 mg m^{-2}. Taking for d_1 the radius of a CMC chain (~ 1 nm [16]) and a reasonable value for the relative dielectric constant in the first Stern layer (ε_r=20), for CMC (ds=0.99) we calculate from equation 4.6 $(\partial\Gamma/\partial pH)_\kappa$ =-0.028 mg m^{-2}, which is in reasonable agreement with our experiments. Equation 4.6 might account for the different values of the slope $(\partial\sigma_{ads}/\partial pH)_\kappa$ as given in table 4.1. As the slope is affected by both d_1 (which is connected to the radius of the polymer backbone) and ε_1 (which depends on the composition of the polymer and the substrate) different numbers for the slope are expected for different combinations of polyelectrolyte and substrate. Despite the crude approximations the model gives a reasonable qualitative (and semi-quantitative) description of the experimental data.

The model implies that the layer adjacent to the surface only contains polymer segments. Any presence of counterions is not taken into account. However, it is not unlikely that counterions are present in the proximity of the polyelectrolyte. These counterions would lower the effective charge of the polymer near the surface in such a way that CMCs varying in ds can have an effectively identical charge density. Screening of charge is well known as counterion condensation for polyelectrolytes in solution [50]. The effective charge density of the polyelectrolyte is not incorporated in the model it would, however, offer a possible explanation for the non-dependence of the adsorption on ds. The independence on ds is further illustrated by means of figure 4.18. In this figure the adsorptions of CMC and oxidised pullulane on TiO_2 in 0.01 mol l^{-1} NaCl as obtained by reflectometry is given at pH=3 and pH=5. The oxidised pullulane samples were prepared by selective oxidation of hydroxyl groups at the 6-position of the pullulane glucose units [51]. As can be seen the adsorption does not depend on the degree of substitution when $ds \geq 0.5$. Since pullulane may be considered as a flexible polysaccharide (its intrinsic persistence length amounts to

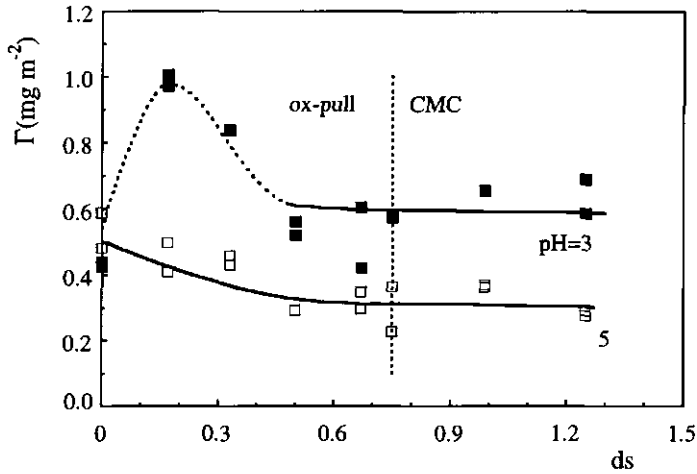

Figure 4.18 Adsorption of CMC and oxidised pullulane (ox-pull) on TiO_2 in 0.01 mol l^{-1} NaCl at pH=3 and pH=5. Measurements were carried out by reflectometry. Points to left of the vertical line refer to adsorption of oxidised pullane, points to the right to adsorption of CMC.

1.3-1.9 nm [52]) the non-dependence is not likely to be connected to the stiffness of the backbone of the polysaccharide. A (nearly) non-dependence of ds in the adsorption of CMC was also observed by Williams et al. [6]. At pH=6.5 they measured the adsorption on $BaSO_4$ in water (no salt was added to the solutions) as 0.45, 0.22, and 0.18 mg m^{-2} for samples with ds=0.45, 0.78, and 1.27 (M_w=250 kg mol^{-1}), respectively. The difference in adsorption between the samples with highest ds is small, which is also found for the adsorption of CMC on rutile and hematite. Furthermore an adsorption behaviour as given in figure 4.18 is also observed by Böhmer et al. [53]. These authors investigated the adsorption of poly vinyl imidazole with different degree of quarternatisation (dq) on silica and yttrium oxide (Y_2O_3) in 0.001 to 0.1 mol l^{-1} KNO_3. On SiO_2 the adsorption shows a broad maximum for dq < 0.15, at higher dq (0.35) the adsorption is nearly independent on dq. For Y_2O_3 also a distinct maximum is observed for dq < 0.15, no dependence of dq is found when dq > 0.15.The kinetics of desorption is connected to both the strong interaction of CMC with the oxidic surface and the rigidity of the backbone. After adsorbing at low pH a substantial increase of the pH is needed to desorb the strongly attached polyelectrolyte from a surface. If the polyelectrolyte is flexible, detachment can take place, in principle, segment by segment. Due to the rigidity of the CMC backbone, however, several bonds to the surface need to be broken simultaneously. The number of bonds to be broken is proportional to the local stiffness of the backbone, characterised by the persistence length (L_p=15 nm [16]), and amounts to about L_p/b = 15 nm/0.52 nm = 29, where b = 0.52 nm [39] is the length of a glucose unit. So, in order to establish simultaneous breaking of a number of strong bonds with the surface a high surplus of adsorbed charge is needed, which manifests itself in desorption of CMC only after

a substantial pH increase.

The strong interaction of CMC with the surface is most likely the result of the formation of ion pairs between CMC carboxylic groups and positively charged surface sites. Strong interaction may also take place due to the formation of a chemical bond between metal ions and glucose hydroxylgroups at the C-2 and C-3 positions. The formation of such a complex has been concluded from infrared measurements by Lui et al. [54] for the adsorption of dextrin on lead hydroxide and by Khosla et al. [55] for the adsorption of starch on hematite. Possibly such a type of interaction is also present in case of CMC adsorption on hematite and rutile.

4.4 Conclusions

The adsorption of CMC on TiO_2 and α-Fe_2O_3 shows features that are commonly encountered in polyelectrolyte adsorption. The adsorbed amount increases with electrolyte concentration and decreases with pH, indicating that electrostatics plays a role in the adsorption process. As below the pzc the surface charge of the substrates increases upon decreasing pH, under these conditions increasing amounts of polymer charge can be accommodated at the surface. Electrolyte screens the charges of the accumulated segments at the surface thereby facilitating higher adsorption. Despite the importance of electrostatics in the adsorption, no influence of the degree of substitution on the adsorption is observed. Probably the presence of counterions near the polymer chain causes screening of charges, which results in a constant effective charge density for all ds.

In both 0.01 mol l^{-1} and 1 mol l^{-1} no dependence of the adsorbed amount of CMC on M_w is observed, which indicates that CMC adsorbs in a flat conformation. From dynamic light scattering experiments, however, a substantial layer thickness is observed. Segments of adsorbed CMC are mainly situated in trains, but apparently a limited amount is present in the form of tails.

A linear dependence of the adsorbed amount on pH near pH=pzc is observed. This linearity is characteristic for the adsorption of a polyelectrolyte on a surface with dissociable hydroxyl groups. As a result of the presence of charged segments at the surface, the surface charge is adjusted such that it becomes linear in pH. In first instance, surface charge is compensated by CMC. However, due to high affinity of CMC for the surface, overcompensation takes place. The amount of overcompensation is mainly determined by the kinetics of the adsorption process. Its magnitude is not affected by the pH but is influenced by the electrolyte concentration.

A distinct hysteresis in the adsorption with respect to pH is observed. When the pH is increased after adsorption at low pH, desorption takes place only after the pH is increased substantially. The arduous desorption originates from a strong interaction with the surface and

is enhanced by the chain rigidity of the CMC backbone. This hysteresis may have important practical consequences. A significant increase in the colloidal stability of rutile or hematite at high pH can be achieved by first adsorbing CMC at low pH and subsequently increasing the pH to the required value. This can, for example, have important implications in papermaking, where rutile is frequently applied as pigment to improve the opacity of paper [56,57]. To ensure optimal realisation it is essential that the pigments are sufficiently stabilised against flocculation by other coating ingredients. In the process of papermaking, pigments are usually added at high pH [57]. With adsorbing CMC at low pH and subsequently increasing the pH the colloidal stability during the coating process can be significantly enhanced. CMC has excellent binding strength [57], which implies that it is capable to penetrate into the cellulose network. The (long) tails are able to penetrate into the network thereby facilitating anchoring the pigments on the paper.

Acknowledgement

The authors want to thank Dr. A.E.J. de Nooy for kindly placing oxidised pullulane samples to our disposal.

References

1. M. Grayson, *Encyclopaedia of Chemical Technology Vol. 5*, John Wiley & Sons, New York (1979).
2. R.L. Whistler, J.N. BeMiller, *Industrial Gums, Polysaccharides and Their Derivatives 2th Ed*, Academic Press, London (1973).
3. H.C.W. Foerst, H. Buchholz-Meisenheimer, *Ullmans Encyklopädie der technischen Chemie*, Urban & Schwarzenberg, Berlin (1970).
4. AQUALON CO, U.S. Patent US 4948-430-A (1990).
5. A. Nag, B. Sadhukhan, and D.K. Chattoraj, *J. Surface Sci. Technol.* **4** (1988) 91.
6. P.A. Williams, R. Harrop, G.O. Phillips, G. Pass, and I.D. Robb, *J. Chem. Soc., Faraday Trans. 1* **78** (1982) 1733.
7. D.R. Bain, M.C. Cafe, I.D. Robb, and P.A. Williams, *J. Colloid Interface Sci.* **88** (1982) 467.
8. E.P.G. Arêas and F. Galembeck, *J. Colloid Interface Sci.* **147** (1991) 370.
9. G.J. Fleer, M.A. Cohen Stuart, J.M.H.M. Scheutjens, T. Cosgrove, B. Vincent, *Polymers at Interfaces*, Chapman & Hall, London (1993).
10. Y.G. Bérubé and P.L. de Bruyn, *J. Colloid Interface Sci.* **27** (1968) 305.
11. J. Ragai and W. Lotfi, *Colloids and Surfaces* **61** (1991) 97.
12. A. Breeuwsma, *Adsorption of ions on hematite (α-Fe_2O_3)*, Ph.D. thesis, Wageningen University (1973).
13. S.J. Gregg and K.S.W. Sing, *Adsorption, Surface Area and Porosity 2th Ed.*, Academic Press, London (1982).
14. T. Hiemstra, J.C.M. de Wit, and W. van Riemsdijk, *J. Colloid Interface Sci.* **133** (1989) 105.
15. J. Westfall and H. Hohl, *Adv. Colloid Interface Sci.* **12** (1980) 265.
16. C.W. Hoogendam, A. de Keizer, M.A. Cohen Stuart, B.H. Bijsterbosch, J.A.M. Smit, J.A.P.P. van Dijk, P.M. van der Horst, and J.G. Batelaan, accepted by *Macromolecules*; chapter 2 in this thesis.

17. H. Struszczyk, K. Wrzesniewka-Tosik, D. Ciechanska and E. Wesolowska in *Cellulose and cellulose derivatives: Physico-chemical aspects and industrial applications*, J.F. Kennedy, G.O. Phillips, P.O. Williams and Lennart Piculell (Eds), Woodhead Publishing Limited, Cambridge (1995).
18. H.M. Spurlin, *J. Am. Chem. Soc.* **61** (1939) 2222.
19. J. Reuben and H.T. Conner, *Carbohydr. Res.* **115** (1983) 1.
20. M. Dubois, K.A. Gillis, J.K. Hamilton, P.A. Rebers, and F. Smith, *Anal. Chem.* **28** (1956) 350.
21. J.C. Dijt, M.A. Cohen Stuart, J.E. Hofman, and G.J. Fleer, *Colloids Surfaces* **51** (1990) 141.
22. J.C. Dijt, M.A. Cohen Stuart, and G.J. Fleer, *Adv. Colloid Interface Sci.* **50** (1994) 79.
23. N.G. Hoogeveen, M.A. Cohen Stuart, and G.J. Fleer, *J. Colloid Interface Sci.* **182** (1996) 133.
24. W.N. Hansen, *J. Optical Soc. Am.* **58** (1968) 380.
25. M. Rinaudo, J. Danhelka, and M. Milas, *Carbohydrate Polymers* **21** (1993) 1.
26. R. Pecorea, *Dynamic Light Scattering, Applications of Photon Correlation Spectroscopy*, Plenum Press, New York (1985).
27. D.E. Koppel, *J. Chem. Phys.* **57** (1972) 4814.
28. N.H.G. Penners, *The preparation and stability of homodisperse colloidal haematite (α-Fe_2O_3)*, Ph..D. Thesis, Wageningen University (1985).
29. C.W. Hoogendam, J.C.W. Peters, R. Tuinier, A. de Keizer, M.A. Cohen Stuart, B.H. Bijsterbosch, accepted by *J. Colloid Interface Sci*; chapter 6 in this thesis.
30. W. Brown and R. Rymden, *Macromolecules* **19** (1986) 2942.
31. M.A. Cohen Stuart, J.M.H.M. Scheutjens, and G.J. Fleer, *J. Polym. Sci.* **18** (1980) 559.
32. F.H. Chowdhury and S.M. Neale, *J. Polym. Sci. A* **1** (1963) 2881.
33. G. Girod, J.M. Lamarche, and A. Foissy, *J. Colloid Interface Sci.* **121** (1987) 265.
34. P.E. Williams, R. Harrop, G.O. Phillips, G. Pass, and I.D. Robb, *J. Chem. Soc., Faraday Trans. 1* **78** (1982) 1733.
35. O.A. Evers, G.J. Fleer, J.M.H.M. Scheutjens, and J. Lyklema, *J. Colloid Interface Sci.* **111** (1986) 446.
36. J. Blaakmeer, M.A. Cohen Stuart, and G.J. Fleer, *Macromolecules* **23** (1990) 2301.
37. A.K. Bajpai and S.K. Bajpai, *Colloid Polym. Sci.* **273** (1995) 1028.
38. H.G.M. van de Steeg, M.A. Cohen Stuart, A. de Keizer, and B.H. Bijsterbosch, *Langmuir* **8** (1992) 2538.
39. E. Ott, H.M. Spurlin, and M.W. Grafflin, *Cellulose Part II, 2th ed.*, Interscience Publishers, New York (1963).
40. M.R. Böhmer, O.A. Evers, and J.M.H.M. Scheutjens, *Macromolecules* **23** (1990) 2288.
41. J. Meadows, P.A. Williams, M.J. Garvey, R.A. Harrop, and G.O. Phyllips, *Colloids Surfaces* **32** (1988) 275.
42. V.A. Hackley, *J. Am. Ceram. Soc.* **80** (1997) 2315.
43. J. Meadows, P.A. Meadows, M.J. Garvey, R. Harrop, and G.O. Philips, *J. Colloid Interface Sci.* **132** (1989) 319.
44. L.G.J. Fokkink, A. de Keizer, and J. Lyklema, *J. Colloid Interface Sci.* **127** (1989) 116.
45. M.A. Cohen Stuart, C.W. Hoogendam, and A. de Keizer, *J. Phys.: Condens. Matter* **9** (1997) 7767; chapter 3 in this thesis.
46. J.C. Dijt, M.A. Cohen Stuart, J.E. Hofman, and G.J. Fleer, *Colloids Surfaces* **51** (1990) 141.
47. J. Lyklema, *Fundamentals of Interface and Colloid Science Volume II: Solid-Liquid Interfaces*, Academic Press, London (1995).
48. A.W.P. Vermeer, F.A.M. Leermakers, and L.K. Koopal, *Langmuir* **13** (1997) 4413.
49. J.E. Gebhart and D.W. Fuerstenau, *Colloids and Surfaces* **7** (1983) 221.
50. T. Odijk, *Biopolymers* **18** (1979) 3111.
51. A.E.J. de Nooy, A.C. Besemer, and H. van Bekkum, *Carbohydr. Res.* **269** (1995) 89.

52. A.E.J. de Nooy, A.C. Besemer, H. van Bekkum, J.A.P.P. van Dijk, and J.A.M. Smit, *Macromolecules* **29** (1996) 6541.
53. M.R. Böhmer, W.H.A. Heesterbeek, A. Deratani, and E. Renard, *Colloids and Surfaces A* **99** (1995) 53.
54. Q.I. Lui and J.S. Laskowski, *J. Colloid Interface Sci.* **130** (1988) 101.
55. N.K. Khosla, R.P. Bhagat, K.S. Gandhi, and A.K. Biswas, *Colloids and Surfaces* **8** (1984) 321.
56. K.W. Britt (Ed.), *Handbook of Pulp and Paper Technology 2th ed.*, Van Nostrand Reinhold Company, New York (1970).
57. J.P Casey (Ed.), *Pulp and Paper, Chemistry and Chemical Technology 2th ed. vol. IV*, John WIley & Sons, New York (1983).

Chapter 5

Adsorption of cellulose derivatives on inorganic oxides

Abstract

Adsorption of hydroxyethyl cellulose (HEC) and quaternary ammonium substituted HEC (QNHEC) on silica and titanium dioxide has been investigated as a function of pH and electrolyte (NaCl) concentration. Adsorbed amounts have been determined by means of reflectometry.

Adsorption of HEC on SiO_2 is constant up to pH=5. At higher pH the adsorption decreases, which is most pronounced at high (0.5 mol l^{-1}) electrolyte concentration. The thickness of the adsorbed layer, obtained by dynamic light scattering, is substantial. This indicates an adsorbed layer with extended conformation having loops and (few) long tails protruding into the solution and possibly having loops. Adsorption on TiO_2 in 0.01 mol l^{-1} NaCl decreases monotonously with increasing pH. In 0.5 mol l^{-1} NaCl the adsorption is constant up to pH=10, beyond which it decreases rapidly. Mechanisms of binding to both surfaces leading to the observed adsorption behaviour are proposed.

Electrostatics dominate the adsorption of QNHEC in 0.01 mol l^{-1} NaCl on both surfaces. The adsorbed amount increases linearly with pH up to pH=10. A decrease is observed for pH > 11. The linearity is interpreted in terms of a molecular condenser which is composed of the surface layer and the polyelectrolyte in the first layer near the surface. In 0.5 mol l^{-1} NaCl adsorption on SiO_2 is constant up to pH=5. A maximum is observed at pH=10. On TiO_2 the adsorption is low.

5.1 Introduction

Natural polymers, such as polysaccharides, have lately gained increasing importance as an alternative for synthetic polymers in, e.g., food chemistry and industrial processes. Within the group of chemically modified natural polymers, cellulose derivatives occupy a prominent position. Cellulose is one of the world's most abundant polymers; it is non-toxic and biodegradable. In papermaking, cellulose derivatives are used as additives to improve the retention of fibers and pigments or to increase the paper strength. They also have practical importance in cosmetics, pharmaceutics, coatings and in wastewater purification [1].

In chapter 4 (see also ref. 2) we reported on the adsorption of carboxymethyl cellulose

(CMC) on inorganic oxides (TiO_2 and Fe_2O_3). In this chapter we will focus on the adsorption of hydroxyethyl cellulose (HEC) and quaternary ammonium substituted hydroxyethyl cellulose (QNHEC) on SiO_2 and TiO_2. Publications concerning the adsorption of hydroxyethyl cellulose on mineral surfaces and other surfaces are scarce, although some data on adsorption of HEC or HEC-related polymers at mineral surfaces [3-7] and non-mineral surfaces [8-10], using different experimental techniques, have been published. Huldén and Sjöblom [3] reported on adsorption of ethylhydroxyethyl cellulose (EHEC) on Al_2O_3 coated TiO_2 particles at pH=8 in 0.1 mol l^{-1} NaCl, whereas on SiO_2 coated TiO_2 particles no adsorption was observed. The structure of adsorbed HEC on Al_2O_3 was investigated by Yamanaka and Esumi [4]. From ESR measurements they obtained the fraction of segments that is situated close to the surface (trains). It was shown that a small fraction of segments is situated in trains, the majority of segments being present in tails and (large) loops.

Although both QNHEC and especially HEC are widely applied, to our knowledge no systematic study has been carried out with respect to the adsorption as a function of pH and electrolyte concentration. HEC is uncharged, whereas QNHEC is a strong polyelectrolyte. Therefore parameters affecting electrostatics (pH and electrolyte concentration) will especially have an effect on the adsorption behaviour of QNHEC. As may be expected, electrostatic interactions have also a major effect on adsorption kinetics [11]. We shall therefore also consider the rate of adsorption.

5.2 Experimental

Hydroxyethyl cellulose (HEC) was procured from Hoechst. Quaternary ammonium HEC (QNHEC) was prepared from this batch by reaction with glycidyl trimethyl ammonium chloride in iso-propanol. Figure 5.1 gives a schematic representation of the structure of HEC and QNHEC. Their backbone consists of D-glucose residues, which are linked through β-1,4 bonds. The average number of hydroxyethyl groups per glucose unit (molar degree of substitution ms) amounted to 1.9. Assuming that the relation between ms and the degree of substitution ds (average number of substituted hydroxyl groups per glucose unit) as experimentally determined by Arisz and Boon [12] is also valid for our sample, ms=1.9 corresponds approximately to ds=1.1. Thus, the average length of the hydroxyethyl side groups amounts to ms/ds=1.73, which means that on the average 0.73 ether groups are present per glucose unit (i.e. in figure 5.1 m=0.73). The average molar mass of HEC was determined by viscometry and amounted to 300 kg mol^{-1}. The degree of substitution by quaternary ammonium groups was determined at 0.39. Assuming that no depolymerisation takes place in the synthesis of QNHEC, QNHEC has an average molar mass of 360 kg mol^{-1}.

Adsorption experiments were carried out on a flat surface using a reflectometer with a stagnation-point flow cell. We will outline the method only briefly; for a detailed description of the experimental set-up the reader is referred to Dijt et al. [13,14].

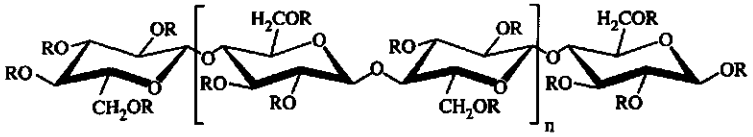

$R = H$ or R_1

$R_1 = (CH_2-CH_2-O)_m-CH_2-CH_2-O-R_2$, $m \geq 0$

HEC : $R_2 = H$

QNHEC : $R_2 = CH_2-\underset{\displaystyle CH_3}{\overset{\displaystyle OH}{\underset{|}{\overset{|}{C}}}}-CH_2-N^+(CH_3)_3$

Figure 5.1 Repeating unit of hydroxyethyl cellulose (HEC) and quaternary ammonium substituted HEC (QNHEC). The D-glucose units are linked through β-1,4 bonds. The average degree of substitution (ds) amounts to 1.1 R_1 groups per glucose unit (m=0.73). The average degree of quaternisation (dq) for QNHEC amounts to 0.39 R_2 groups per glucose unit.

A polymer solution is transported under well-defined hydrodynamic conditions towards an adsorbing surface. The polymer flux depends on the experimental set-up, the viscosity of the solution, the diffusion coefficient of the polymer, and the polymer concentration. As substrates we used an oxidised silicon wafer and a silicon wafer which was coated with a TiO_2 layer. The wafers were obtained from Philips Laboratories, Eindhoven (The Netherlands). Streaming potential measurements showed that the pzc of the TiO_2 coated wafer is about pH=4, which indicates that the TiO_2 layer is probably not rutile but amorphous TiO_2 [15]. The pzc of the oxidised silicon wafer amounted to about 2-3 [15].

The adsorbed amount is measured on-line and is obtained from changes in reflectivities of the parallel and perpendicular components of a laser beam (wavelength 632.8 nm). The adsorption is proportional to the reflectometer signal. The latter is converted into an adsorbed amount according to Abeles' method [16]. The conversion factor depends among other parameters (such as the thickness and the refractive index of the oxide layers, the index of refraction of the solution and the wavelength of the laser beam) on the refractive index increment (dn/dc) of the polymer (0.131 $cm^3 g^{-1}$ [21]). By comparing the change in reflectivities of our wafers with those of wafers with known oxide layer thickness (as determined by ellipsometry) the thicknesses of the SiO_2 and TiO_2 layers were determined at 110 and 25 nm, respectively.

Solutions of HEC and QNHEC (50 to 250 mg l^{-1}) were prepared by first dissolving dry polymer in demineralised water and stirring at room temperature during 15 hours. Next, the ionic strength was adjusted by adding NaCl solution. Prior to the adsorption experiments, dust particles that interfere in the optical detection were removed by centrifuging the solutions whereafter the required pH was set. The wafers were cleaned with an UV-ozone oxidation procedure.

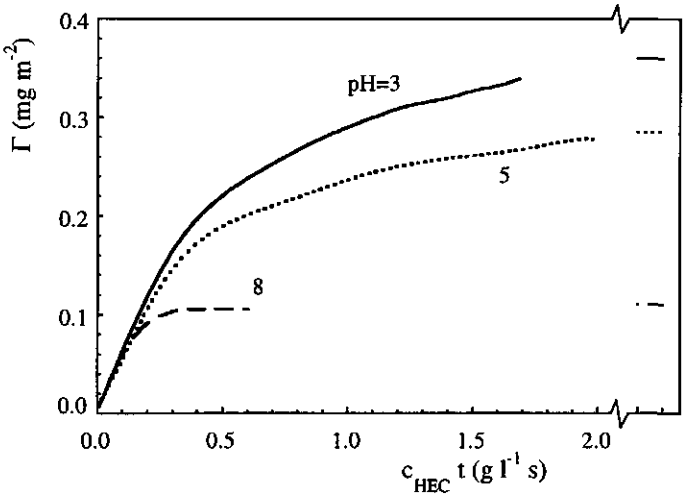

Figure 5.2 Adsorption of HEC on SiO_2 in 0.01 NaCl at different pH values (indicated in the figure) as a function of the product of polymer concentration (c_{HEC}) and time. Adsorbed amounts after 1800 s are indicated separately.

The hydrodynamic layer thickness of adsorbed HEC was obtained by dynamic light scattering. For details about obtaining δ_h from dynamic light scattering the reader is referred to ref. 2. Spherical, nearly monodisperse silica particles were used in the light scattering experiments. These particles were prepared according to Bogush et al. [17,18] by a hydrolysis reaction of tetraethyl orthosilicate and water at 298 K. The radius of the bare particles as obtained by dynamic light scattering was 290 nm. Analysis by means of the method of cumulants showed a slight difference (about 3%) in the radii of the bare particles between using a first or second order polynomial. This indicates that the silica sample is slightly polydisperse.

5.3 Results and discussion

5.3.1 Adsorption of HEC on SiO_2

Experiments on adsorption kinetics were carried out with different polymer concentrations. To compare experiments with different polysaccharide concentrations, the adsorbed amount (Γ) is presented as a function of the product of concentration and time ($c_{HEC}t$). In figure 5.2 this is shown for HEC on SiO_2 in 0.01 mol l^{-1} NaCl. Similar curves were found in 0.5 mol l^{-1} NaCl. The adsorption process is characterised by three stages. Initially, the adsorption increases linearly in time. This stage of the adsorption process is solely determined by mass transfer from solution to the interface. As the adsorption increases,

molecules approaching the surface experience a gradually increasing hindrance, prohibiting them to adsorb directly after coming in the proximity of the surface; consequently, the adsorption is no longer linear in time. For neutral molecules, as for HEC, this hindrance is usually attributed to loops and tails of already adsorbed molecules obstructing the approach towards the surface [13]. The last stage in the adsorption process is characterised by a levelling off of the adsorption curve. Due to the higher surface coverage the resistance to adsorption has grown to such an extent that the rate of adsorption becomes low and the adsorbed amount hardly increases anymore. In our experiments this stage is usually reached after about 1800 s. The adsorbed amount after 1800 s is shown in figure 5.2 after the break in the horizontal axis.

In the initial stage, at low surface coverage, the condition of a perfect sink is satisfied, i.e. all molecules approaching the surface are adsorbed [13]. The flux of polymer towards the surface (J in kg m^{-2} s^{-1}) can be derived from the hydrodynamics of the stagnation point flow set-up:

$$J / c_b = 0.776 \nu^{1/3} R^{-1} D^{2/3} (\bar{\alpha} Re)^{1/3} \qquad (5.1)$$

where ν (m^2 s^{-1}) is the kinematic viscosity, R (m) the radius of the inlet tube of the flow cell, D (m^2 s^{-1}) the polymer diffusion coefficient, $\bar{\alpha}$ a dimensionless streaming intensity parameter, Re the Reynolds number and c_b (kg m^{-3}) the concentration of polymer in the bulk. It is assumed that D can be obtained from the Stokes-Einstein relation by using the radius of gyration of the polymer, implying that $D \sim 1/R_g$. The latter can be obtained from the length of a polymer chain (contour length L_c) and the persistence length (L_p). In a first approximation, i.e. omitting excluded volume effects, one can calculate the radius of gyration according to $R_g^2 \approx \frac{1}{3} L_c L_p$ [19]. From the molar mass (300 kg mol^{-1}), the molar mass of the monomer M_0 (246 g mol^{-1}) and the length of a monomer b (0.52 nm [20]) one obtains $L_c = bM/M_0 = 630$ nm. As $L_p = 15$ nm [21], R_g amounts to 55 nm. From the corresponding value of D and the parameters of our experimental set-up, we calculated $J/c_b = 4.5\ 10^{-7}$ m s^{-1}. The experimental initial adsorption rate ($1/c_b(d\Gamma/dt)_{t=0} = 6.1\ 10^{-7}$ m s^{-1}) agrees reasonably with the calculated flux, indicating that mass transport towards the surface is the rate determining step indeed. This is confirmed by the observation (see figure 5.2) that the initial stages in the adsorption coincide for different polymer concentrations ($d\Gamma/dt \sim c_b$, so $\Gamma \sim c_b t$) and are independent of pH.

The adsorbed amounts of HEC on SiO_2 after 1800 s as a function of pH at two different electrolyte concentrations are shown in figure 5.3. At pH below 5 the adsorption is not affected by the pH. Increasing the pH results in a decrease in the adsorbed amount, which is most pronounced at high salt concentration. At high pH no adsorption is observed any more. The observed adsorption behaviour shows strong resemblance with the adsorption of polyethylene oxide (PEO) on SiO_2 [22,23]. PEO adsorption is constant up to pH≈8 beyond

which it decreases strongly, until above pH=10.5 adsorption no longer takes place [23]. In agreement with our observations, Huldén et al. [3] found no adsorption of ethylhydroxyethyl cellulose on SiO_2 at pH=8 in 0.1 mol l^{-1} NaCl. As stated by Van der Beek [23] the adsorption of PEO on SiO_2 is a consequence of the formation of hydrogen bridges between ether groups in the PEO chain and silanol (Si-OH) surface sites.

The substituents in HEC also contain ether groups, in fact they are short PEO side chains. Hence, HEC also has the capability of hydrogen bonding to the silica surface. By way of comparison, at pH=3 in 1 mol l^{-1} NaCl, carboxymethyl cellulose (CMC) does not adsorb on to silica. At pH=3 the silica surface is uncharged, whereas electrostatic repulsion between charged segments is screened to a large extent. So, under these experimental conditions electrostatics will be of little importance in the adsorption of CMC. The absence of adsorption of CMC on SiO_2 at pH=3 in 1 mol l^{-1} NaCl indicates that binding between the glucose residues and the silica surface does not take place. Therefore we conclude that in case of HEC, the adsorption is caused by ether groups in the hydroxyethyl side groups, i.e. HEC has the same mechanism of binding as PEO (adsorption takes place by hydrogen bonding).

Similar to PEO adsorption, the adsorption of HEC on silica at low pH is not significantly affected by the pH. Upon increasing the pH both PEO and HEC show a decreasing adsorption. Potentiometric titrations (see for instance ref. 24) indicate that up to pH=5 the number of non-dissociated Si-OH groups is constant and does not depend on the salt concentration. Above pH=5 the Si-OH groups gradually dissociate. Assuming a surface coverage of 5 Si-OH nm^{-2} [25] one can calculate from the surface charge density that at, e.g., pH=9 the number of non-dissociated Si-OH groups is lowered by only 15%. Thus, the amount of surface sites that is available for HEC binding is not diminished to a large extent.

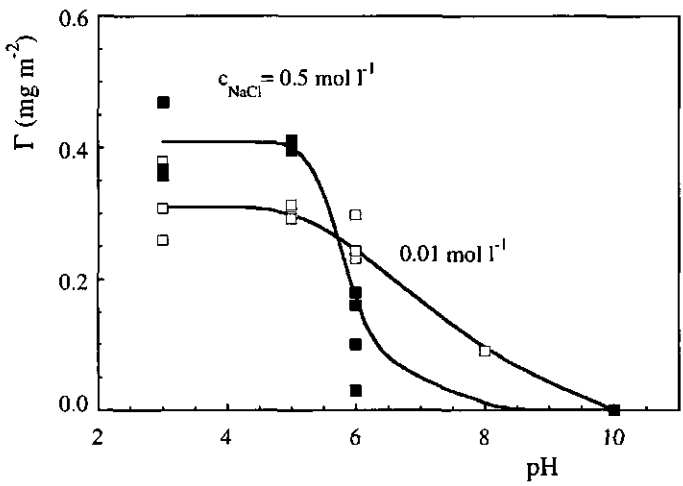

Figure 5.3 Adsorption of HEC on SiO_2 after 1800 s as a function of pH in 0.01 and 0.5 mol l^{-1} NaCl.

Yet, a clear decrease in the adsorption is observed upon at pH > 5 (i.e. at increasing surface charge). A decrease in the adsorption of PEO on silica with increasing surface charge has also been found by Eremenko and Sergienko [26]. As the number of charged surface sites increases with pH, the number of Na^+ ions at the surface will also increase. A possible explanation for the observed decrease in the adsorbed amount is that Na^+ ions act as a displacer for the HEC segments [27].

The adsorption is affected by the electrolyte concentration. At low pH a higher adsorption is observed upon increasing the salt concentration, an effect that is in case of polyelectrolyte adsorption often observed. Salt screens any charges on the chain so that their mutual repulsion is reduced, which results in an increased adsorption. However, HEC carries no charges, hence the increased adsorption cannot be attributed to screening of charges on the chain. One could argue that the solvent quality is lowered by the addition of electrolyte. Lowering the solvent quality results in a decrease of the attraction between polymer segments and solvent, which in effect comes down to an increase in the adsorption energy [27] thereby giving higher adsorption. The solvent quality also affects the dimensional properties of polymers in solution. In a poor solvent the chain will be less extended. However, light scattering experiments by Brown et al. [21] show no significant difference in the radius of gyration of HEC in 0.5 mol l^{-1} NaCl and solutions without added salt. So, the higher adsorption cannot be attributed to the difference in solvent quality. Another possible explanation is that polymer segments in salt solutions are more easily dehydrated, which also facilitates binding to the silica [27]. At high electrolyte concentration the adsorption levels off more sharply than in 0.01 mol l^{-1} NaCl, corresponding to a more rapid increase of the surface charge with pH at 0.5 mol l^{-1} NaCl.

In figure 5.4 the hydrodynamic layer thickness (δ_h) of adsorbed HEC in 0.01 mol l^{-1} NaCl as obtained from dynamic light scattering is given as a function of pH. Initially, HEC (35 mg l^{-1}) was added to a dispersion (concentration 2.5 ppm w/w) of spherical silica particles (radius 290 nm) at pH=10.5. Within experimental error the radius of the bare particles is the same as at pH=3 which indicates that at pH=10.5 no, or at the least only a slight, dissolution of silica takes place. At pH=10.5 adsorption does not take place, so δ_h=0. The pH of the sample is decreased stepwise. About one hour after each step δ_h is measured. Before and after each light scattering experiment the pH was measured; within 0.5 unit no changes in the pH were observed. As the pH is decreased, adsorption takes place, which results in an increase in the hydrodynamic layer thickness, causing slower diffusion of the silica particles. The decrease cannot be attributed to aggregation of particles, which would also result in a decrease in the diffusion coefficient (D), as the decrease in D is not accompanied by a change in the intensity of the scattered light. The latter is highly sensitive to the particle size. Again, a similarity with the adsorption behaviour of PEO on SiO_2 is observed. For PEO at high pH Van der Beek found δ_h=0 [22]. Decreasing the pH resulted in an increase of δ_h, eventually

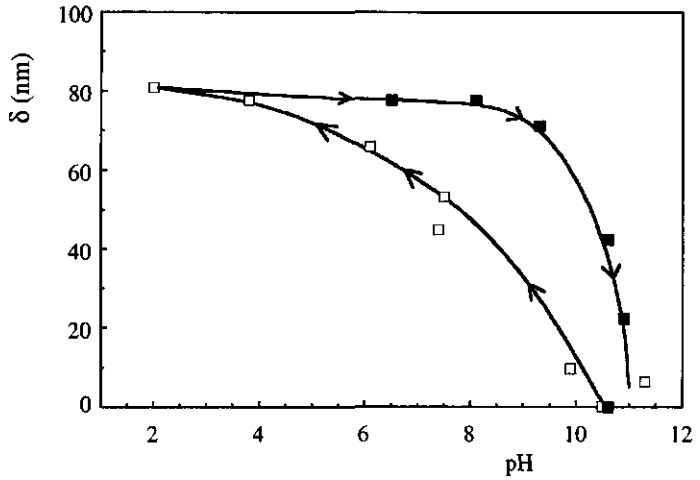

Figure 5.4 Hydrodynamic layer thickness (δ_h) of adsorbed HEC on spherical (radius 290 nm) SiO_2 particles. Symbols □ refer to HEC adsorption starting at high pH, whereafter the pH was decreased. Symbols ■ refer to a subsequent pH increase of the same sample, starting at pH=2.

reaching a plateau. As shown in figure 5.4 the thickness of the adsorbed layer is considerable. A high layer thickness was also found for CMC adsorbed on hematite (α-Fe_2O_3) [2]. In case of CMC the high layer thickness was interpreted in terms of long tails protruding into the solution. In our opinion, long tails may also cause the high hydrodynamic layer thickness of HEC. The large value of δ_h is in line with the ESR measurements of Yamanaka et al. [4]. These authors concluded that HEC adsorbed on Al_2O_3 has only a small fraction (a few percent) in trains. Most segments are situated in tails and (large) loops. Since we have not investigated the effect of the molar mass on adsorption, we cannot substantiate that the conformation of HEC on SiO_2 also contains a small amount of trains. However, the hydrodynamic layer thickness is comparable to the diameter of the coil ($\sim 2R_g = 110$ nm) which indicates that the conformation might be comparable to that in solution (i.e. the adsorbed layer has large loops and short trains).

After reaching pH=2, the pH was increased stepwise, which resulted in a clear hysteresis in δ_h. A common property in the adsorption of polymers is the (apparent) slow desorption after adsorption has taken place. Using reflectometry, Dijt et al. [14] studied the effect of rinsing with polymer-free solvent after adsorption had taken place. The general finding is a small decrease in the adsorbed amount with time, i.e. the process of desorption is a very slow one. The process of desorption can be accelerated by diminishing the number of binding sites of the substrate. In case of HEC adsorbed on SiO_2 this can be achieved by increasing the pH. Up to pH≈5 the number of binding sites on the silica surface remains almost constant, so below pH=5 desorption is not expected to take place. Further increasing the pH, thereby

increasing the number Na^+ ions at the surface, however, initially does not lead to a decrease in δ_h. The hydrodynamic layer thickness initially remains constant, but beyond pH=9 it drops rapidly. The fact that δ_h retains its value over a broad pH range indicates that desorption does not take place. In our opinion this is related to the stiffness of the polymer backbone. Irrespective of the fraction of segments that is situated in trains being low or not, they do provide the bonding of the polymer to the surface. For flexible polymers, in principle, detachment of adsorbed segments can take place segment by segment resulting in a decrease in the hydrodynamic layer thickness. Due to the rigidity of the HEC backbone, however, several bonds to the surface need to be broken simultaneously. The number of bonds to be broken is proportional to the local stiffness of the backbone, characterised by the persistence length (L_p=15 nm [21]), and amounts to about L_p/b = 15 nm/0.52 nm ≈ 30. The rigidity of the backbone implies a strong bonding to the surface. As several adjacent segments are in contact with the surface, this corresponds to the adsorption of a larger segment with length L_p. The adsorption energy will roughly correspond to the sum of the individual adsorption energies. Though a single segment may have a low adsorption energy, stiff or semi-flexible polymers have long segments with high adsorption energy. Therefore we expect that, in general, such polymers show a stronger adsorption than flexible polymers.

5.3.2 Adsorption of QNHEC on SiO_2

In figure 5.5 the adsorbed amount of QNHEC on SiO_2 in 0.01 mol l^{-1} NaCl as a function of the product of polymer concentration and time is given for four pH values. Similar to HEC, initially the adsorption increases linearly in time. As for the adsorption of HEC, we calculated the polymer flux towards the surface. The initial adsorption rate $1/c_b(d\Gamma/dt)_{t=0}$ ($5.9\ 10^{-7}$ m s^{-1}) corresponds fairly well with J/c_b ($4.2\ 10^{-7}$ m s^{-1}). As for HEC, the initial stages coincide for different polymer concentrations.

Unlike HEC, the chain of QNHEC is charged. Hence electrostatics will affect the kinetics of the adsorption process. In chapter 3 (see also ref. 11) we presented a model which deals with electrostatics in the kinetics of the adsorption process. The model has been used to interpret the adsorption behaviour of carboxymethyl cellulose (CMC) on rutile (TiO_2) and hematite (α-Fe_2O_3) [2]. The number of charged groups per glucose monomer which amounted for QNHEC to 0.39 is considerably less than that for CMC (0.75 to 1.25). In order to assess the effect of the chain charge density on the adsorption we applied the same model [11], which implies calculating the resistance that a charged molecule encounters when approaching a (charged) surface. This resistance is the sum of the transport resistance in solution and the barrier resistance coming from repulsive electrostatic forces that act in the proximity of the surface where adsorption takes place. The former can be assessed experimentally from the linear region in the time dependent adsorption curves. The latter is

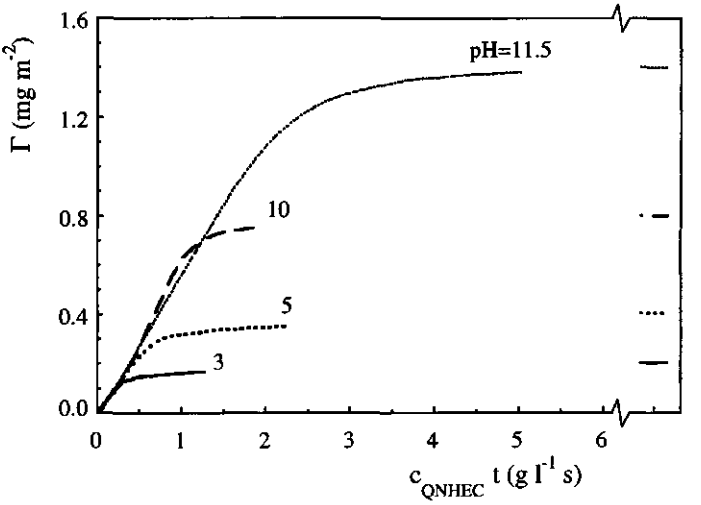

Figure 5.5 Adsorption of QNHEC on SiO_2 in 0.01 NaCl at different pH values (indicated in the figure) as a function of the product of polymer concentration (c_{QNHEC}) and time. Adsorbed amounts after 1800 s are indicated separately.

calculated numerically with the use of a lattice model [27,28]. In this way we can calculate the barrier for adsorption at different stages of the adsorption process (i.e. as a function of the adsorbed amount). Finally, the adsorption as a function of time is obtained by solving the differential equation for the rate of adsorption numerically [11]. Calculations were carried out for a linear polymer consisting of 100 segments with charge densities ranging from 0.25 to 1 charges per segment. The concentration was chosen 10 mg l^{-1}, the adsorbed amount (θ_{ads}) is expressed in equivalent monolayers. All interaction parameters, except the interaction between polymer segments and the surface, were chosen zero. Relative permittivities were set to ε_r=80 for all components. Non-electrostatic interactions between polymer and interface were taken into account by incorporating an adsorption energy (U_{ads}=2 kT).

Although most adsorption experiments are carried out for a charged surface, in the model calculations we used an uncharged surface. As shown in refs. 2 and 11 the height of the barrier is affected by the net charge at the interface (i.e. the sum of the surface charge and the adsorbed charge). As long as the surface charge is not compensated there is no electrostatic barrier for adsorption. If the surface charge is only slightly overcompensated the electrostatic barrier is lower than the resistance due to transport in solution. Both situations lead to an adsorption dependency which is linear in time. For polyelectrolyte adsorption, deviation from the linearity begins if electrostatics become the dominating factor in the adsorption process, i.e. when the adsorbed polymer charge substantially exceeds the surface charge. Since the net charge at the surface is a leading parameter in the adsorption, it is legitimate to make a qualitative comparison between model calculations using an uncharged surface and

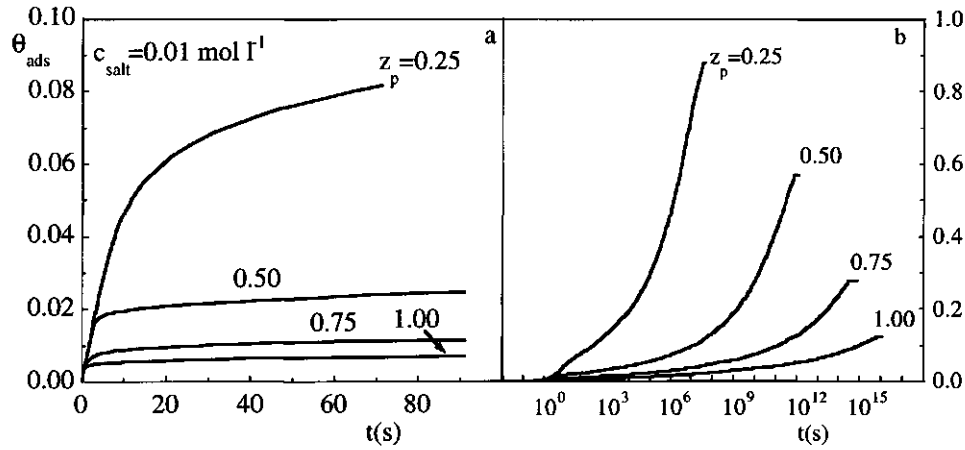

Figure 5.6 Calculated time dependent adsorption (U_{ads}= 2 kT) of a polyelectrolyte (10 mg l^{-1}) with fixed charge density on an uncharged surface in a 0.01 mol l^{-1} 1-1 electrolyte solution. The average number of charged groups per segment, z_p, is indicated in the figure. In figure a the adsorption is given on a time scale which is comparable with adsorption experiments, figure b shows the complete curve (i.e. time needed to reach equilibrium). The adsorption is expressed in equivalent monolayers.

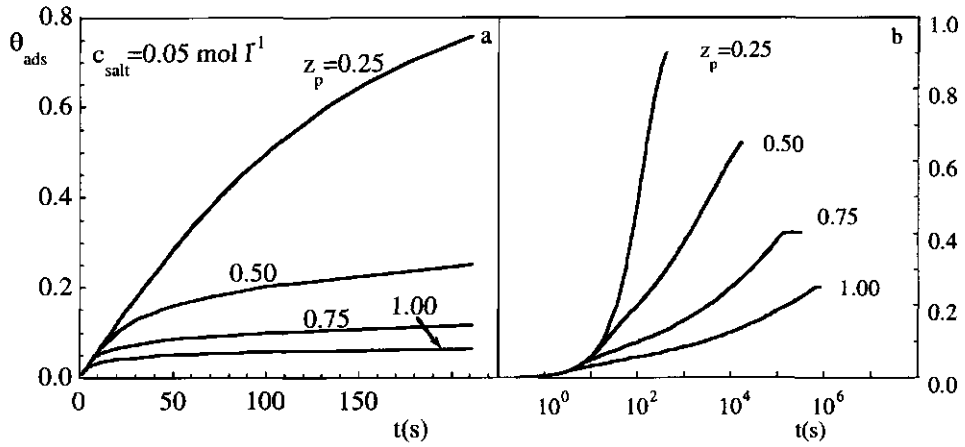

Figure 5.7 Calculated time dependent adsorption (U_{ads}= 2 kT) of a polyelectrolyte (10 mg l^{-1}) with fixed charge density on an uncharged surface in a 0.05 mol l^{-1} 1-1 electrolyte solution. The average number of charged groups per segment, z_p, is indicated in the figure. In figure a the adsorption is given on a time scale which is comparable with adsorption experiments, figure b shows the complete curve (i.e. time needed to reach equilibrium). The adsorption is expressed in equivalent monolayers.

experiments.

Figure 5.6a shows the time dependent adsorption on the time scale of an experiment for a strong polyelectrolyte on an uncharged surface in the presence of 0.01 mol l^{-1} 1-1 electrolyte.

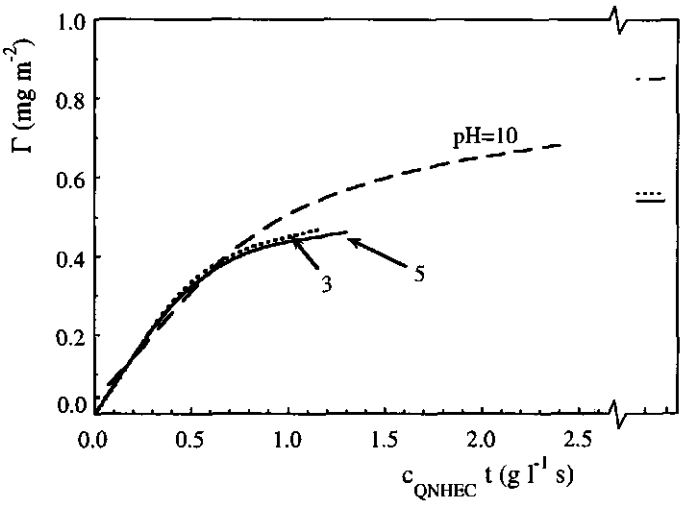

Figure 5.8 Adsorption of QNHEC on SiO_2 in 0.5 NaCl at different pH values (indicated in the figure) as a function of the product of polymer concentration (c_{QNHEC}) and time. Adsorbed amounts after 1800 s are indicated separately.

The effect of the polymer charge density on the adsorption on the full time scale (adsorption reaching equilibrium) is given in figure 5.6b, end points referring to the adsorption when equilibrium is reached. The calculations clearly illustrate the effect of the charge density on the kinetics of the adsorption process. For the two highest charged polyelectrolytes, the linear part in the adsorption is hardly affected by the polymer charge density. For polyelectrolytes having lower charge densities the linear region is increased considerably. As the electrostatic repulsion between already adsorbed molecules and segments approaching the surface is less for lower charged polyelectrolytes, the height of the barrier for the adsorption will increase with polymer charge. For highly charged polyelectrolytes the calculations show that extremely long times are needed to reach equilibrium in the adsorption. On the time scale of an adsorption experiment ($\approx 10^4$ s in case of our reflectometry experiments) about 10% of the adsorption at equilibrium is reached for the highly charged polymers. In 10^4 s a substantially higher adsorption is reached for the lowest charged polyelectrolyte, however equilibrium is not obtained. Regarding the charge density of QNHEC, about 0.4 charged groups per glucose unit, it can be concluded that the adsorption is closer to equilibrium compared to fully dissociated CMC, although the adsorption in 0.01 mol l^{-1} NaCl may still not be at equilibrium. Calculated adsorption for polyelectrolytes having charge densities ranging from 0.25 to 1 charges per monomer, but at higher electrolyte concentration (0.05 mol l^{-1}) are shown in figure 5.7. The effect of the higher salt concentration on lowering the barrier for adsorption first shows up in the linear region which has a longer range than in 0.01 mol l^{-1} electrolyte (figure a). The effect is more pronounced for the lowest charged polyelectrolytes

than for the ones with higher charge densities. The adsorption up to equilibrium is given in figure 5.7b. The time to reach adsorption equilibrium is considerably decreased in the presence of a higher amount of electrolyte. For the polyelectrolytes with the lowest charge densities equilibrium is now reached on the time scale of an experiment. On account of these model calculations we conclude that the adsorption of QNHEC at low salt concentration (0.01 mol l^{-1} NaCl) is likely not at equilibrium, whereas at the higher salt concentration (0.5 mol^{-1} NaCl) equilibrium is reached during our experiments.

In figure 5.8 the adsorption of QNHEC on SiO_2 at various pH values in 0.5 mol l^{-1} NaCl is given as a function of the product of polymer concentration and time. In comparison with adsorption in 0.01 mol l^{-1} NaCl (figure 5.5) after the linear part a more gradual increase in the adsorption is observed. The difference in adsorption was already inferred from our model calculations, which again illustrates the influence of electrostatics on the adsorption (kinetics). The linear part in the adsorption seems not to be affected by the pH. Although the surface charge increases with pH, all curves show a linear part up to 0.35 mg m^{-2}. At low salt concentration such a behaviour is not observed. In fact the shape of the curves in 0.5 mol l^{-1} NaCl is comparable with the adsorption curves of HEC. This indicates that the barrier is mainly caused by loops and tails of already adsorbed chains, electrostatics being of minor importance. Such a behaviour was not found for CMC [2]. For CMC the range of the linear region increases with electrolyte concentration. As CMC has a higher charge density, higher electrolyte concentrations are needed to screen charges.

Adsorption of QNHEC on SiO_2 after 1800 s as a function of pH at two NaCl concentrations is shown in figure 5.9. At low salt concentration the adsorption increases linearly with pH up to pH=10. In chapter 4 (see also ref. 2) we noted that this feature is

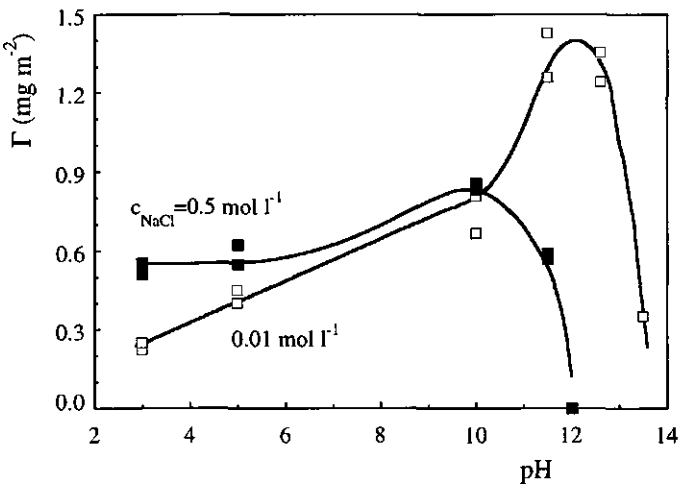

Figure 5.9 Adsorption of QNHEC on SiO_2 after 1800 s as a function of pH in 0.01 and 0.5 mol l^{-1} NaCl.

encountered more often for adsorption of (strong) polyelectrolytes on oxidic surfaces which have a high coverage with dissociable hydroxyl groups. In ref. 2 we quantified the slope $(\partial\Gamma/\partial pH)_\kappa$, i.e. $\partial\Gamma/\partial pH$ at constant electrolyte concentration, by using the properties of a molecular condenser. The adsorbed charge comprises the sum of the charge on the surface (surface charge compensation) and an excess amount (surface charge is overcompensated by adsorbed polymer). A linear relation between Γ and pH at fixed electrolyte concentration is obtained if the excess amount does not depend on the surface charge (i.e. on the pH), but is solely determined by the amount of electrolyte in solution. This is true, as we showed in refs. 2 and 11, if the adsorption is kinetically limited. In a previous paragraph we reasoned that the adsorption at low salt concentration is not at equilibrium, whereas adsorption at higher salt concentration is likely to be at equilibrium. The equation for the slope $(\partial\Gamma/\partial pH)_\kappa$ reads [2]:

$$\left(\frac{\partial\Gamma}{\partial pH}\right)_\kappa = -\frac{2.3\,RT}{F^2}\frac{M_0}{ds}\frac{\varepsilon_r}{d_p} \tag{5.2}$$

where M_0 is the molar mass of a monomer, ε_r is the permittivity of the adsorbed polymer and d_p the thickness of the molecular condenser; RT and F have their usual meaning. Taking for d_p the radius of a cellulose chain (~ 1 nm [29]) and a reasonable value for the relative dielectric constant in the Stern layer (ε_r=20), for QNHEC we calculate $(\partial\Gamma/\partial pH)_\kappa = 0.068$ mg m^{-2}, which is in reasonable agreement with our experiments (0.081 mg m^{-2}).

Comparing the adsorption of QNHEC with HEC in 0.01 mol l^{-1} NaCl, it turns out that the former has slightly lower adsorption at pH=3. Increasing the pH causes higher adsorption. Because upon increasing the pH the negative charge on the substrate surface increases, more charge has to be compensated by adsorbed polyelectrolyte which results in an increased adsorption. At low pH the adsorption increases with electrolyte concentration. Moreover, at pH $\leq$ 5 the adsorption in 0.5 mol l^{-1} NaCl the adsorption reaches the level of HEC (1.8 μmol m^{-2}), i.e. QNHEC behaves as a quasi neutral polymer.

Van de Steeg et al. [30] theoretically investigated the adsorption of strong polyelectrolytes on (un)charged surfaces. According to their calculations, both an increase or decrease can occur upon increasing the electrolyte concentration. Which of the two prevails depends on parameters like polymer charge density, surface charge density and the non-electrostatic surface affinity. According to the classification of Van de Steeg, QNHEC adsorption at low pH is of the screening-enhanced type. Screening-enhanced adsorption is expected to take place when besides electrostatic, also non-electrostatic interactions act in the adsorption process. Because QNHEC has still the possibility of forming H-bridges this condition is met. Since upon increasing the ionic strength, the electrostatic interaction between QNHEC and the SiO_2 surface is screened, adsorption is ultimately only a result of H-bridge interaction. When merely electrostatic interactions determine the adsorption and

non-electrostatic interactions are weak (or absent) the screening-reduced regime occurs [30]. Opposite to the screening-enhanced regime, in the screening-reduced regime a decrease in the adsorption takes place upon increasing the electrolyte concentration. Since the electrostatic interactions between polyelectrolyte and the surface are screened, the driving force for adsorption becomes less and the adsorption decreases when the electrolyte concentration is increased. For QNHEC at pH > 7, in 0.5 mol l^{-1} NaCl a lower adsorption than in 0.01 mol l^{-1} NaCl is observed, so at high pH the adsorption is of the screening-reduced type. The number of dissociated silanol groups increases with pH, which results in a decrease of non-electrostatic interactions (the number of H-bridges becomes less). On the other hand the surface charge increases, which enhances the polyelectrolyte-surface interaction. According to Van de Steeg et al. [30] the boundary of both regimes depends on the non-electrostatic interaction parameter χ_s. For high and moderate χ_s the adsorption is, except for high surface charge, merely of the screening-enhanced type. This situation is reversed for a system with low χ_s: adsorption is reduced upon increasing the electrolyte concentration, except for low surface charge [30]. Both increasing the surface charge and decreasing the non-electrostatic interaction occur upon increasing the pH, which explains the change from the screening-enhanced adsorption at low pH to screening-reduced adsorption at higher pH. When the electrolyte concentration is increased to 2 mol l^{-1} the adsorption at high pH even decreases further, which again illustrates that at high pH adsorption of QNHEC is of the screening-reduced type.

Having established that electrostatics determines the driving force for adsorption in 0.01 mol l^{-1} NaCl at high pH we return to the maximum in the adsorption in figure 5.9. Two explanations may account for this maximum. The first refers to the possibility that small ions might be more efficient in compensating the surface charge. As the surface charge increases small ions will then increase their contribution to charge compensation, resulting in lower polyelectrolyte adsorption and in a maximum in the pH-dependency. The second argument refers to the deprotonation of glucose hydroxyl groups. Hoogeveen et al. [15] observed a maximum in the pH-dependency for the adsorption of AMA (polydimethylaminoethyl methacrylate) on TiO_2, whereas the adsorption of AMA^+ (polytrimethylaminoethyl methacrylate) did not show a maximum in the pH range 2 to 11. Unlike AMA^+, which is a strong polyelectrolyte (charges are fixed), AMA has weak basic groups. Hoogeveen et al. ascribe the maximum in adsorption of AMA to deprotonation of the amine groups. At pH≈10 AMA is completely deprotonated, so that from this pH on no adsorption of AMA takes place (i.e. there is no non-electrostatical interaction). Transferring this deprotonation argument to our case, we note that at high pH (pH > 12) glucose hydroxyl groups start to dissociate [20]. However, one can imagine that dissociation of these groups (thereby creating negative charges) can occur more easily if the chain carries intrinsic positive charges. In solution, the intramolecular repulsion between the negative charges is opposed by the also present opposite charges. At the surface the density of segments is much higher, whereas the opposing effect

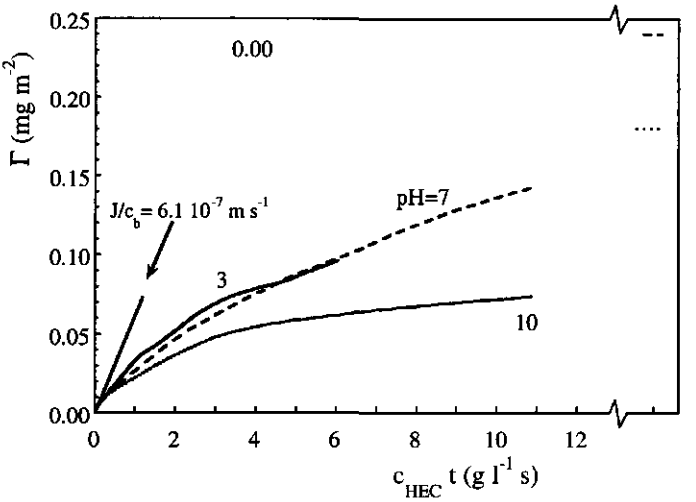

Figure 5.10 Adsorption of HEC on TiO_2 in 0.01 NaCl at different pH values (indicated in the figure) as a function of the product of polymer concentration (c_{HEC}) and time. Adsorbed amounts after 1800 s are indicated separately. The straight line represents the adsorption when mass transfer is rate determining. For pH=3 the adsorption reaches a value of 0.55 mg m^{-2} (not shown in the figure).

of the positive charges is smaller due to their interaction with the surface. Nonetheless, deprotonation may obstruct accumulation of QNHEC at the surface, which shows up in a decrease in the adsorption at high pH and thus a maximum in the pH dependency.

5.3.3 Adsorption of HEC on TiO_2

In figure 5.10 the adsorption of HEC on TiO_2 is given as a function of the product of c_{HEC} and time in 0.01 mol l^{-1} NaCl for three values of pH. Adsorption at 0.5 mol l^{-1} (not shown) exhibits similar behaviour. The shape of the adsorption curves shows a considerable difference with those for the adsorption on SiO_2. The latter start with a linear region in the adsorption (straight line indicated in figure). Such a region is absent on TiO_2, where the adsorption gradually increases to its end point. The absence of a linear region may point to a slow rate of attachment of HEC to the TiO_2 surface. If the rate of attachment is low compared to the mass transport to the surface, it is likely that the process of unfolding is also slow compared to mass transport. So, molecules that are partially attached to the surface, thereby maintaining their extended solution conformation, obstruct the approach of additional polymers. Polymer concentrations are in the same range as with HEC adsorption on SiO_2 (50 to 250 mg l^{-1}), so the polymer flux towards the surface is comparable. The lower rate of attachment on TiO_2 is likely related to the fact that formation of bonds between HEC and the TiO_2 surface has a higher activation energy than on SiO_2. It must be concluded that the

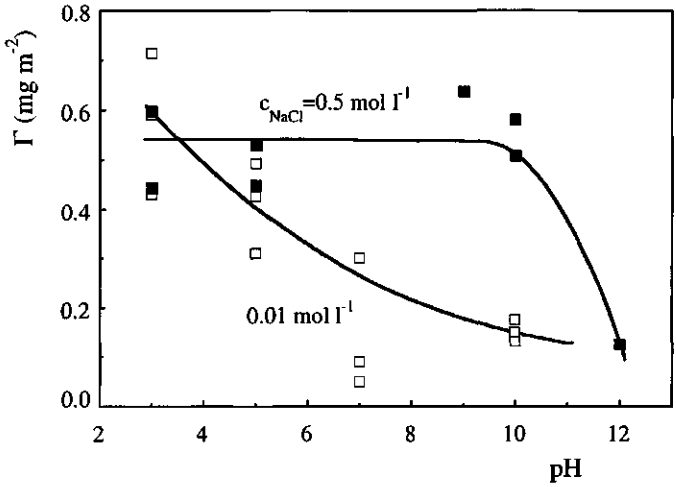

Figure 5.11 Adsorption of HEC on TiO_2 after 1800 s as a function of pH in 0.01 and 0.5 mol l^{-1} NaCl.

mechanism of binding to TiO_2 is different from the binding to SiO_2.

Adsorption of HEC on TiO_2 after 1800 s as a function of pH at two NaCl concentrations is shown in figure 5.11. As can be seen from figures 5.3 and 5.11 the adsorption behaviour on SiO_2 and TiO_2 shows considerable differences. At low electrolyte concentration the adsorption on TiO_2 decreases monotonously. Increasing the electrolyte concentration causes the adsorption to increase. Up to pH=10 the adsorption is constant, then it drops rapidly to zero. Separate experiments (not shown here) reveal that PEO does not adsorb onto TiO_2, therefore the adsorption of HEC cannot be attributed to H-bridging between HEC ether groups and OH-groups at the titania surface. Laskovski et al. [31] reported dextrin adsorption on lead hydroxide. The binding mechanism proposed by these authors comprises the formation of a chemical bond between hydroxyl groups at C2 and C3 positions in the glucose unit and Pb-OH groups at the surface, thereby releasing a H_3O^+ ion. The same mechanism is proposed by Subramanian et al. [32] for the binding of starch on hematite. Since the backbone of HEC is also composed of glucose units and the TiO_2 surface also has metal-OH groups, it is not unlikely that a similar binding mechanism is also valid for the adsorption of HEC on TiO_2. Transferring this idea about the mechanism to the adsorption of HEC on TiO_2 the binding is accomplished by a chemical bond of free (i.e. non-substituted) hydroxyl groups at C2 and C3 positions in glucose units and Ti-OH groups. As a result of the release of a H_3O^+ ion, a negative charge is created at the surface. At pH < 4, where the surface is positively charged, a negative charge can easily be created. The surplus of positive charges already present stabilises the created negative charge. If the number of positive charges decreases, or even changes in to a surplus of negative charge, stabilisation is not easily achieved. This

mechanism would explain the decreasing adsorption of HEC with increasing pH.

The effect of higher electrolyte concentration is an increased screening of charges. So, creation of negative charges on the surface can more easily be achieved at high (0.5 mol l^{-1}) NaCl concentration. This is reflected in the adsorption of HEC at high NaCl concentration. At low pH, negative charge is created in a surplus of positive charged sites. Hence, the effect of salt on the adsorption is expected to be negligible. At higher pH, especially above the pzc, the number of negative charges on the surface increases. Now the screening of salt has its effect on the adsorption; substantially higher adsorption is observed in 0.5 mol l^{-1} NaCl as compared to 0.01 mol l^{-1} NaCl.

5.3.4 Adsorption of QNHEC on TiO_2

Finally we discuss the adsorption of QNHEC on TiO_2. In figure 5.12 the adsorbed amount is plotted as a function of the product of the polymer concentration and time for four pH values in 0.01 mol l^{-1} NaCl. At pH=3 the rate of adsorption is very low, Γ increases slowly to a plateau value. At pH=3 the TiO_2 surface is positively charged. Hence, an electrostatic barrier will slow down the rate of adsorption. Above pH=4 the surface is charged oppositely to QNHEC. Now, for low adsorbed amounts the electrostatic barrier is missing, which shows up in a linear increase in the initial stage. As observed for adsorption on SiO_2 the range of the linear part in the time dependent adsorption curves increases with pH. The fact that at pH $\geq$ 5 QNHEC adsorption shows a linear region, which is not found for HEC,

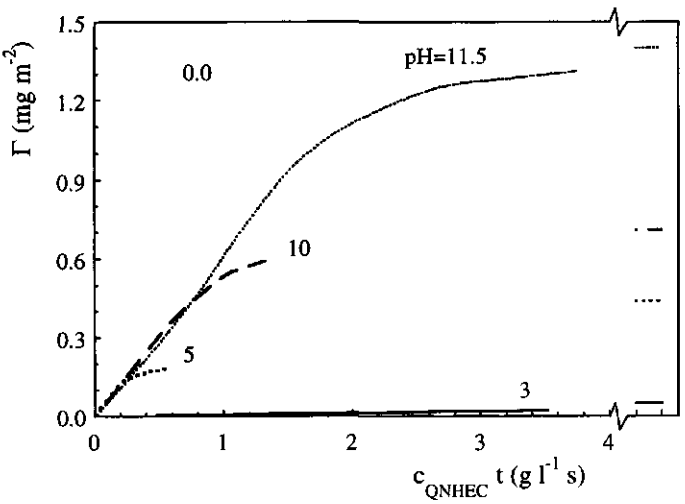

Figure 5.12 Adsorption of QNHEC on TiO_2 in 0.01 NaCl at different pH values (indicated in the figure) as a function of the product of polymer concentration (c_{QNHEC}) and time. Adsorbed amounts after 1800 s are indicated separately.

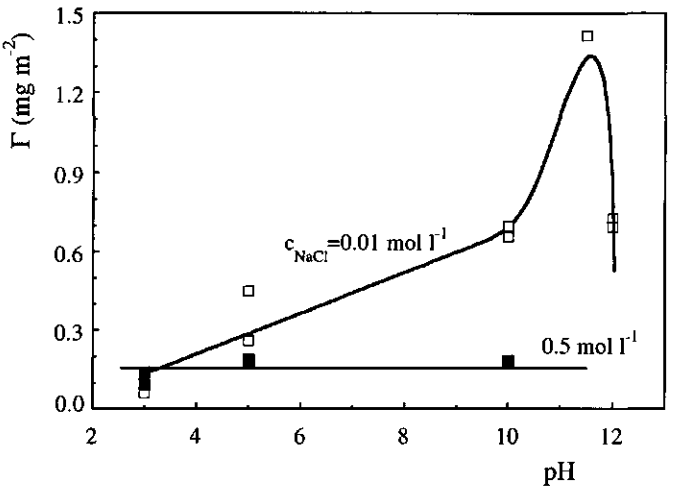

Figure 5.13 Adsorption of QNHEC on TiO_2 after 1800 s as a function of pH in 0.01 and 0.5 mol l^{-1} NaCl.

indicates that attachment of QNHEC is different from HEC. In case of QNHEC the interaction between opposite charges provides a good (and fast) anchoring to the surface. The linear region in the first stage of the adsorption ($1/c_b(d\Gamma/dt)_{t=0} = 6.1\ 10^{-7}$ m s^{-1}) shows good agreement with the initial adsorption rate of QNHEC on SiO_2. In 0.5 mol l^{-1} NaCl (not shown) the adsorption shows a similar behaviour as found for pH=3 in 0.01 mol l^{-1} NaCl.

In figure 5.13 the adsorption of QNHEC on TiO_2 after 1800 s at two NaCl concentrations is shown as a function of pH. At low electrolyte concentration the adsorption behaviour shows strong resemblance to adsorption on SiO_2. Up to pH=10 the adsorption increases linearly with pH ($(\partial\Gamma/\partial pH)_\kappa$ =0.066 mg m^{-2}), a maximum is observed at pH≈11. This similarity indicates that in 0.01 mol l^{-1} NaCl electrostatics dominate the adsorption. The pH dependency at 0.5 mol l^{-1} NaCl, however, is quite different. The adsorption is not affected by the surface charge, which indicates that at high electrolyte concentration electrostatics are of minor importance. As observed for HEC the adsorption is constant up to pH=10. The adsorbed amount, however, is considerably less than for HEC. The lower adsorption is probably related to differences in size of the substituents. As electrostatics are screened, adsorption takes place as for HEC. However, due to the presence of the considerable bulky substituents the glucose hydroxyl groups in QNHEC are not able to come close to the surface. The result is less interaction with the surface, which results in lower adsorption. On SiO_2 the adsorption of QNHEC at 0.5 mol l^{-1} NaCl is also the result of non-electrostatic interactions. However, the groups that facilitate binding to the SiO_2 surface (ether groups) are situated outside the backbone whereas the glucose hydroxyl groups that are operating in the binding to TiO_2 are situated in the backbone, which means that the bulky substituents in QNHEC cause

less hindrance for the adsorption on SiO_2. This could account for the fact that the adsorption of QNHEC on SiO_2 at low pH is higher compared to the adsorption on TiO_2.

5.4 Conclusions

Adsorption of HEC on SiO_2 is facilitated by hydrogen bonding between HEC ether groups and Si-OH (silanol) groups at the substrate surface. The number of dissociated silanol groups increases with pH. As a consequence the number of Na^+ ions increases, thereby displacing HEC segments which causes a decrease of the adsorption with pH. On TiO_2 adsorption does not take place by hydrogen bonding. Probably in this case the mechanism is a reaction between non-substituted C2 and C3 glucose hydroxyl groups and Ti-OH surface groups [31,32]. As this mechanism involves a chemical reaction at the surface, the rate of attachment may be lower as compared to binding originating from physical interaction (like H-bridging or electrostatic interaction).

Dynamic light scattering experiments reveal a high (~80 nm) hydrodynamic layer thickness of HEC adsorbed on SiO_2. This indicates a rather extended conformation of the adsorbed layer with loops and (few) long tails protruding into the solution. A hysteresis in δ_h is observed with respect to pH. This hysteresis is related to the fact that for desorption of a semi-flexible polymer, such as HEC, several bonds with the surface need to be broken simultaneously, which hampers desorption.

At low electrolyte concentration (0.01 mol l^{-1} NaCl) the adsorption of QNHEC on both SiO_2 and TiO_2 is merely determined by electrostatics. A linear increase in the adsorption is observed up to pH=10. The linearity is interpreted in terms of a molecular condenser which is composed of the charged surface layer and the polyelectrolyte charge in the first layer near the surface. Model calculations indicate that it is likely that on both surfaces in 0.01 mol l^{-1} NaCl equilibrium in adsorption is not reached. Due to a non-electrostatical interaction, overcompensation of surface charge can take place. The extent of overcompensation is less than at equilibrium. A repulsive potential between the surface (which is equally charged due to some overcompensation) and polyelectrolytes approaching the surface inhibits reaching equilibrium on the time scale (~1800 s) of our experiments. In 0.5 mol l^{-1} NaCl charges are screened to such an extent that equilibrium is reached. On SiO_2 at low pH the adsorption is of the screening-enhanced type (adsorption increases with electrolyte concentration) [30], whereas at high pH adsorption is of the screening-reduced type (decrease in adsorption with increasing electrolyte concentration). On TiO_2 the adsorption is low. Bulky substituents of QNHEC inhibit interaction between glucose hydroxyl groups and the TiO_2 surface.

References

1. M. Grayson, *Encyclopaedia of Chemical Technology, Vol. 5*, John Wiley & Sons, New York (1979).
2. C.W. Hoogendam, A. de Keizer, M.A. Cohen Stuart, B.H. Bijsterbosch, J.G. Batelaan, and P.M. van der Horst, *Langmuir* **14** (1998) 3825, chapter 4 in this thesis.
3. M. Huldén and E. Sjöblom, *Prog. Colloid Polym. Sci.* **82** (1990) 28.
4. Y. Yamanaka and K. Esumi, *Colloids and Surfaces* **122** (1997) 121.
5. M. Malmsten and B. Lindman, *Langmuir* **6** (1989) 357.
6. B.H. Pettersen, L. Bergflodt, and J. Sjöblom, *Colloids and Surfaces A* **127** (1997) 175.
7. V. Shubin, *Langmuir* **10** (1994) 1093.
8. J.E. Glass, H. Ahmed, S.D. Seneker, and G.J. McCarthy, *Colloids and Surfaces* **21** (1986) 323.
9. J.F. Argillier, R. Ramachandran, W.C. Harris, and M. Tirrell, *J. Colloid Interface Sci.* **146** (1991) 242.
10. K. Furusawa and T. Tagawa, *Colloid Polymer Sci.* **263** (1985) 353.
11. M.A. Cohen Stuart, C.W. Hoogendam, and A. de Keizer, *J. Phys.: Condens. Matter* **9** (1997) 7767, chapter 3 in this thesis.
12. P.W. Arisz and J.J. Boon, *J. Anal. Appl. Pyrolysis* **25** (1993) 371.
13. J.C. Dijt, M.A. Cohen Stuart, J.E. Hofman, and G.J. Fleer, *Colloids and Surfaces* **51** (1990) 141.
14. J.C. Dijt, M.A. Cohen Stuart, and G.J. Fleer, *Adv. Colloid Interface Sci.* **50** (1994) 79.
15. N.G. Hoogeveen, M.A. Cohen Stuart, and G.J. Fleer, *J. Colloid Interface Sci.* **182** (1996) 133.
16. W.N. Hansen, *J. Optical Soc. Am.* **58** (1968) 380.
17. G.H. Bogush, M.A. Tracy, and C.F. Zukoski, *J. of Non-Crystaline Solids* **104** (1988) 95.
18. W. Stöber, A. Fink, and E. Bohn, *J. Colloid Interface Sci.* **26** (1968) 62.
19. H. Yamakawa, *Modern Theory of Polymer Solutions*, Harper & Row, New York (1971).
20. E. Ott, H.M. Spurlin, and M.W. Grafflin, *High Polymers Vol. V Cellulose and Cellulose Derivatives part II*, Interscience Publishers, Inc. New York (1954).
21. W. Brown, D. Henley, and J. Öhman, *Makromolekulare Chem.* **162** (1962) 407.
22. G.P. van der Beek and M.A. Cohen Stuart, *Langmuir* **7** (1991) 327.
23. G.P. van der Beek, *Displacement of Adsorbed Polymers*, Ph.D. thesis Wageningen Agricultural University (1991).
24. T.P. Goloub, L.K. Koopal, B.H. Bijsterbosch, and M.P. Sidorova, *Langmuir* **12** (1996) 3188.
25. L.T. Zhuralev, *Langmuir* **3** (1987) 316.
26. B.V. Eremenko and Z.A. Sergienco, *Colloid J. USSR* **41** (1977) 422.
27. G.J. Fleer, M.A. Cohen Stuart, J.M.H.M. Scheutjens, T. Cosgrove, and B. Vincent, *Polymers at Interfaces*, Chapman & Hall, London (1993).
28. M.R. Böhmer, O.A. Evers, and J.M.H.M. Scheutjens, *Macromolecules* **23** (1990) 2288.
29. C.W. Hoogendam, A. de Keizer, M.A. Cohen Stuart, B.H. Bijsterbosch, J.A.M. Smit, J.A.P.P. van Dijk, and P.M. van der Horst, accepted by *Macromolecules*, chapter 2 in this thesis.
30. H.G.M. Van de Steeg, M.A. Cohen Stuart, A. de Keizer, and B.H. Bijsterbosch, *Langmuir* **8** (1992) 2538.
31. Q.I. Lui and J.S. Laskowski, *J. Colloid Interface Sci.* **130** (1988) 101.
32. S. Subramanian and K.A. Natarajan, *Minerals Engineering* **1** (1988) 241.

Chapter 6

Depletion thickness and thickness of the adsorbed layer of cellulose derivatives on inorganic oxides

Abstract

The diffusion of silica particles with radii ranging from 12 to 510 nm in dilute solutions of carboxymethyl cellulose (M_w=180 to 1200 kg mol^{-1}, c_{CMC}=5 to 1000 mg l^{-1}) was investigated by means of dynamic light scattering at pH=5 in 0.01 mol l^{-1} NaCl. The viscosity of the polymer solution as experienced by the silica probes (the "microscopic" or effective viscosity η^{eff}) differs from the viscosity as determined by capillary viscometry (η^{p}). For small particles η^{eff} nearly equals the viscosity of the solvent (η^{0}). The effective viscosity increases with the size of the probe particles and the polymer concentration, but remains less than η^{p}.

The effective viscosity is interpreted in terms of a model in which the particle is surrounded by a layer of polymer free solution ($\eta=\eta^{0}$). The thickness of the polymer-free layer is assumed to be equal to the depletion layer (λ_d). Applying this model, a decrease in λ_d as a function of CMC concentration is observed. At low concentration λ_d equals the radius of gyration.

The hydrodynamic layer thickness (δ_h) of cellulose derivatives (carboxymethyl cellulose and hydroxyethyl cellulose) adsorbed on inorganic oxide surfaces (α-Fe_2O_3 and SiO_2) is also investigated by dynamic light scattering. Upon using η^{p} maxima in δ_h are found. However, these maxima are a consequence of an incorrect choice of the viscosity. Using the viscosity as obtained from inert probe diffusion no anomalies are observed.

6.1 Introduction

Many applications of polymers, e.g. in paints or as additives in food [1,2], are related to their capability of stabilising particles in dispersions. This capability is associated with the fact that polymers adsorb at the solid-liquid interface, thereby covering the surface which prevents coagulating of particles. The thickness of the adsorbed polymer layer is an important parameter in colloidal stabilisation. Experimentally, the hydrodynamic layer thickness can be determined by dynamic light scattering. This technique measures the diffusion coefficient, from which the size (the hydrodynamic radius) of the particles is usually calculated using the Stokes-Einstein relation. It has been shown, see for instance refs. 3-8, that for particles

dispersed in a polymer solution the Stokes-Einstein relation can noticeably fail if the solution viscosity is set equal to the bulk viscosity. It turns out that the viscosity experienced by the diffusing particles (so called effective or "microscopic" viscosity) is lower than the bulk (shear) viscosity. As a result, obtaining the thickness of the adsorbed layer becomes obfuscated.

In this chapter we use the microscopic viscosity determined from the diffusion of a series of inert probes (i.e. particles on which polymer does not adsorb) to obtain the layer thickness of adsorbed cellulose derivatives (carboxymethyl cellulose, CMC, and hydroxyethyl cellulose, HEC) on inorganic oxides (Fe_2O_3, TiO_2 and SiO_2). In addition we will use the diffusion behaviour to obtain the thickness of the layer from which CMC is depleted from a solid-liquid interface. For this purpose we will apply a model proposed by Donath et al. [9].

6.2 Diffusion of particles in a polymer solution

For spherical particles the diffusion coefficient D ($m^2\ s^{-1}$) in a liquid medium is often interpreted in terms of the well-known Stokes-Einstein (SE) relation:

$$D = \frac{kT}{6\pi\eta\ R} \tag{6.1}$$

where η is the viscosity of the medium in which the sphere is suspended, R the hydrodynamic radius of the sphere and kT has its usual meaning. Henceforth we will discuss mostly the viscosity in terms of the dimensionless relative viscosity η_r (i.e. the viscosity with respect to that of the solvent η^0). The SE relation assumes the medium to be a continuum. In case of a polymer solution this assumption may be plausible if the size of the particles is much larger than the dimension of the polymer in solution. On the other hand, if the particles are much smaller they can easily penetrate into the polymer coil, not hindered by the presence of segments, i.e. their motion will be affected mainly by solvent molecules. Therefore, we expect the assumption of considering the medium as a continuum to be valid for particles which are much larger than polymer molecules and for very small particles. In case of the former the viscosity will be equal to that of the bulk ($\eta_r=\eta_r^b$) and for the latter it will be equal to the viscosity of the solvent ($\eta_r=1$). Within these limits, η_r will have a value ranging from 1 to η_r^b.

In literature various attempts [3-5,7] can be found to describe the diffusion of spherical particles in polymer solutions. Many end up with scaling relations, which tend to $D/D_0=0$ (i.e. $\eta_r=\infty$) for large spheres. We applied a model proposed by Donath et al. [9] to evaluate our experimental data concerning the diffusion of inert probes in a polymer solution. In the following we will discuss this model briefly and only give the relevant equations. For a detailed discussion the reader is referred to ref. 9.

Donath et al. consider the liquid flow in a polymer solution with viscosity η_r around an inert (non-adsorbing) spherical particle with radius R under creeping flow conditions (i.e. flow which is characterised by a low Reynolds number). In the proximity of the particle surface the viscosity is lower than the bulk viscosity. This reduction is related to the fact that polymer segments are depleted from the surface. Because the polymer concentration is lower as compared with the bulk concentration, the viscosity is also lower than in the bulk. It is assumed that the reduced viscosity is a function of the distance from the surface r : $\eta_r(r)=\eta_r^b f(r)$, f(r) representing the radial dependency of the viscosity and η_r^b the viscosity at large distance from the surface. In their paper Donath et al. choose $\eta_r^b=\eta_r^p$, i.e. at large distance from the particle surface the viscosity equals the viscosity of a polymer solution as obtained from viscometry. Assuming a quasi-flat surface for the sphere and taking the viscosity profile into account an expression for the velocity profile is obtained. Applying the hydrodynamic boundary conditions for the normal and tangential velocities at the surface the following expression for the effective viscosity η_r^{eff} is obtained [9]:

$$\eta_r^{eff} = \eta_r^b \frac{R + 2\eta_r^b K}{R + 3\eta_r^b K} \tag{6.2}$$

where K is given by:

$$K = \frac{1}{\eta_r^b}\int_0^\infty \left(\frac{1}{f(r)} - 1\right) dr \tag{6.3}$$

where r=0 corresponds to the particle surface. In order to evaluate equation 6.3 an expression for f(r) is needed. We applied a simple step function, i.e. $f(r)=1/\eta_r^b$ for $r \le \lambda_d$ and f(r)=1 for $r > \lambda_d$, where λ_d is assumed to be equal to the thickness of the depletion layer. Inserting (6.3) in (6.2) for the viscosity step profile one arrives at:

$$\eta_r^{eff} = \eta_r^b \frac{1 + (2\lambda_d/R)(\eta_r^b - 1)}{1 + (3\lambda_d/R)(\eta_r^b - 1)} \tag{6.4}$$

For large particles ($R\rightarrow\infty$) equation 6.4 yields $\eta_r^{eff}=\eta_r^b$. While one would expect $\eta_r^{eff}=1$, equation 6.4 yields $\eta_r^{eff}=\frac{2}{3}\eta_r^b$ in the limit of small particles ($R\rightarrow 0$). We can give no explanation for the incorrect behaviour at small particle size. In ref. 9 the authors do not make any remark about the validity of their theory for small particles. Possibly equation 6.4 fails for small particle size since it has been derived under the assumption of a quasi-flat surface.

Table 6.1 Characteristics of cellulose polymer samples.

Polymer	M_w (kg mol^{-1})	M_n (kg mol^{-1})	M_w/M_n	R_g (nm)	$[\eta]$ (l g^{-1})
CMC1	1200	570	2.0	105	1.4
CMC2	640	390	1.6	85	1.1
CMC3	180	80	2.3	28	0.39
CMC4	30	---	---	13	0.10
HEC	300	---	---	55	0.61

6.3 Experimental

Both HEC and CMC have a cellulose backbone that consists of D-glucose residues, which are linked through β-1,4 bonds. HEC was procured from Hoechst. The average number of hydroxyethyl groups ($[CH_2\text{-}CH_2\text{-}O]_m\text{-}CH_2\text{-}CH_2\text{-}O\text{-}H$, $m \geq 1$) per glucose unit (molar degree of substitution ms) is 1.9, which corresponds approximately to ds=1.1 [10,11] (average number of substituted hydroxyl groups per glucose unit). The average molar mass of HEC (M_w) was determined by viscometry and amounted to 300 kg mol^{-1}. The sodium salt of carboxymethyl cellulose was prepared by AKZO Nobel in a homogeneous reaction, by treating alkali cellulose (cotton linters) in iso-propanol with sodium mono chloroacetate in nitrogen atmosphere. The degree of substitution of carboxymethyl groups (CH_2COONa) was 0.99. CMC was treated with hydrogen peroxide, which cleaves the cellulose chain at random position. By adding different amounts of hydrogen peroxide a series of CMCs varying in molecular mass was obtained. In table 6.1 some characteristics of cellulose derivatives that are used are given. The molecular masses of the CMC samples were obtained from SEC-MALLS at pH=7 in 0.1 mol l^{-1} $NaNO_3$ [12], the radius of gyration (R_g) at pH=5 in 0.01 mol l^{-1} NaCl was calculated from the electrostatic worm model [12,13].

Light scattering experiments were carried out using a He-Ne laser (wavelength 632.8 nm) at a constant scattering angle of 90°. By means of an ALV 5000 digital correlator fluctuations in the intensity of scattered light were processed into an intensity auto-correlation function. We used the method of cumulants [14,15] for data analysis. By fitting the natural logarithm of the intensity auto-correlation function to a second order polynomial the average translational diffusion coefficient (D) of the particles can be obtained. Then the effective viscosity (η^{eff}) is obtained via the Stokes-Einstein relation:

$$\eta^{eff} = \frac{kT}{6\pi RD} \tag{6.5}$$

The hydrodynamic layer thickness is obtained in a similar way:

$$\delta_h = \frac{kT}{6\pi\eta^{eff}D_p} - R \tag{6.6}$$

where D_p is the diffusion coefficient in the presence of adsorbed CMC.

Spherical, nearly monodisperse particles were used. Silica particles, with different radii ranging from 12 to 510 nm, were prepared according to Bogush et al. [16,17] by a hydrolysis reaction of tetraethyl orthosilicate and water at 298 K. Hematite particles (R=42 nm) were prepared according to Penners [18] by nucleation in a $FeCl_3/HClO_4$ solution at 373 K. The radii of the bare particles were obtained from dynamic light scattering. Analysis by means of the method of cumulants showed a slight difference (about 3%) in the radii of the bare particles between using a first or second order polynomial. This indicates that the samples are slightly polydisperse.

6.4 Results and discussion

In figure 6.1 the relative viscosity experienced by spherical silica particles (lower curve) is compared to the bulk viscosity (upper curve) for HEC solutions with concentrations of 5 to 350 mg l^{-1}. The former was determined from the diffusion coefficient of silica particles (R=290 nm), the latter with a capillary viscometer. All data are obtained in 0.01 mol l^{-1} NaCl at pH=11. At pH=11 HEC does not show any adsorption on silica [10], so these measurements are very well suitable for obtaining η_r^{eff}. As can be seen from figure 6.1, η_r^{eff} is always below the bulk viscosity. Curves similar to those in figure 6.1 are given for CMC in figure 6.2. The upper curve relates to the bulk viscosity of CMCs with different molar mass at pH=3 in 0.01 mol l^{-1} NaCl, the lower curves relate to the effective viscosity as experienced by silica particles of size 12 and 510 nm. As observed for HEC the effective viscosity is always

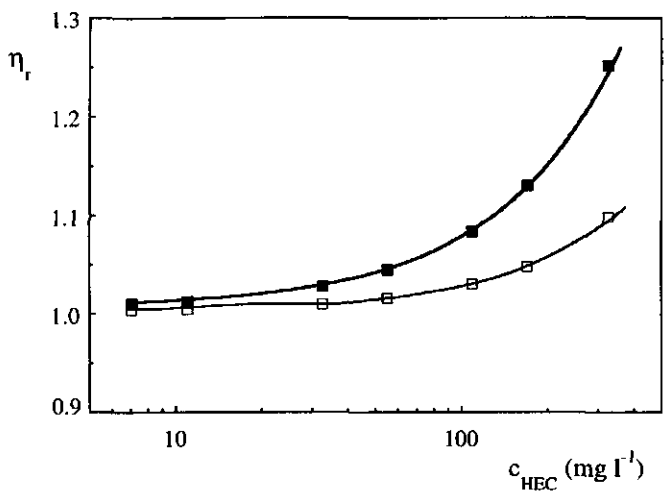

Figure 6.1 Relative viscosity of HEC solutions at pH=11 in 0.01 mol l^{-1} NaCl. ■: obtained by capillary flow viscometry, □: as experienced by spherical silica particles (R=290 nm).

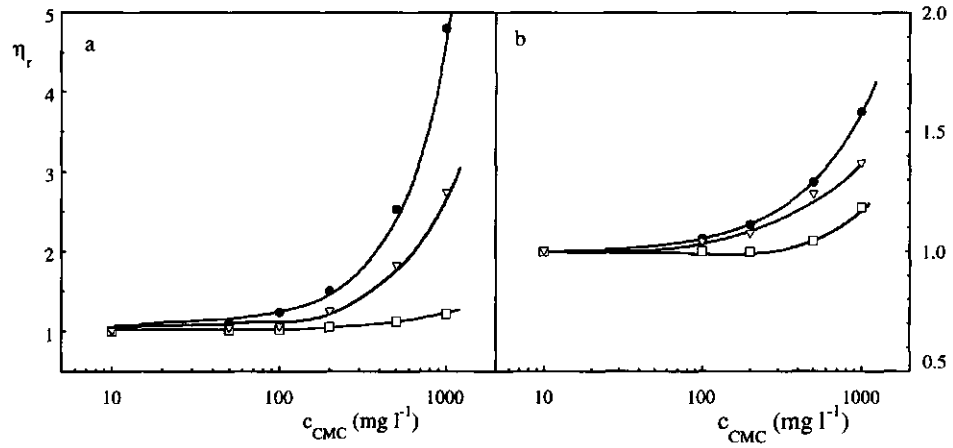

Figure 6.2 Relative viscosity of CMC solutions at pH=5 in 0.01 mol l^{-1} NaCl. ■: obtained by capillary flow viscometry, □: R=12 nm, ∇: R=510 nm. Figure a relates to CMC3, figure b relates to CMC1.

lower than the bulk viscosity. In case of the smallest silica particle the effective viscosity is close to the viscosity of the solvent ($\eta_r \approx 1$). Only at high CMC concentrations (~ 500 mg l^{-1}) increases the effective viscosity somewhat, so it seems that the motion of small particles is not affected to a large extent by the presence of polymer of both low and high molar mass CMC. In comparison with the particles with R=12 nm the motion of particles with R=510 nm is more affected by the presence of polymer in solution. The effective viscosity is considerably higher for the large silica particle. Yet it is still lower than the bulk viscosity, albeit for the CMC3 solution the effective viscosity is closer to the bulk viscosity than for CMC1.

The dependency of the relative effective viscosity on the particle size is shown more clearly in the figures 6.3 and 6.4. The meaning of the solid curves will be explained further on. Figure 6.3 shows the size dependency of η_r^{eff} in CMC1 solutions with three concentrations at pH=5 in 0.01 mol l^{-1} NaCl. For small particle size the effective viscosity tends to $\eta_r^{eff}=1$. Upon increasing the size of the particles the effective viscosity increases. Comparing η_r^{eff} for the largest particle to the shear viscosities of the CMC1 solutions (η_r^p=1.5, 2.5, and 4.8 for solutions with concentration of 200, 500, and 1000 mg l^{-1}, respectively) it is clear that those levels are not reached. So, the size of the particles is still too small that the polymer solution may be considered as a continuum. Figure 6.4 shows the effective viscosity in c_{CMC}= 1000 mg l^{-1} for CMCs with different molar mass. In case of CMC2 the effective viscosity is still lower than the shear viscosity, albeit the ratio η_r^p/η_r^{eff} for the largest silica particle is lower (1.4) than for CMC1 (η_r^p/η_r^{eff}=1.7). However, in case of

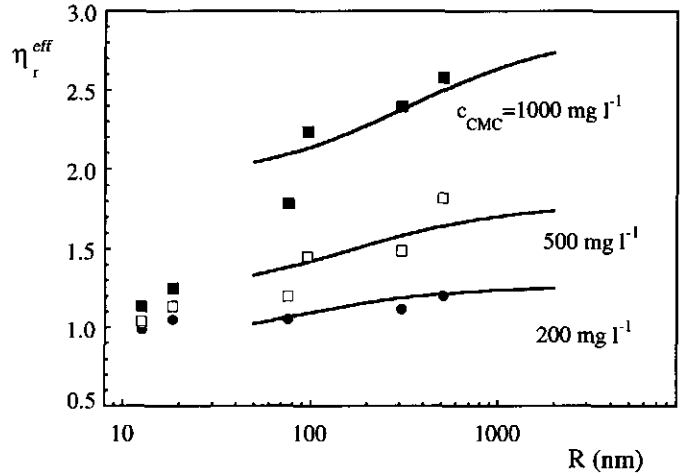

Figure 6.3 Relative effective viscosity experienced by spherical SiO_2 particles dispersed in solutions of CMC1 at pH=5 in 0.01 mol l^{-1} NaCl. CMC concentration is indicated in the figure. Curves were calculated according to Donath [9] (see text).

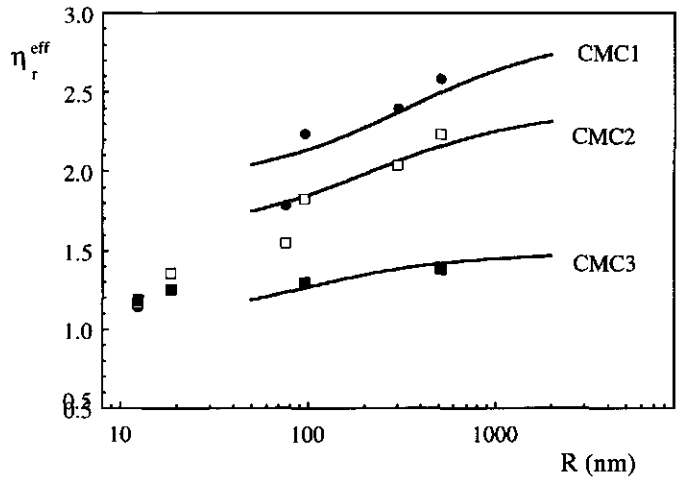

Figure 6.4 Relative effective viscosity experienced by spherical SiO_2 particles dispersed in CMC solutions (c_{CMC}=1000 mg l^{-1}) of different molar masses at pH=5 in 0.01 mol l^{-1} NaCl. CMC sample numbers are indicated in figure. Curves were calculated according to Donath [9] (see text).

CMC3 η_r^{eff} comes rather close to the bulk viscosity (η_r^p/η_r^{eff}=1.2). As the size of the largest silica particle is about twenty times the size of the polymer this agrees with our expectation that a polymer solution may be considered as a continuum if the size of the probe particle is much larger than that of the polymer.

One could think that the effective viscosity as obtained from the diffusion coefficient

(using equation 6.5) is obfuscated by aggregation of SiO_2 particles. If aggregation takes place, larger particles are formed which have lower diffusion coefficient. However, the decrease in D is not accompanied by a change in the intensity of the scattered light. As the scattered intensity is proportional to the sixth power of the size of the scattering particle [14], the decrease in D can be attributed to changes in the effective viscosity rather than to aggregation.

We applied the model by Donath et al. to the data presented in figures 6.3 and 6.4. As equation 6.4 can easily be linearised the thickness of the depletion layer can be derived from the slope (which is equal to $3\lambda_d/R$) when plotting $-(\eta_r^{eff} - \eta_r^b)/(\eta_r^{eff} - \frac{2}{3}\eta_r^b)$ as a function of $(\eta_r^b - 1)$. We choose $\eta_r^b = \eta_r^p$. Then performing the procedure we obtain depletion thicknesses which vary from 60 to 600 nm, the values depending on the particle radius and the mass of the polymer. Comparing these data to radii of gyration of the CMCs (R_g=28 and R_g=105 nm for CMC3 and CMC1, respectively) the values of λ_d are much larger. Theoretical predictions on the thickness of the depletion layer near a flat surface indicate that, as long as the polymer concentration is below the overlap concentration (c*), λ_d is roughly equal to the radius of gyration of the polymer [19]. For concentrations higher than the overlap concentration λ_d decreases with the polymer concentration. These predictions relate to neutral polymers depleted from an uncharged surface. As the CMC chain is charged (the silica surface is nearly uncharged at pH=5 [20]), λ_d may be higher than R_g. Furthermore, for curved surfaces possibly there might be a dependence on the size of the particle, however, to our opinion, such high values as 60 to 600 nm are questionable.

Because the analysis described in the previous paragraph does not yield physical realistic values for λ_d we used a somewhat different approach to analyse our data. In our analysis the viscosity outside the depletion layer was chosen equal to the viscosity as determined by a capillary viscometer. However, one must bare in mind that the method of capillary viscometry is based on a Poiseuille flow (i.e. the flow through a cylindrical tube). Furthermore, it is generally known that the experimentally determined viscosity of a polymer solution depends on the conditions of flow in the particular instrument [21,22]. As the flow of liquid around a spherical particle is very different from a Poiseuille flow, the viscosity outside the depletion layer may also be different (lower) than the viscosity obtained by capillary viscometry. Unfortunately, as far as we know, there is no information available about the choice for the viscosity outside the particle depletion layer. Therefore we choose to use η_r^b as well as λ_d as fit parameters. For this purpose we used the following procedure. First it is assumed that η_r^b does not depend on the size of the particle but only on the polymer concentration. We defined the function $\chi^2(\{R\}, \eta_r^b, \lambda_d) = \Sigma_i[y_i - y(R_i, \eta_r^b, \lambda_d)]^2$. In this function $y_i = (D_{i,0}/D_i)(1/\eta_r^b)$, where D_0 and D are the diffusion coefficients of the particles in solution without CMC and solution containing CMC, respectively, $y(R_i, \eta_r^b, \lambda_d)$ equals η_r^{eff}/η_r^b (equation 6.4), and {R} is

a series of particle sizes. As χ^2 cannot be linearised the fit parameters have to be found by a non-linear procedure. The values for the best fit can be found by minimising χ^2 with respect to η_r^b and λ_d, for which we used the Levenberg-Marquardt algorithm [23]. In the minimising procedure not all data points are used. As the Donath model is derived for a quasi-flat surface, it is not correct to involve data points relating to particles with small radii. By taking R=96 nm as the lower limit, the best fits to our experimental data are those represented by the solid curves in figures 6.3 and 6.4.

As figures 6.3 and 6.4 show, our experimental data can be described rather satisfactorily with the Donath model. The thickness of the depletion layer as obtained with the non-linear fit, as a function of the CMC concentration, is given in figure 6.5. For CMC1 and CMC2 a decrease of λ_d as a function of concentration is observed. Though not clearly, the data presented tend to indicate that λ_d does not depend on the CMC concentration for the low molar mass CMC. As mentioned in the previous paragraph, for uncharged polymers above the overlap concentration λ_d decreases, reaching λ_d=0 for high polymer concentrations (volume faction of polymer≈1). Introducing charges on the chain causes a different behaviour. It has been shown theoretically that the depletion thickness at low concentration amounts to about the radius of gyration, however, already below the overlap concentration it decreases [19]. The overlap concentration can be readily estimated from the intrinsic viscosity [η] according to $c^* \approx 1/[\eta]$, so c* is expected at 2500, 900 and 700 mg l^{-1} for CMC3, CMC2, and CMC1, respectively. The effect of the decrease in the depletion layer thickness at

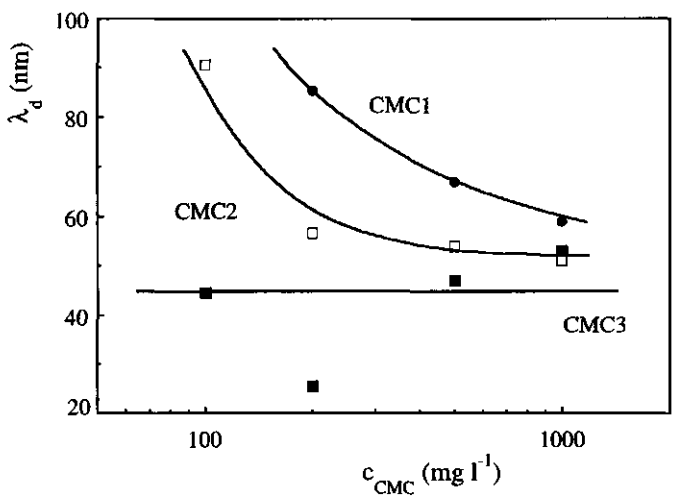

Figure 6.5 Depletion layer thickness on SiO_2 (λ_d) as a function of CMC concentration at pH=5 in 0.01 mol l^{-1} NaCl. CMC sample numbers are indicated in figure.

concentration lower than c* is caused by the build up of a Donnan potential gradient across the depletion zone which opposes the depletion of polyelectrolyte chains from the surface [19]. Unfortunately, there is very little experimental data to compare with ours. We note that a decreasing thickness of the depletion layer with polymer concentration for $c<c^*$ is also observed by Cosgrove et al. [24] for polystyrene sulphonate depleted from a spherical silica surface.

The hydrodynamic layer thickness (δ_h) of HEC adsorbed on SiO_2 (2 mg l^{-1}, R=290 nm) at pH=3 in 0.01 mol l^{-1} NaCl as assessed from dynamic light scattering is shown in figure 6.6. No increase in the intensity of the scattered light was observed. The data in this figure were obtained from the diffusion coefficient by using three different viscosities. In the upper curve the viscosity was set to that of the solvent, i.e. any effect of the polymer is neglected. A monotonous increase in δ_h reaching high values is observed, but neglecting the effect of polymers on the viscosity of the solution is, of course, very unrealistic. Taking the viscosity as η_p the lower curve in figure 6.6 is obtained. At low HEC concentration no difference in δ_h is observed. Upon increasing the polymer concentration δ_h increases, however to a lower extent than when the solvent viscosity is used. Furthermore the hydrodynamic layer thickness reaches a maximum at $c_{HEC} \approx 40$ mg l^{-1}. There is no physical reason for the existence of a maximum in the thickness of the adsorbed layer. Hence, the occurrence of the maximum is a result of an incorrect choice of the viscosity. The middle curve is obtained by putting the viscosity equal to the microscopic viscosity as experienced by the bare silica particles at pH=11 (inert probe viscosity). The now observed dependency of δ_h on the polymer concentration does not show a maximum anymore but increases with polymer concentration. The increase of δ_h with concentration can be explained from the polydisperisty of the polymer sample. It has been shown both theoretically and experimentally [19] that long polymer chains adsorb preferentially over short ones. Cellulose polymers are polydisperse [12]. In our experiments the surface area on which adsorption takes place is kept constant, while the HEC concentration is increased. At low concentration both short and long chains will be adsorbed on the surface. Upon increasing the polymer concentration, the number of long chains also increases. Hence, the contribution of long chains to the adsorption will also increase. As the value of δ_h is mainly determined by tails of adsorbed polymers, which in length increase with the chain length, δ_h increases with the HEC concentration.

We are very well aware that the procedure we applied to obtain δ_h is not fully correct. The effective viscosity was determined using silica particles which are smaller than the covered ones, whilst is was applied for particles which are larger (290 nm + δ_h). As can be seen from figures 6.3 and 6.4, for particles with a size of about 300 nm the effective viscosity increases only slightly (i.e. compared to smaller particles) with the particle size. If it is assumed that the size dependency of the effective viscosity in HEC solutions resembles that

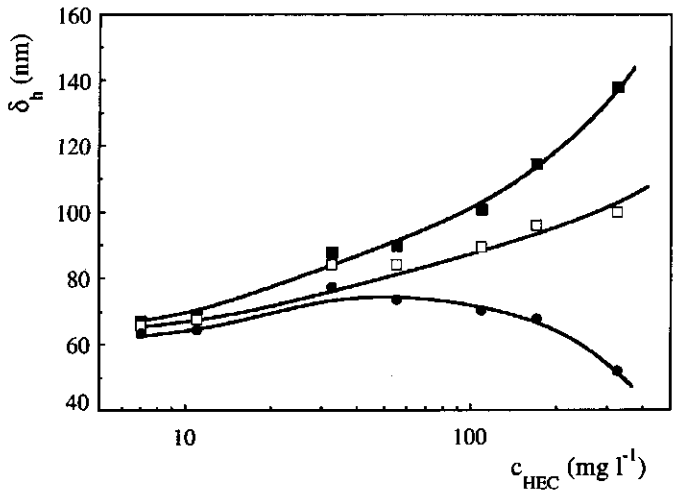

Figure 6.6 Hydrodynamic layer thickness (δ_h) of adsorbed HEC on SiO_2 at pH=3 in 0.01 mol l^{-1} NaCl. Symbols refer to different viscosities used in Stokes-Einstein for obtaining δ_h. ■: $\eta=\eta_{water}$; ●: $\eta=\eta_{bulk}$; □: $\eta=\eta_{eff}$. See text for details.

of CMC, than neglecting the size of the depletion layer does not lead to large errors when R=290 nm. Secondly, we assumed that the particles with adsorbed polymer are rigid. Masliyah et al. [25] calculated the drag force that acts on a composite sphere (i.e. a solid sphere surrounded with a permeable layer). According to Masliyah et al. the drag force of a composite sphere is always less than the drag force of a solid sphere with the same radius. Hence, the effective viscosity to be used is less than the one we applied. Despite the errors, we believe that quite reliable data can be obtained when determining the microscopic viscosity with the use of an inert probe with a size which is about the same as the covered particle.

In figure 6.7a the hydrodynamic layer thickness of CMC with various molar mass as adsorbed on hematite is presented as a function of the polymer concentration. No increase in the intensity of the scattered light was observed. Data in figure 6.7a were obtained using the bulk viscosity in the Stokes-Einstein relation. A similar anomalous behaviour as observed for HEC (i.e. a maximum in the thickness of the layer) is also observed for the two high molar mass CMCs. We used the microscopic viscosity as obtained from probe diffusion (data presented figures 6.3 and 6.4) to calculate a more reliable value of the layer thickness. We are aware that the CMC covered particles (42 nm+δ_h) are not completely comparable with solid particles with size 42 nm+δ_h. Unlike the silica particles used in figure 6.6, the size dependency of the effective viscosity is higher, however the effective viscosity is at least a more proper one to use than the bulk viscosity. The data shown in figure 6.7b are assessed as follows. First from the diffusion coefficient of the polymer covered particle the apparent

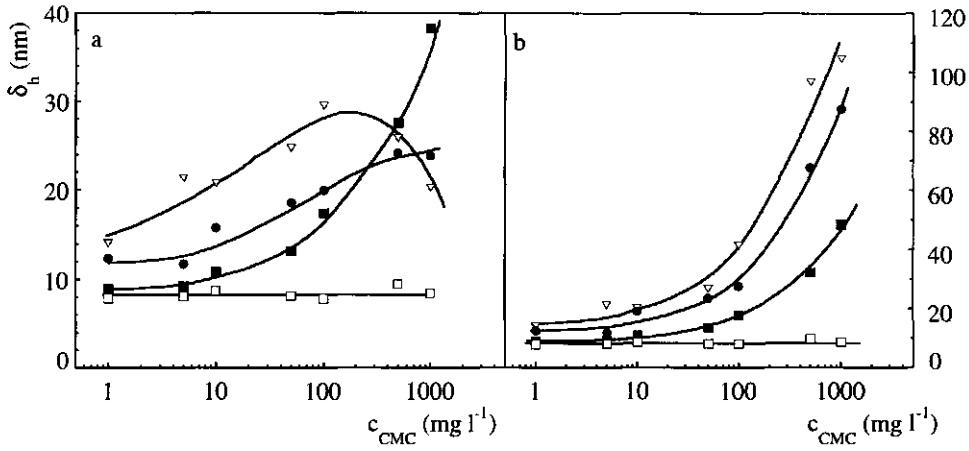

Figure 6.7 Hydrodynamic layer thickness (δ_h) of CMC adsorbed on spherical hematite particles (R=42 nm) at pH=3 in 0.01 mol l^{-1} NaCl. Symbols refer to different CMC sample numbers, ∇: CMC1 ●: CMC2, ■: CMC3, □: CMC4. The data in figure a were calculated using the viscosity as obtained from capillary flow, in figure b the effective viscosity as determined from inert probe diffusion was used.

radius ($R+\delta_h$) was calculated using the polymer bulk viscosity. Then the effective viscosity corresponding to the apparent radius was determined from the probe diffusion measurements, whereafter the size of the covered particle is again calculated. This step is repeated several times until the calculated size does not change anymore. As for the high molar mass CMCs, no anomalies are observed anymore. In case of CMC4 only small differences as compared to figure 6.7a are observed. Because the solution viscosity is low (comparable to the solute viscosity) differences are not expected. For CMC3 higher layer thickness are found for the high concentration range. Though the adsorption of CMC does not depend on the molar mass, which indicates a flat adsorption, the observed layer thickness for CMC3 and CMC4 is substantial. As the hydrodynamic layer thickness is merely determined by tails [19] we may conclude that CMC adsorbs in a flat conformation, with few tails protruding in the solution.

The data relating to CMC1 and CMC2 are merely to illustrate the effect of the choice of the viscosity. Because the size of these CMCs (which is not the case for CMC3 and CMC4) exceeds that of the hematite particles one deals with adsorption of hematite particles on CMC coils rather than with adsorption of CMC chains on a hematite surface.

In a previous paper [26] we discussed the adsorption of CMC adsorption on hematite. Since the process involves the adsorption of a charged polymer on a charged surface it is likely that electrostatics influence the adsorption. As we concluded in our paper concerning the adsorption of anionic quaternary ammonium hydroxyethyl cellulose [10], equilibrium can

be reached on the time scale of an experiment for polymers which have moderate charge densities (≈ 0.4 charges per segment). In case of highly charged polyelectrolytes equilibrium will not be reached on the time scale of an experiment. With respect to CMC adsorption this means that at pH values were CMC has a high degree of dissociation the adsorbed amount will be kinetically limited, whereas at low degree of dissociation the adsorption may be considered at equilibrium, i.e. whether adsorption is at equilibrium or not depends on the pH at which an experiment has been carried out. An aspect of reaching equilibrium is the displacement of small polymer chains by larger ones. Displacement can only take place if polymer chains are able to come close the surface, i.e. if there is only a low electrostatic barrier for reaching the surface. In the following we examined if displacement of low M_w CMC by higher M_w CMC takes place. Because the longer chains will form more and larger loops, in general the process of displacement is accompanied by an increase of the adsorbed amount. However, for CMC the adsorbed amount does not depend on the molar mass [26]. So, this quantity cannot be used as a tool to get information about any displacement taking place. As the hydrodynamic layer thickness, however, is a much more sensitive parameter [19] we used this property to investigate the displacement process.

In a relevant experiment, CMC4 was adsorbed at pH=3 in 0.01 mol l^{-1} NaCl. After increasing the pH to pH≈6 the hydrodynamic layer thickness was again measured. We observed an increase from δ_h=8 nm to δ_h=20 nm. As the charge density on the chain becomes higher because of the increased dissociation of the carboxylic groups, the tails will adapt a more stretched conformation resulting in an increase in δ_h. Subsequently, at pH=6 CMC3 was added to the solution. No increase in δ_h was observed. However, when the CMC3 was added at pH=3 δ_h increases from 8 to 18 nm; upon subsequently increasing the pH to pH≈6, δ_h augments to 29 nm. This increase at pH=3 is very likely related to the displacement of small molecules by larger ones, the increase at pH=6 again resulting from the stretching of the tails. At high pH no increase of the hydrodynamic layer thickness is observed when CMC3 is presented to a surface on which originally CMC4 is adsorbed. As the barrier for reaching the surface is possibly too high, molecules cannot, or at the least to very low extent, reach the surface. So, at high pH displacement does not take place (or the process will be very slow).

In figure 6.8 data are presented on the adsorbed layer thickness of CMC on TiO_2. The CMC concentration was chosen at 30 mg l^{-1}, so that $\eta \approx \eta_0$. Initially CMC was adsorbed at pH=9, whereafter the pH was decreased stepwise until pH=3. At the initially high pH CMC adsorbs to a very small extent [26], so δ_h=0. Upon decreasing the pH, an increase in δ_h up to δ_h=26 nm is observed. As the adsorbed amount increases, the layer thickness also increases. From pH=3 on the pH is subsequently increased. As the charge of the surface becomes less positive (or even negative) a surplus of adsorbed charge is created which may cause detachment of segments resulting in desorption of CMC. Upon increasing the pH, however, no decrease in δ_h is observed. Even at pH=9 the value corresponding to pH=3 is maintained.

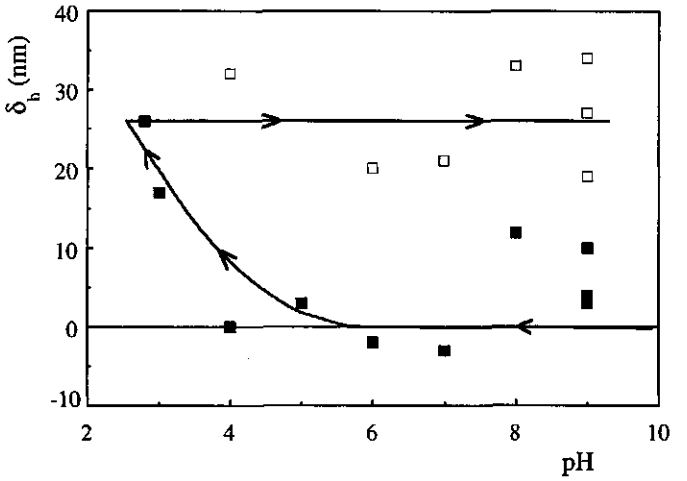

Figure 6.8 Hydrodynamic layer thickness (δ_h) of CMC1 adsorbed on spherical TiO_2 particles (R=115 nm) in 0.01 mol l^{-1} NaCl. Symbols □ refer to CMC adsorption starting at high pH, whereafter the pH was decreased. Symbols ■ refer to a subsequent pH increase of the same sample, starting at pH=3. CMC concentration is 30 mg l^{-1}.

In an earlier paper [26] we presented similar data on the layer thickness of CMC on hematite. In that case CMC was adsorbed at pH=3, whereafter the pH was increased stepwise to pH=11. The hydrodynamic layer thickness was found to increase up to pH≈9, whereafter it decreases. For CMC on TiO_2 the behaviour is different. The difference is possibly related to the adsorbed amount being present when the pH is increased. For TiO_2 used in this study pH=3 corresponds to pzc-pH=1, whereas for hematite this corresponds to pzc-pH=5. Because at pH=3 the hematite surface has a higher charge density than the TiO_2 surface, the adsorbed amount at pH=3 will be lower on the titania surface. As the density of segments is lower the repulsion between charged segments, which is a motive for desorption, is also lower for CMC adsorbed on TiO_2. In addition, desorption is hampered (both on the hematite and titania surface) because of both the stiffness of the backbone of the polymer and the strong adsorption to the surface, as we argued in previous papers [10,26].

6.5 Conclusions

The viscosity experienced by spherical silica particles suspended in a polymer solution differs considerably from the viscosity obtained from capillary viscometry. If the particles are dispersed in a solution containing a polymer which does not adsorb on the surface, the surface is surrounded by a layer which has a lower viscosity than the bulk viscosity (so called depletion layer). The thickness of this layer, or at least a physically reasonable estimate, can

be obtained by the model proposed by Donath et al. [9]. In this model the depletion layer is assumed to be free of polymer segments. The depletion thickness decreases with CMC concentration and molar mass, at low concentration it equals the radius of gyration of CMC. The viscosity outside the depletion layer is lower than the viscosity determined by a capillary flow viscometer.

The use of η_p for obtaining the thickness of adsorbed CMC or HEC (δ_h) gives rise to an unrealistic dependency of δ_h on the polymer concentration (the dependency shows a maximum). Upon using the effective viscosity as obtained from inert probe measurements, a more consistent dependency is obtained (δ_h increases monotonously with the polymer concentration). So, in experiments involving the thickness of the adsorbed layer the effective viscosity has to be chosen carefully.

References

1. M. Grayson, *Encyclopedia of Chemical Technology Vol. 5*, John Wiley & Sons, New York (1979)
2. R.L. Whistler and J.N. BeMiller, *Industrial Gums, Polysaccharides and Their Derivatives 2th Ed*, Academic Press, London 1973.
3. W. Brown and R. Rymdén, *Macromolecules* **20** (1987) 2867.
4. G.D.J. Phillies, C. Malone, K. Ullmann, G.S. Ullmann, J. Rollings, and L.P. Yu, *Macromolecules* **20** (1987) 2280.
5. T.H. Lin and G.D.J. Phillies, *J. Phys. Chem.* **86** (1982) 4073.
6. D. Gold, C. Onyenemezu, and W.G. Miller, *Macromolecules* **29** (1996) 5700.
7. G.S. Ullmann, K. Ullmann, R.M. Linder, and G.D.J. Phillies, *J. Phys. Chem.* **89** (1985) 692.
8. X. Cao, R. Bansil, D. Gantz, E.W. Moore, N. Niu, and N.H. Afdhal, *Biophys. J.* **73** (1997) 1932.
9. E. Donath, A. Krabi, M. Nirschl, V.M. Shilov, M.I. Zharkikh, and B. Vincent, *J. Chem Soc., Faraday Trans.* **93** (1997) 115.
10. C.W. Hoogendam, I. Derks, A. de Keizer, M.A. Cohen Stuart, and B.H. Bijsterbosch, accepted by *Colloids and Surfaces A*, chapter 5 in this thesis.
11. P.W. Arisz and J.J. Boon, *J. Anal. Appl. Pyrolysis* **25** (1993) 371.
12. C.W. Hoogendam, A. de Keizer, M.A. Cohen Stuart, B.H. Bijsterbosch, J.A.M. Smit, J.A.P.P. van Dijk, P.M. van der Horst, and J.G. Batelaan, accepted by *Macromolecules*, chapter 2 in this thesis.
13. R.M. Davis, *Macromolecules* **24** (1991) 1149.
14. R. Pecora, *Dynamic Light Scattering, Applications of Photon Correlation Spectroscopy*, Plenum Press, New York (1985).
15. D.E. Koppel, *J. Chem. Phys.* **57** (1972) 4814.
16. G.H. Bogush, M.A. Tracy, and C.F. Zukoski, *J. of Non-Crystaline Solids* **104** (1988) 95.
17. W. Stöber, A. Fink, and E. Bohn, *J. Colloid Interface Sci.* **26** (1968) 62.
18. N.H.G. Penners, *The preparation and stability of homodisperse colloidal haematite (α-Fe_2O_3)*, Ph.D. Thesis, Wageningen Agricultural University (1985).
19. G.J. Fleer, M.A. Cohen Stuart, J.M.H.M. Scheutjens, T. Cosgrove, and B. Vincent, *Polymers at Interfaces*, Chapman & Hall, London (1993).
20. T.P. Goloub, L.K. Koopal, B.H. Bijsterbosch, and M.P. Sidorova, *Langmuir* **12** (1996) 3188.

21. D. McIntyre (Ed.), *Characterisation of Macromolecular Structure*, National Academy of Sciences Washington, D.C., Washington D.C. (1968).
22. F.R. Eirich (Ed.), *Rheology, Theory and Applications*, Academic Press Inc. Publishers, New York (1956).
23. W.H. Press, S.A. Teukolsky, W.T. Vetterling, *Numerical Recipes*, Cambridge University Press, New York (1989).
24. T. Cosgrove, T.M. Obey, and K. Ryan, *Colloids Surfaces* **65** (1992) 1.
25. J.H. Masliyah, G. Neale, K. Malysa, and T.G.M van de Ven, *Chem. Engng. Sci.* **42** (1987) 245.
26. C.W. Hoogendam, A. de Keizer, M.A. Cohen Stuart, B.H. Bijsterbosch, J.G. Batelaan, and P.M. van der Horst, *Langmuir* **14** (1998) 3825; chapter 4 in this thesis.

Summary

Cellulose derivatives, in particular carboxymethyl cellulose (CMC) are used in many (industrial) applications. The aim of this work is to obtain insight into the adsorption mechanism of cellulose derivatives on solid-liquid interfaces.

In **chapter 1** of this thesis we discuss some applications of cellulose derivatives. Application of CMC in pelleting of iron ore and in papermaking and the role of adsorption are given in more detail. Further we present a short introduction in the adsorption of polyelectrolytes.

A set of 20 CMC samples was used in this study. Samples with four different degrees of substitution (ds=0.75, 0.91, 0.99, and 1.25) were prepared by AKZO Nobel by reaction of cellulose with NaOH and sodium monochloro acetate ($ClCH_2COONa$). Samples were subjected to a random cleavage reaction with hydrogen peroxide yielding samples with molar masses ranging from M_w=30 to 10^3 kg mol^{-1}. Characterisation of the CMC samples by size exclusion chromatography in combination with multi-angle laser light scattering (SEC-MALLS) and potentiometric titrations has been described in **chapter 2**. Size exclusion chromatography separates molecules according to their size. The radius of gyration (R_g) and the molar mass (M_w) of each eluted fraction are then obtained on-line by multi-angle laser light scattering (via a Zimm-plot), yielding information about the molecular mass distribution of each sample. SEC-MALLS characterisation has been carried out at pH=7 in 0.02 and 0.1 mol l^{-1} $NaNO_3$. It turns out that the distribution depends on the salt concentration and the method of extrapolation of the scattered intensity to zero scattering angle in the Zimm-plot (i.e. using a linear or a non-linear extrapolation). Such a non-linearity is often attributed to the presence of aggregates. Because a CMC solution is supposed to contain more aggregates at high electrolyte concentration it is expected that the molar mass distribution will be shifted to higher molar mass when obtained in 0.1 mol l^{-1} $NaNO_3$ in comparison with 0.02 mol l^{-1} $NaNO_3$. However, the experiments show the opposite trend, indicating that the lack of coincidence of distributions obtained at both salt concentrations is probably not caused by the presence of aggregates.

Because SEC-MALLS gives both the molar mass and the radius of gyration of each eluted fraction, it is a highly suitable experimental technique to obtain the relation between M and R_g. We applied the electrostatic wormlike chain model as well as Odijk's theory concerning the dimension of a polyelectrolyte to analyse this relation (both M and R_g were obtained from the non-linear extrapolation method). A meaningful parameter in these models is the persistence length (L_p) of a polymer, L_p characterising the length scale on which a polymer may be considered as rigid. The persistence length of a polyelectrolyte has two additive contributions. The first is the intrinsic or bare persistence length (L_{p0}) which

characterises the stiffness of the polymer backbone, the second accounts for the stretching of the chain due to electrostatic repulsion (electrostatic persistence length L_{pe}). Using the electrostatic wormlike chain theory, L_{p0} is assessed at 16 nm, indicating that CMC can be considered as a semiflexible polymer. A somewhat lower value (12 nm) has been obtained from the theory of Odijk. The value of L_{p0} does not depend on ds. The difference in L_{p0} between both models arises from the fact that in the Odijk model the contribution of L_{pe} to L_p is higher as compared to the electrostatic wormlike chain model. Furthermore the Odijk model assumes the chain as infinitely long. The electrostatic wormlike chain theory gives a more complete description of a polyelectrolyte chain as it takes molecular properties (such as the length and the cross-section of the molecule) and the details of the electrostatics into account.

Potentiometric titrations were used to characterise the dissociation behaviour of CMC as a function of the NaCl concentration and pH. From the titration data the cross-section (radius) of CMC was obtained. Considering CMC as a uniformly charged cylinder radii of 0.95 nm (ds=0.75) up to 1.15 nm (ds=1.25) were obtained. Applying Katchalsky's theory for the dissociation of a polyelectrolyte, L_{p0} could be also determined from the titration data. In comparison to the analysis of the SEC-MALLS data Katchalsky's model gives a lower value (L_{p0}=5.9 nm). The difference is probably related to an incorrect evaluation of the electrostatic energy in Katchalsky's model.

In **chapter 3** the kinetics of polyelectrolyte adsorption has been investigated theoretically. Analogous to Kramers' rate theory for chemical reactions a model is presented which is based on the assumption that a polyelectrolyte encounters a barrier in its motion towards an adsorbing surface. The barrier is composed of the resistance due to transport in solution and to the presence of an electrical field. As soon as one segment touches the surface the chain is assumed to be adsorbed, i.e. the resistance that a chain encounters in the process of spreading out is neglected.

We consider the motion of a strong polyelectrolyte with only one segment positioned at the front of the moving chain, all other segments are lagging behind the front segment. At each distance the chain explores all possible configurations, i.e. one needs to calculate the partition function of a chain with one segment at $z=z^*$ and all other segments at $z > z^*$ ($Q(z^*)$). Such a partition function is readily evaluated from the numerical procedure proposed by Scheutjens and Fleer. Using this self-consistent-field (SCF) lattice model the resistance of an entering polyelectrolyte chain is calculated as a function of the distance from the surface. It turns out that the profile of the potential energy felt by the moving chain shows a strong resemblance with the interaction curve of colloidal particles, i.e. we observed a resemblance between the attachment process and the classical DLVO theory.

Summing the contributions over the entire trajectory yields the barrier for adsorption R_b. The barrier is calculated as a function of the adsorbed amount, and the results are inserted in the equation for the rate of the adsorption process. Finally, integration at a fixed concentration

of polyelectrolyte leads to the time dependent adsorption. Endpoints in the calculated time dependent adsorption refer to equilibrium at that particular polyelectrolyte concentration.

Parameters that affect the height of the barrier are the net charge at the interface (i.e. the surface charge plus the charge of the adsorbed polyelectrolyte), the charge density of the chain and the electrolyte concentration. Consider the adsorption of a polyelectrolyte on an oppositely charged surface. As long as the surface charge is not compensated there is no electrostatic barrier for adsorption, i.e. the rate of adsorption is determined by the rate of transport in solution to the surface. The height of the barrier strongly decreases with the electrolyte concentration. Consequently, the time needed to reach adsorption equilibrium also strongly depends on the electrolyte concentration. For low electrolyte concentration (0.01 mol l^{-1}) an extremely long time is needed (~10^{15} s), at a moderate concentration (0.2 mol l^{-1}) it takes about 10 s. Hence, compared to the time scale of an experiment (~10^5 s) adsorption equilibrium will not be accomplished for low electrolyte concentrations.

The adsorption of carboxymethyl cellulose on rutile (TiO_2) and hematite (α-Fe_2O_3) is discussed in **chapter 4**. Data were obtained by batch adsorption experiments (depletion method) and by reflectometry, the latter yielding information about the kinetics of the adsorption. Systematically, we examined the influence of pH (pH=3 to 11), electrolyte concentration (c_{NaCl}= 0.01 to 1 mol l^{-1}) , molar mass (M_w=35 to 1200 kg mol^{-1}) and degree of substitution (ds=0.75 to 1.25). Adsorption isotherms are of the high affinity type and have well-defined plateau values. Plateau values in the adsorption decrease with increasing pH and increase with salt concentration. The adsorbed amount depends neither on ds nor on M_w, the latter indicating a (rather) flat conformation of adsorbed CMC. The non-dependence on ds is possibly related to the fact that counter ions in the proximity of the polyelectrolyte chain lower the effective charge in such a way that CMCs varying in ds can have an identical effective charge density.

On both surfaces a strong hysteresis in the adsorption with respect to pH is observed: in the high pH range a substantially higher adsorbed amount can be obtained by initially adsorbing at low pH and subsequently increasing the pH than by measuring the adsorption directly at any specified pH value. Desorption of CMC only takes place after the pH is increased substantially, which indicates a (very) strong interaction between CMC and the surface. Strong binding is likely related to the formation of ion pairs between the carboxylic groups of CMC and positively charged surface groups. Furthermore the desorption becomes even more difficult due to the chain rigidity of the CMC backbone, i.e. several bonds to the surface need to be broken simultaneously.

Both the dissociation of the OH groups of the mineral surfaces and of the carboxylic groups of CMC depends on pH and electrolyte concentration. Furthermore the adsorption of a weak polyelectrolyte on such variable charged surfaces induces additional charges on the surface as well as on the polyelectrolyte. These characteristics cause the adsorption of a weak

polyelectrolyte on a mineral surface to be very complicated. The model as presented in chapter 3 is used to elucidate this kind of adsorption. We calculated the adsorption and the charge of the surface at 10^5 s (a time which is comparable to the duration of an experiment). Because the short-range interaction between CMC and the surface is strong, the charge of adsorbed CMC can exceed the surface charge. The amount of overcompensation (or excess adsorbed charge σ_{exc}) depends on the possibility that molecules reach the surface, i.e. on the height of the barrier for adsorption. As this barrier is a function of the net charge at the interface, σ_{exc} at a fixed electrolyte concentration does not depend on the pH. Increasing the electrolyte concentration lowers the barrier which allows higher σ_{exc}. The calculations in chapter 4 show that at pH values where a weak polyelectrolyte is fully dissociated (i.e. acts as a strong polyelectrolyte) the adsorbed amount decreases linear with pH. Our experiments are in qualitative agreement with these calculations. The shape of the calculated time dependent adsorption curves also shows qualitative agreement with reflectometry experiments.

In **chapter 5** we discuss the adsorption of hydroxyethyl cellulose and quaternary ammonium substituted HEC (QNHEC) on silica and titanium dioxide. The adsorption has been investigated as a function of pH (pH=2 to 12) and electrolyte concentration (c_{NaCl}=0.01 and 0.5 mol l^{-1}) by means of reflectometry.

The adsorption of HEC on SiO_2 shows a strong resemblance with the adsorption of polyethylene oxide. The adsorption is constant up to pH=5 in both 0.01 and 0.5 mol l^{-1} NaCl, albeit in the latter case the adsorption is higher. At pH > 5 the adsorption decreases, which is most pronounced at the high salt concentration, reaching the level of zero adsorption at pH≈9. On TiO_2 the adsorption decreases monotonously with pH in 0.01 mol l^{-1} NaCl. At high salt concentration it is constant up to pH=10, beyond which it decreases rapidly. The adsorption of HEC on SiO_2 is facilitated by hydrogen bonding between HEC ether groups and Si-OH surface groups, whilst the mechanism on TiO_2 is probably an interaction between non-substituted glucose hydroxyl groups and Ti-OH surface groups. The latter involves a chemical reaction, which may account for the fact that the time dependent adsorption of HEC on TiO_2 lacks a region where the adsorption increases linearly in time (i.e. mass transport in the solution is not the rate determining step even when the adsorption is low).

Just as for CMC, in the adsorption of QNHEC there is an electrostatic barrier for adsorption. We compared the time dependent adsorption of QNHEC with calculations obtained from the model presented in chapter 3. It appears that in the case of QNHEC equilibrium is very likely not reached in 0.01 mol l^{-1} NaCl, whereas in 0.5 mol l^{-1} NaCl equilibrium is reached. As the charge density of QNHEC is lower (0.4 charged groups per glucose unit) than for CMC, the electrostatic barrier is also lower. In 0.01 mol l^{-1} NaCl both on SiO_2 and TiO_2 the adsorption increases linearly with pH up to pH=10. This linearity is interpreted in analogous to the CMC adsorption. The adsorption reaches a maximum at pH≈12, then it decreased rapidly. According to the classification of van de Steeg the

adsorption of QNHEC on SiO_2 in 0.5 mol l^{-1} NaCl is of the screening-enhanced type up to pH ≅ 10, whereas at higher pH it is of the screening-reduced type. On TiO_2 the adsorbed amount is low and does not depend on pH.

In **chapter 6** the diffusion of spherical silica particles (with radii ranging from 12 to 510 nm) in dilute CMC solutions (M_w=180 to 1200 kg mol^{-1}, c_{CMC}=5 to 1000 mg l^{-1}) was investigated by means of dynamic light scattering. From the diffusion coefficient the viscosity as experienced by these inert probes (the "microscopic" or effective viscosity) is obtained. The smallest particles experience a viscosity which is slightly higher than the solvent viscosity, which may be interpreted in terms of the motion of these particles hardly being affected by the presence of polymer. The effect of polymer on the motion of the probes increases with the size of the probes. However, the value of the viscosity as obtained from capillary viscosimetry (bulk viscosity) is still not reached for the largest sphere, albeit for CMC M_w=180 kg mol^{-1} the effective viscosity comes rather close to the bulk viscosity.

The thickness of the CMC/HEC layer adsorbed on Fe_2O_3/SiO_2 is also investigated in chapter 6. The layer thickness as obtained using the bulk viscosity shows a maximum as a function of the polymer concentration. The origin of the maximum is a consequence of an incorrect choice of the viscosity. Using the viscosity as obtained from the inert probe diffusion the layer thickness increases monotonously with polymer concentration.

The diffusion behaviour of the inert probes is discussed in terms of a model in which the particles are surrounded by a layer of polymer free solution. This layer is assumed to be equal to the thickness of the depletion layer. According to this model the thickness of the depletion layer decreases with the CMC concentration, at low concentration approaching the radius of gyration of CMC.

The work described in this thesis has led to the following publications and submitted manuscripts:

C.W. Hoogendam, A. de Keizer, M.A. Cohen Stuart, B.H. Bijsterbosch, J.A.M. Smit, J.A.P.P. van Dijk, P.M. van der Horst, and J.G. Batelaan, "*Persistence length of carboxymethyl cellulose as evaluated from size exclusion chromatography and potentiometric titrations*" accepted by *Macromolecules* (chapter 2).

M.A. Cohen Stuart, C.W. Hoogendam, and A. de Keizer, "*Kinetics of polyelectrolyte adsorption*", *J. Phys.: Condens. Matter* **9** (1997) 7767 (chapter 3).

C.W. Hoogendam, A. de Keizer, M.A. Cohen Stuart, B.H. Bijsterbosch, J.G. Batelaan, and P.M. van der Horst, "*Adsorption mechanisms of carboxymethyl cellulose on mineral surfaces*", *Langmuir* **8** (1998) 3825 (chapter 4).

C.W. Hoogendam, I. Derks, A. de Keizer, M.A. Cohen Stuart, and B.H. Bijsterbosch, "*Adsorption of cellulose derivatives on inorganic oxides*", accepted by *Colloids and Surfaces A* (chapter 5).

C.W. Hoogendam, J.C.W. Peters, R. Tuinier, A. de Keizer, M.A. Cohen Stuart,and B.H. Bijsterbosch, "*Depletion thickness and thickness of the adsorbed layer of cellulose derivatives on inorganic oxides*", accepted by *Journal of Colloid and Interface Science* (chapter 6).

N.G. Hoogeveen, C.W. Hoogendam, R. Tuinier, and M.A. Cohen Stuart, "*Adsorption of weak polyelectrolytes on amphoteric oxide surfaces*", *Int. J. Polymer Analysis & Characterization* **1** (1995) 315.

Samenvatting

Adsorptie en desorptie van cellulose derivaten

Polymeren zijn lange moleculen die bestaan uit een groot aantal kleinere identieke moleculen (monomeren). Het belang van het gebruik van polymeren in onze moderne samenleving wordt algemeen erkend. Ruwweg kunnen de toepassingen van polymeren worden verdeeld in plastics (bijvoorbeeld PVC of verpakkingsmaterialen), als verdikkings middelen (bijvoorbeeld in yoghurt of in verf), en als coatings. Het werk, zoals beschreven in dit proefschrift, heeft betrekking op de laatste toepassing. Veelal worden synthetische polymeren gebruikt in coatings. Echter, chemisch gemodificeerde natuurlijke polymeren worden steeds vaker als alternatief voor synthetische polymeren gebruikt. Met name polysacchariden, zoals zetmeel en cellulose, worden veel gebruikt als chemisch gemodificeerd natuurlijke polymeren. Deze materialen zijn ruimschoots voorradig (cellulose is het belangrijkste bestanddeel van planten), zijn vaak niet giftig en door hun afbreekbaarheid zijn ze minder belastend voor het milieu. Het onderwerp van dit promotie onderzoek spitst zich toe op het gebruik van chemisch gemodificeerde cellulose polymeren (cellulose derivaten). Dit werk is uitgevoerd om inzicht te krijgen in het gedrag van dergelijke polymeren aan een vast-vloeistof grensvlak. Inzicht hierin kan resulteren in verbetering van huidige toepassingen of kan leiden tot nieuwe toepassingen.

Eén van de belangrijkste vertegenwoordigers van de cellulose derivaten is carboxymethyl cellulose (CMC). CMC wordt gebruikt in onder andere de papierindustrie en bij de bereiding pellets van ijzererts. In CMC zijn waterstof atomen van glucose moleculen (glucose is het monomeer in een cellulose polymeer) vervangen door CH_2COOH groepen. De CH_2COOH groepen kunnen een H^+ deeltje afsplitsen (dissociatie), dit betekend dat CMC in water is opgelost, bijna altijd negatief geladen is. Een geladen polymeer (positief of negatief geladen) wordt een polyelectroliet genoemd.

In dit onderzoek is een serie van 20 verschillende CMC monsters gebruikt. De monsters variëren in substitutiegraad (ds=0.75, 0.91, 0.99, en 1.25) en molecuul massa (M_w=30 kg mol^{-1} tot 10^3 kg mol^{-1}). De substitutiegraad geeft het gemiddeld aantal aangebrachte chemische groepen per glucose molecuul weer. Karakterisering van de CMC monsters wordt beschreven in **hoofdstuk 2**. Bij de karakterisering is gebruik gemaakt van size exclusion chromatografie (ook wel gelpermeatie chromatografie genoemd) gecombineerd met een multi-hoek lichtverstrooiings detector (SEC-MALLS) en potentiometrische titraties. Bij de eerstgenoemde techniek worden de monsters over een kolom geleid die deze scheidt op grootte. Doordat de grootste moleculen het gemakkelijkst door de kolom heen bewegen, komen deze als eerste door de kolom, de kleinste moleculen worden het meeste vertraagd. De grootte van de moleculen, die wordt gekarakteriseerd door de gyratiestraal R_g en de molecuul

massa M_w van een fractie die van de kolom komt, wordt direct bepaald met de lichtverstrooiings detector (via een Zimm plot). Op deze manier is de molecuulmassa verdeling vastgesteld. Het blijkt dat deze verdeling afhangt van de methode van extrapolatie (een lineaire of niet-lineaire extrapolatie) van de intensiteit van het verstrooide licht naar een strooihoek van 0°. Een niet-lineair gedrag in een Zimm plot wordt in het algemeen toegeschreven aan de aanwezigheid van geaggregeerde moleculen (moleculen die samengeklonterd zijn). SEC-MALLS karakterisering is uitgevoerd in 0.02 en 0.1 mol l^{-1} $NaNO_3$ oplossingen bij een zuurgraad van pH=7. Bij pH=7 zijn de CMC moleculen volledig geladen. Omdat de ladingen op de ketens de vorming van aggregaten bemoeilijken, mag worden verwacht dat de molecuulmassa verdeling bepaald in 0.1 mol l^{-1} $NaNO_3$ een verschuiving geeft naar hogere molecuul massa in vergelijking met de verdeling bepaald in 0.02 mol l^{-1} $NaNO_3$. Uit de experimenten blijkt echter het tegengestelde, hetgeen aangeeft dat de CMC oplossingen geen of heel weinig aggregaten bevatten.

Aangezien SEC-MALLS voor elke fractie direct zowel R_g als M_w geeft, is deze techniek bijzonder geschikt om experimenteel de relatie tussen de molecuul massa en de gyratiestraal te bepalen. Voor de analyse van deze relatie (bepaald via een niet-lineaire extrapolatie) is gebruik gemaakt van het electrostatische wormachtige ketenmodel en de theorie van Odijk voor de beschrijving van de afmeting van polyelectrolieten in een vloeistof. Centrale parameter in deze modellen is de lengte waarover een molecuul als stijf mag worden opgevat, de persistentiel engte L_p. De persistentie lengte is samengesteld uit twee bijdragen die bij elkaar kunnen worden opgeteld. De eerste bijdrage, de intrinsieke of kale persistentie lengte L_{p0}, wordt bepaald door de stijfheid van het molecuul zelf, de tweede bijdrage brengt de strekking van de keten als gevolg van de repulsie tussen ladingen op de keten in rekening (electrostatische persistentie lengte L_{pe}). Met behulp van het wormachtige ketenmodel wordt een waarde van L_{p0} van 16 nm gevonden, hetgeen aangeeft dat CMC mag worden opgevat als een semi-flexibel polymeer (d.w.z. CMC is geen staafvormig molecuul, maar ook geen volkomen flexibel molecuul). De theorie van Odijk geeft een waarde voor L_{p0} van 12 nm. De waarde van L_{p0} hangt niet af van de substitutiegraad. In het model van Odijk is de bijdrage van L_{pe} aan L_p groter dan in het wormachtige ketenmodel, daarom wordt met het eerstgenoemde model een lagere waarde voor L_{p0} bepaald. Behalve dat ladingseffecten meer gedetailleerd wordt beschreven, houdt het wormachtige ketenmodel rekening met moleculaire eigenschappen, zoals de lengte en de doorsnede van de keten (deze ontbreken in het gebruikte model van Odijk).

De potentiometrische titraties zijn uitgevoerd om het dissociatie gedrag van CMC als functie van de concentratie zout (NaCl) en de zuurgraad (pH) te bepalen. Uit het dissociatie gedrag is het mogelijk de straal van de CMC keten te bepalen. Onder aanname dat de CMC keten als een uniform geladen cilinder mag worden opgevat, is een straal van 0.95 nm (ds=0.75) tot 1.15 nm (ds=1.25) gevonden. Het model voor de dissociatie van een polyelectroliet zoals beschreven door Katchalsky is gebruikt om L_{p0} te bepalen uit het

dissociatie gedrag. Vergeleken met de analyse van de SEC-MALLS gegevens levert toepassing van dit model een lager waarde voor L_{p0} op (L_{p0}=5.9 nm). De reden van het verschil is waarschijnlijk toe te schrijven aan een incorrecte beschrijving van de electrostatische energie in het model van Katchalsky.

In **hoofdstuk 3** wordt aandacht besteed aan een theoretische beschrijving van de kinetiek van de adsorptie van polyelectrolieten. In analogie met de theorie van Kramers voor de snelheid van chemische reacties wordt een model gepresenteerd dat gebaseerd op de aanname dat een polyelectroliet een barrière ondervindt in zijn beweging naar het oppervlak toe. Deze barrière is opgebouwd uit de weerstand die een polymeer ondervindt bij beweging in de vloeistof en uit de weerstand die het gevolg is van de aanwezigheid van een electrisch veld. In het gepresenteerde model wordt verondersteld dat zodra één monomeer het oppervlak weet te bereiken de keten niet meer los kan komen (het polymeer is geadsorbeerd). Met de weerstand die wordt ondervonden bij de spreiding over het oppervlak wordt geen rekening gehouden.

Een polymeer dat de minste weerstand ondervindt bij beweging naar het oppervlak toe, is een polymeer met één monomeer in de richting van het oppervlak terwijl de overige monomeren zich achter dit ene monomeer bevinden. Er wordt verondersteld dat op elke afstand van het oppervlak de keten alle mogelijke configuraties kan aannemen. Dit betekent dat de partitie functie van een keten met een monomeer op $z=z^*$ en de overige monomeren op $z > z^*$ ($Q(z^*)$) moet worden berekend. Het berekenen van een dergelijke partitie functie kan worden uitgevoerd met het numerieke model van Scheutjens en Fleer. De zelf consistente veld theorie van Scheutjens en Fleer is gebruikt om de weerstand voor adsorptie te berekenen als functie van de afstand van het oppervlak. De berekeningen laten zien dat het profiel van de potentiële energie een sterke overeenkomst vertoont met de interactiecurve van colloïdale deeltjes, m.a.w. het adsorptieproces vertoont overeenkomsten met de klassieke DLVO theorie.

Door alle bijdragen over het traject waarover het polymeer beweegt bij elkaar op te tellen wordt de barrière voor adsorptie, R_b, berekend. Vervolgens wordt R_b berekend als functie van de hoeveelheid geadsorbeerd polymeer aan het oppervlak. Door deze berekende waarden in te vullen in de vergelijking voor de snelheid van het adsorptieproces kan na integratie van deze vergelijking de adsorptie als functie van de tijd worden berekend. De eindpunten in de berekeningen komen overeen met de evenwichtswaarden behorend bij een gegeven concentratie polyelectroliet. Uit de berekeningen kan dus worden afgeleid hoe veel tijd er nodig is voordat evenwicht in de adsorptie is bereikt.

Parameters die de hoogte van de barrière bepalen zijn de netto lading aan het oppervlak (de oppervlaktelading plus de lading van het geadsorbeerde polyelectroliet), de ladingsdichtheid van de keten en de zoutconcentratie. Beschouw het geval dat een polyelectroliet adsorbeert aan een tegengesteld geladen oppervlak. Zolang de oppervlaktelading niet is gecompenseerd door het polyelectroliet, is er geen electrostatische barrière voor adsorptie (immers, tegengestelde ladingen trekken elkaar). De netto lading aan

het oppervlak blijft tegengesteld aan de lading van het polyelectroliet zolang er geen sprake is compensatie van de oppervlakte lading. Bij afwezigheid van een electrostatische barrière wordt de adsorptie snelheid dan alleen bepaald door het transport van polyelectroliet naar het oppervlak toe. Zodra de lading van geadsorbeerd polyelectroliet groter is dan de oppervlakte lading wordt het moeilijker om het oppervlak te bereiken aangezien de netto oppervlakte lading en het polyelectroliet gelijk in teken zijn (er is nu sprake van een electrostatische barrière). De hoogte van de electrostatische barrière neemt af met de zoutconcentratie. Om deze reden hangt de tijd die nodig is voor het bereiken van evenwicht sterk samen met de zoutconcentratie. In het geval van een lage concentratie (0.01 mol l^{-1}) duurt de evenwichtsinstelling extreem lang (~ 10^{15} s), bij een middelgrote zoutconcentratie (0.2 mol l^{-1}) wordt evenwicht bereikt in ongeveer 10 seconden. De berekeningen geven aan dat in het geval van lage zoutconcentraties er geen evenwicht wordt bereikt op de tijdschaal van een experiment (~ 10^5 s).

De adsorptie van CMC aan rutiel (TiO_2) en hematiet (α-Fe_2O_3) wordt besproken in **hoofdstuk 4**. De invloed van de pH (pH= 3 tot 11), concentratie zout (c_{NaCl}= 0.01 mol l^{-1} tot 1 mol l^{-1}), molecuul massa (M_w= 35 tot 1200 kg mol^{-1}) en substitutiegraad (ds=0.75 tot 1.25) op de adsorptie is systematisch onderzocht. Voor de bepaling van de geadsorbeerde hoeveelheid is gebruik gemaakt van batch adsorptie experimenten (depletie methode) en van reflectometrie, waarbij de laatstgenoemde methode informatie geeft over de kinetiek van het adsorptieproces. Adsorptie isothermen bepaald met de depletie methode zijn van het hoge affiniteit type en hebben een goed gedefinieerde plateau waarde. Het plateau in de adsorptie neemt af met de pH en neemt toe met de zoutconcentratie. De adsorptie hangt niet af van de molecuul massa, hetgeen aangeeft dat de conformatie van de geadsorbeerde laag (vrij) vlak is. Ook blijkt de adsorptie niet af te hangen van de substitutiegraad. Een mogelijke verklaring hiervoor is dat tegenionen die zich dicht in de buurt van de keten bevinden de effectieve lading van de keten beïnvloeden zodat CMCs die variëren in ds toch een vrijwel gelijke effectieve ladingsdichtheid hebben.

Op zowel het hematiet en rutiel oppervlak wordt een sterke hysterese ten aanzien van de pH waargenomen: bij een hoge pH-waarde kan een belangrijk hogere hoeveelheid geadsorbeerd CMC worden verkregen door eerst bij lage pH te adsorberen en vervolgens de pH te verhogen dan direct bij hoge pH te adsorberen. Desorptie (loslaten van het oppervlak) van CMC vindt alleen maar plaats na een aanzienlijke pH verhoging. Dit geeft aan dat er een sterke binding is tussen CMC en de gebruikte oppervlakken. Deze sterke binding is mogelijk het gevolg van de vorming van ionparen tussen de carboxyl groepen van CMC en positief geladen groepen van het oxide oppervlak. Verder speelt de stijfheid van de cellulose keten een rol: in het geval van CMC moeten een aantal bindingen gelijktijdig worden verbroken om te kunnen desorberen.

De oxidische oppervlakken bevatten OH groepen die deze oppervlakken lading geven. Zowel de dissociatie van deze groepen als die van de carboxyl groepen van CMC hangen af

van de pH en de concentratie zout. Bovendien worden zowel de lading van het oppervlak en van CMC door de adsorptie beïnvloed. Deze ladingsinductie maakt de adsorptie van een zwak polyelectroliet op een mineraal oppervlak zeer ingewikkeld. In hoofdstuk 4 wordt het model uit hoofdstuk 3 gebruikt om de adsorptie van CMC aan de oxidische oppervlakken te beschrijven. De adsorptie en de oppervlaktelading in aanwezigheid van geadsorbeerd polyelectroliet is berekend na 10^5 s (vergelijkbaar met de tijd van een experiment). De sterke interactie tussen CMC en de oxidische oppervlakken maakt het mogelijk dat de lading van geadsorbeerd polyelectroliet hoger kan zijn dan de oppervlaktelading. De mate van overcompensatie (excess geadsorbeerde lading σ_{exc}) hangt af van de mogelijkheid van de moleculen om het oppervlak te bereiken (van de hoogte van de barrière). Aangezien de hoogte van de barrière bepaald wordt door de netto lading aan het oppervlak, hangt bij een constante zoutconcentratie de waarde van σ_{exc} niet af van de pH. Verhoging van de zout concentratie verlaagt de barrière waardoor een hogere waarde voor σ_{exc} mogelijk wordt. De berekeningen in hoofdstuk 4 laten zien dat bij pH-waarden waar een zwak polyelectroliet volledig is gedissocieerd de geadsorbeerde hoeveelheid lineair afneemt met de pH. Een dergelijk gedrag is ook waargenomen in de adsorptie experimenten. Ook vertoont de berekende tijdafhankelijke adsorptie een goede kwalitatieve overeenkomst met reflectometrie experimenten.

In **hoofdstuk 5** wordt de adsorptie van hydroxyethyl cellulose (HEC) en quaternair ammonium gesubstitueerd HEC (QNHEC) aan siliciumoxide en titaan oxide besproken. HEC is een ongeladen cellulose derivaat, QNHEC heeft een constante positieve lading. De adsorptie is met behulp van reflectometrie onderzocht als functie van de pH (pH= 2 tot 12) en zout concentratie (c_{NaCl}= 0.01 mol l^{-1} en 0.5 mol l^{-1}).

De adsorptie van HEC op SiO_2 vertoont een sterke overeenkomst met de adsorptie van polyethylene oxide. Zowel in 0.01 en 0.5 mol l^{-1} NaCl is de geadsorbeerde hoeveelheid constant tot pH=5, zij het dat de adsorptie voor de hoogste zoutconcentratie hoger is. Voor pH > 5 daalt de adsorptie, bij pH≈9 vindt geen adsorptie meer plaats. Op TiO_2 daalt de adsorptie monotoon met de pH in het geval van 0.01 mol l^{-1} NaCl. Voor de hoge zout concentratie is de geadsorbeerde hoeveelheid constant to pH=10, daarna daalt de adsorptie snel. De adsorptie van HEC aan SiO_2 wordt mogelijk gemaakt door de vorming van waterstofbruggen tussen HEC ether groepen en Si-OH oppervlakte groepen (silanol groepen). Het mechanisme voor de binding aan TiO_2 is waarschijnlijk het gevolg van een chemische interactie tussen niet-gesubstitueerde glucose hydroxyl groepen en Ti-OH groepen.

QNHEC is, net als CMC, een polyelectroliet. Er zal daarom ook sprake zijn van een electrostatische barrière voor de adsorptie. De tijdafhankelijk adsorptie van QNHEC is vergeleken met berekeningen verkregen met het in hoofdstuk 3 gepresenteerde model. De berekeningen geven aan dat in 0.01 mol l^{-1} NaCl er geen evenwicht wordt bereikt in de adsorptie experimenten, in 0.5 mol l^{-1} NaCl wordt het evenwicht wel bereikt. Omdat de

ladingsdichtheid van QNHEC (gemiddeld 0.4 geladen groepen per glucose monomeer) lager is dan voor CMC, is de electrostatische barrière ook lager. In 0.01 mol l^{-1} NaCl neemt de adsorptie aan SiO_2 en TiO_2 lineair toe met de pH tot pH=10. Bij pH≈12 bereikt de geadsorbeerde hoeveelheid een maximum, waarna deze snel afneemt. Binnen de classificatie volgens van de Steeg is de adsorptie van QNHEC op SiO_2 in 0.5 mol l^{-1} NaCl van het type screening-enhanced tot pH≈10, bij hogere pH is het screening-reduced type van toepassing. Op TiO_2 is de adsorptie laag en hangt deze niet af van de pH.

Het diffusie gedrag van bolvormige SiO_2 deeltjes (met straal van 12 tot 510 nm) in verdunde CMC oplossingen (M_w=180 to 1200 kg mol^{-1}, c_{CMC}=5 to 1000 mg l^{-1}) wordt besproken in **hoofdstuk 6**. Uit de diffusie coëfficiënt, bepaald met behulp van dynamische lichtverstrooiing, is de viscositeit zoals deze wordt ondervonden door deze inerte probe deeltjes ("microscopische" of effectieve viscositeit) bepaald. Inerte probe deeltjes zijn deeltjes waaraan een polymeer niet adsorbeert. De kleinste deeltjes ervaren een viscositeit die iets hoger is dan de viscositeit van het oplosmiddel, hetgeen aangeeft dat de beweging van de deeltjes nauwelijks wordt beïnvloed door aanwezigheid van polymeer in oplossing. De invloed van de aanwezigheid van polymeer neemt toe met de grootte van de probe deeltjes. De waarde van de bulk viscositeit (bepaald met capillaire viscometrie) wordt, zelfs voor het grootste probe deeltje, nog niet bereikt. In het geval van CMC M_w=180 kg mol^{-1} neemt de waarde van de effectieve viscositeit bijna de waarde van de bulk viscositeit aan.

De laagdikte van geadsorbeerd CMC/HEC aan Fe_2O_3/SiO_2 wordt ook besproken in hoofdstuk 6. Wanneer de bulkviscositeit wordt gebruikt om de laagdikte te berekenen wordt een maximum als functie van de polymeerconcentratie gevonden. Dit maximum is het gevolg van een incorrecte keuze van de viscositeit. Wanneer de viscositeit zoals verkregen door middel van inerte probe metingen wordt gebruik, wordt een monotone toename van de laagdikte gevonden als functie van de polymeerconcentratie.

Het diffusie gedrag van de inerte probe deeltjes wordt beschreven met een model waarbij wordt verondersteld dat de deeltjes zijn omgeven door een laag vloeistof die geen polymeer bevat. Verondersteld wordt dat de dikte van deze laag gelijk is aan de dikte van de depletie laag rond deze deeltjes. De analyse van de experimenten geeft aan dat de dikte van de depletie laag afneemt met de concentratie CMC. Bij lage concentratie is de dikte gelijk aan de gyratiestraal van CMC.

Levensloop

Cornelis Willem (in het dagelijks leven René) Hoogendam aanschouwde op zaterdag 10 april 1965 om 12 uur 36 in Zeist het levenslicht. Na het doorlopen van de middelbare school (MAVO, HAVO en Atheneum-B aan het Revius Lyceum te Doorn) werd in 1986 begonnen aan een studie Scheikunde aan de Rijksuniversiteit Utrecht (tegenwoordig Universiteit Utrecht). In september 1991 werd de studie afgerond met specialisaties Halfgeleiderelectrochemie, Chemische Informatica (als bijvakken), en Oppervlakte Chemie (als hoofdvak). In januari 1992 trad de auteur van dit proefschrift in dienst bij de vakgroep Fysische en Kolloïdchemie (tegenwoordig het Laboratorium voor Fysische Chemie en Kolloïdkunde) van de Landbouwuniversiteit Wageningen. Als Assistent In Opleiding deed hij onderzoek naar de adsorptie van cellulose derivaten aan anorganische oxiden. Begin 1998 werd het onderzoek afgerond met de voltooiing van het schrijven van dit proefschrift.

Nawoord

Beste lezer, voor u liggen de laatste bladzijden van dit proefschrift. Dit proefschrift, dat het eindproduct is van een lange (misschien wel een iets te lange) periode van onderzoek doen en het op papier zetten van de resultaten daarvan. Het is een cliché, dat weet ik ook wel, maar een proefschrift maak je niet alleen. Op deze bladzijden is het mij gegeven enige woorden te richten aan mensen die, in min of meerdere mate, er toe hebben bijgedragen dat het dan toch uiteindelijk zo ver gekomen is.

Mijn directe begeleiders op het lab waren Bert Bijsterbosch, Arie de Keizer en Martien Cohen Stuart. Het is voor mij een plezierige en leerzame ervaring geweest om met jullie samen te werken. Bert, vooral in de eindfase heb ik veel aan jou gehad. Wanneer ik weer een ei (hoofdstuk of artikel) had gelegd, kreeg ik het terug met suggesties om de tekst beter leesbaar te maken. Ik weet zeker dat het ook daarom is dat alle artikelen in één keer zijn geaccepteerd. Uitkomsten van experimenten werden regelmatig door Arie op een goudschaaltje gelegd. Arie, mede dankzij door jouw kritische blik bleef ik er aan herinnerd altijd op mijn hoede te blijven voor valkuilen op het wetenschappelijke pad. Martien lijkt wel voor bijna elk probleem een goeie suggestie voor een oplossing te hebben. Als ik dacht "hoe zou je dit nu weer kunnen verklaren?" of "hoe gaan we dit probleem nu weer aanpakken?" ontsproot er uit jouw brein wel weer een origineel idee dat mij dan weer op weg hielp.

Regelmatig werd er overleg over de voortgang van het promotie onderzoek gepleegd. Een bijdrage van buiten Wageningen in het overleg werd geleverd door Jan Batelaan en Peter van der Horst (beide van AKZO Nobel in Arnhem). De CMCs in dit onderzoek zijn gesynthetiseerd door Peter, m.a.w. zonder Peter had het onderzoek nooit uitgevoerd kunnen worden. Jan en Peter bekijken de chemie vanuit een andere hoek: vanuit een Organisch Chemische hoek. Dit gaf regelmatig aanleiding tot levendige discussies die mij als Fysisch Chemicus er toe aanzette om problemen ook eens vanuit een andere gezichtspunt te bekijken. Jan en Peter: ik heb jullie betrokkenheid bij het onderzoek altijd zeer op prijs gesteld.

Met Jan Smit en John van Dijk heb ik in Leiden gewerkt aan de karakterisering van de CMCs. We kamen al snel tot ontdekking dat we niet met het meest gemakkelijke polymeer te maken hadden. De resultaten die uit de SEC-MALLS metingen volgden waren niet altijd even duidelijk. We hebben veel gepuzzeld, nagedacht en dingen geprobeerd. Soms bekroop mij het gevoel van "komt dit nog goed ?". Nu kan ik zeggen: het is allemaal goed gekomen.

Mijn werkplek heb ik lange tijd gedeeld met Henri Bijsterbosch. Als polymeer AIO's hebben we vaak over onze onderzoeken gepraat. Leuker vond ik eigenlijk onze discussies over de ontwikkelingen in de Nederlandse voetbal competitie (vooral omdat we het daar lang niet altijd over eens waren). Ik ben Henri altijd nog dankbaar dat hij mij er op heeft geattendeerd dat er namen van bergen in een lijstje voor de Tour de France Pool kwamen. Die namen zijn geschrapt en vervangen door andere namen. Ik heb dat jaar wel de pool gewonnen! Met Joanne Klein Wolterink heb ik het laatste jaar de werkplek gedeeld. Joanne,

ik ben blij dat jij -net als ik- vrijwel altijd de zonnewering gesloten houdt. Ik wens je veel succes met je onderzoek naar (stervormig) humus zuur.

De koffiekamer (met name het gedeelte rechts als je binnen komt) is een prima locatie voor het voeren van niet-wetenschappelijke discussies. Daar tref je mensen aan als Ben Spee, Rob Vullings, Ab van der Linde, Wim Threels, Ronald Wegh en Bert Torn. Deze mensen, vooral Ben en Bert, hebben mij regelmatig advies gegeven bij het invullen van mijn voetbal toto formulieren. Ik heb nooit een grote klapper gemaakt, maar als dat ooit nog gebeurd krijgen jullie dat te horen !

Data verzamelen is de eerste aanzet tot een figuur. Voor de afwerking van de figuren is Gert Buurman de persoon bij uitstek. In de schrijffase ben ik vaak bij Gert langs geweest om "de beste lijn" door de punten te laten tekenen. Gert, jouw bijdrage is op bijna elke pagina terug te vinden.

Dubbellikkers (dat zijn ijslollies) zijn verkoelend bij warm weer. Het was dan ook in warme perioden dat er "Goldberg Discussions" plaatsvonden in de kelder van het lab. De discussies, onder het genot van een ijslollie, met Monique Bremer, Marcel Giesbers en Remco Fokkink waren een welkome afwisseling op het werk. Ook voor interessante conversaties (nou ja ?!) met Rob maakte ik graag even wat tijd vrij.

Remco Tuinier, Ingrid Derks en Jenke Peters hebben bij mij een afstudeervak gedaan. Remco en Jenke hebben zich bezig gehouden met vooral de bepaling van de effectieve viscositeit van polymeer oplossingen. Een lastig onderwerp. Jullie werk heeft er, denk ik, toe bij gedragen dat er weer tipje van de sluier van het onderwerp effectieve viscositeit is opgelicht. Ingrid heeft onderzoek gedaan naar de adsorptie van HEC en QNHEC. De reflectometer opstelling werkte niet altijd mee, maar uiteindelijk is alles toch nog goed gekomen. Bedankt, jullie werk heeft zeker bijgedragen aan dit boekje.

Een goed begin van de werkdag is altijd prettig. En hoe kun je een dag beter beginnen dan met een vers bakkie koffie. Dankzij Annie Homan en Anneke van der Kraats was er altijd zo'n bakkie om de dag te starten. Annie en Anneke, bedankt voor al die liters uitstekende koffie (nou ja, niet overdrijven) die ik in de afgelopen jaren heb mogen drinken.

Als laatste wil ik mijn ouders bedanken. Zij hebben mij altijd gestimuleerd om door te leren. Zij hebben mij ook bijgebracht om vooral nooit op te geven, het is dan ook zeker dankzij mijn vader en mijn moeder dat dit proefschrift er dan toch uiteindelijk ligt.

Ik heb een lange tijd doorgebracht op het lab op de Dreijen. Het was niet altijd gemakkelijk, maar ik heb het wel naar mijn zin gehad. Tijd om de laatste woorden uit te spreken:

tot ziens, tot kijk, ,
allemaal bedankt !!!

René